Review | Open Access

Energy Z

Chen *et al. Energy Z* **2026**, *2*, 200019 **DOI:**10.20517/energyz.2026.17

Advanced electrolyte engineering for solid electrolyte interphase regulation on Si anodes in Li batteries

Yang Chen[1], Haoxuan Liu[1,*], Anqi Duan[1], Zhihui Xu[1], Jiafeng Cao[1], Chao Wu[2,*], Aruuhan Bayaguud[1,*]

Keywords:
Silicon anode, electrolyte, solid electrolyte interphase, solvation structure

Citation: Chen, Y.; Liu, H.; Duan, A.; Xu, Z.; Cao, J.; Wu, C.; Bayaguud, A. Advanced electrolyte engineering for solid electrolyte interphase regulation on Si anodes in Li batteries. *Energy Z* **2026**, *2*, 200019. https://dx.doi.org/10.20517/energyz.2026.17

Received: 9 Apr 2026
First Decision: 12 May 2026
Revised: 27 May 2026
Accepted: 14 Jul 2026
Published: 11 Sep 2026

Academic Editor:
Yuping Wu
Copy Editor:
Shu-Yuan Duan
Production Editor:
Shu-Yuan Duan

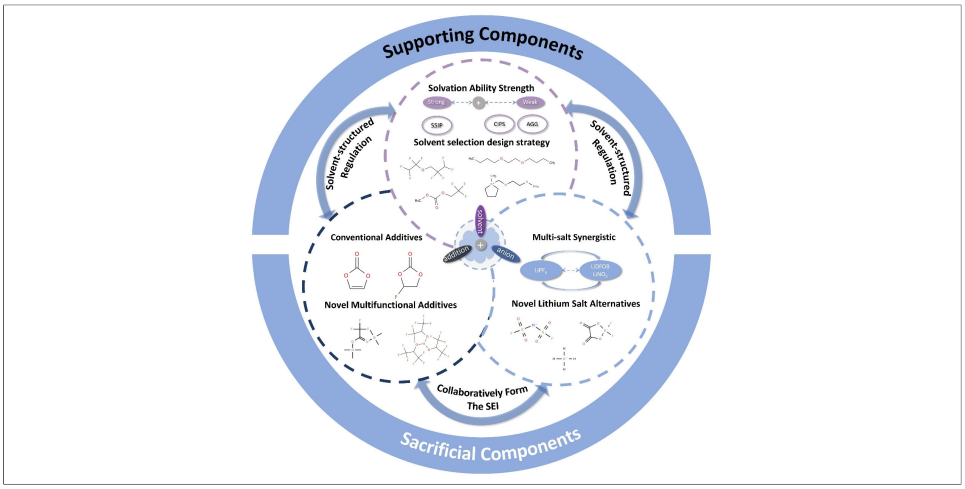

Abstract

Silicon has emerged as one of the most promising anodes for next-generation high-energy-density Li-ion batteries (LIBs) owing to its abundant resource, high theoretical capacity, and low redox potential. However, the drastic volume changes of Si anodes during lithiation/delithiation lead to continuous rupture and reformation of the solid electrolyte interphase (SEI), ultimately resulting in low Coulombic efficiency (CE) and poor cycling stability. Currently, electrolyte engineering has attracted increasing attention because it directly governs SEI formation, composition, and mechanical stability. This review highlights the challenges in developing functional electrolytes and summarizes recent progress in electrolyte engineering for constructing stable SEIs on Si anodes, with particular emphasis on the roles of solvation structure regulation and anion/additive decomposition pathways in SEI formation and stability. Finally, key perspectives are proposed to guide the rational design of electrolytes for high-energy-density Si-based LIBs.

[1]Department of Materials Science and Engineering, Inner Mongolia University of Technology, Hohhot 010051, Inner Mongolia, China.
[2]Institute of Energy Materials Science (IEMS), University of Shanghai for Science and Technology, Shanghai 200093, China.

[*]**Correspondence to:** Dr. Haoxuan Liu, Prof. Aruuhan Bayaguud, Department of Materials Science and Engineering, Inner Mongolia University of Technology, Hohhot 010051, China. E-mail: liuhx@imut.edu.cn; jinaruhan@imut.edu.cn; Prof. Chao Wu, Institute of Energy Materials Science (IEMS), University of Shanghai for Science and Technology, Shanghai 200093, China. E-mail: chaowu@usst.edu.cn

INTRODUCTION

Lithium-ion batteries (LIBs) have played a vital role in meeting the urgent demand for efficient and sustainable energy storage. Since their commercialization in the 1990s, LIBs have dominated the rechargeable battery market due to their high energy density, long cycle life, and negligible memory effects, enabling the widespread adoption of portable electronic devices and electric vehicles[1,2]. However, conventional graphite anodes are constrained by a limited theoretical specific capacity of 372 mAh g^{-1}, making it difficult to meet the demands of next-generation high-energy-density batteries and driving the development of advanced anode materials with higher energy/power density[3-5]. In this context, Si anodes, with a theoretical capacity of 3,579 mAh g^{-1} and a low operating potential (0.1-0.5 V *vs.* Li/Li^+), have emerged as promising candidates to overcome the energy density limitations of current LIBs[6-8]. However, the drastic volume expansion of Si (~ 300%-400%) during lithiation/delithiation not only causes mechanical pulverization of electrodes and detachment of active material from the current collector but also induces continuous regeneration of the solid electrolyte interphase (SEI). This interfacial instability results in irreversible consumption of active Li^+ ions and electrolyte, increased interfacial impedance, and reduced Coulombic efficiency (CE), ultimately limiting the cycle life of Si-based LIBs (typically less than 100 cycles)[11-15]. Therefore, mitigating the volume expansion of Si anodes and the associated interfacial instability remains a central challenge for practical Si-based anodes.

To address these challenges, current strategies could be broadly classified into three categories: (1) structural design of Si-based anodes to accommodate the volume expansion[16-18]; (2) binder functionalization to improve the electrode integrity[19-21]; (3) electrolyte engineering to regulate the SEI layer[22-24]. Compared with the first two strategies, electrolyte engineering offers a direct and chemically tunable route to improving the interfacial stability of next-generation Si anodes[25]. Although numerous electrolyte engineering strategies have been developed to construct a robust SEI on graphite anodes, they could not be directly transferred to the Si-based anode because of the low lithiation potential and large volume fluctuation of Si. The low operating potential promotes the reduction of solvent molecules, leading to the formation of a fragile organic-rich SEI, such as $ROCO_2Li$ species. Meanwhile, the drastic volume expansion of Si imposes mechanical stresses on this organic-rich SEI, exposing fresh Si surfaces and triggering continuous electrolyte decomposition, thereby producing a spatially heterogeneous and mechanically unstable interphase[26-30]. During delithiation, the Si particles undergo volume contraction, creating voids between the Si surface and the pre-existing SEI. Upon subsequent lithiation, additional SEI continuously forms to fill these void regions[31]. As a result, SEI growth persists rather than reaching a steady state during repeated cycling. Such uncontrolled SEI accumulation progressively depletes the electrolyte, consumes Li^+ ions, and thus accelerates the capacity fading and calendar aging. In addition, the accumulated SEI fragments may promote localized current distribution and facilitate the nucleation and growth of Li dendrites, raising safety concerns. Those thickened SEIs can also increase the desolvation barrier and interfacial resistance, thereby impeding the transport kinetics of Li^+ ions[32]. Thus, rationally tailoring the chemical and physical properties of the SEI on Si anodes is crucial for achieving safe, long-lifespan, and high-energy-density LIBs.

Recently, extensive efforts have been devoted to addressing these interfacial challenges of Si anodes through electrolyte engineering, including the design of novel solvents and salts, the introduction of functional additives, and the development of electrolyte systems, such as high-concentration electrolytes (HCEs) and localized high-concentration electrolyte (LHCEs)[22-24,33,34]. Herein, this review systematically summarizes the electrolyte engineering strategies for regulating the SEI formation on Si anodes from the perspective of functional electrolyte components. Specifically, we first introduce the formation mechanisms and the requirements of the SEI on Si anodes, followed by a comprehensive discussion of current electrolyte engineering strategies from two perspectives, i.e., supporting components and sacrificial components, with particular emphasis on their roles in regulating interfacial reaction pathways and tailoring solvation

structures. Furthermore, insights from advanced electrolyte engineering on lithium metal anodes (LMAs) and Si/C composite anodes are discussed to inspire new approaches for addressing the intrinsic challenges of Si anodes. Finally, future research directions are outlined to guide the rational design of electrolyte engineering for high-performance and long-lifespan Si-based LIBs.

SEI ON SI ANODES

Formation Mechanisms and Functional Roles of SEI

The stability of the electrode-electrolyte interphase [EEI, including the SEI and cathode-electrolyte interphase (CEI)] is critical for governing the electrochemical stability window (ESW) and battery cycle life[35-37]. In lithium batteries, SEI formation on the anode surface is inevitable because of the intrinsically low chemical potential of the anode. In a pioneering study, the surface passivation of the Li metal upon immersion in organic electrolytes was first reported by A.N. Dey in 1977[38]. Two years later, Peled introduced the concept of SEI and proposed its fundamental characteristics, namely electronic insulation coupled with lithium-ion conductivity[39]. Subsequently, Li_2CO_3 and lithium alkyl carbonates were identified as major SEI components derived from electrolyte decomposition[40,41]. Further, extensive studies revealed that the compact inner layer of SEI is rich in inorganic species, such as LiF and Li_2O, whereas the porous outer layer mainly consists of organic compounds, laying the foundation for the bi-layer SEI structure proposed in the early 1990s[42-46]. Meanwhile, Li^+-solvent co-intercalation into graphite was found to induce the formation of a protective surface layer that suppresses further solvent co-intercalation[47]. Based on these foundational studies, Peled proposed the mosaic SEI model in which organic and inorganic species are heterogeneously distributed throughout the interphase[48]. Furthermore, it was recognized that solvents play a decisive role in determining the chemical composition of the SEI species. For instance, lithium alkoxide (ROLi) and lithium carboxylates (RCOOLi) were predominant in SEIs formed in solvents such as tetrahydrofuran (THF), ethylene glycol dimethyl ether (DME), and methyl formate, whereas Li_2CO_3, Li dicarbonates [$(ROCO_2Li)_2$], and semicarbonates ($ROCO_2Li$) are the main products in carbonate-based electrolytes[49-51].

In 2010, Goodenough *et al.* proposed a detailed mechanistic framework for SEI formation based on frontier orbital theory[52]. According to this theory, when the chemical potential of the anode (μA) exceeds the lowest unoccupied molecular orbital (LUMO) energy level of the electrolyte, electrons spontaneously transfer from the anode to electrolyte molecules, triggering reductive decomposition and SEI formation. Figure 1A summarizes the evolution of SEI formation theories and highlights key advances in understanding the interfacial stability of Si anodes. With an improved understanding of electrolyte solvation, researchers have gradually recognized that the solvation structure of Li^+ plays a decisive role in governing the dynamic process of SEI formation. As illustrated in Figure 1B, Li^+ migrates through the electrolyte as solvated coordination complexes, where it is coordinated by surrounding solvent molecules [e.g., ethylene carbonate (EC), dimethyl carbonate (DMC)] and anions (e.g., PF_6^-) to form a solvation sheath. Upon approaching the electrode surface, these solvated Li^+ complexes first enter the outer Helmholtz plane (OHP) under the influence of the interfacial electric field[53]. Upon entering the inner Helmholtz plane (IHP), which is much thinner (≈ 0.5 nm) than the solvation sheath, Li^+ must partially or completely shed coordinated species before entering the electrode as a free ion. This desolvation process requires overcoming a substantial energy barrier and is generally regarded as a rate-determining step for Li^+ ion deposition/intercalation[54,54]. Incomplete desolvation promotes preferential decomposition of solvents or anions in the first solvation sheath of Li^+ at the electrode surface, contributing to SEI formation[56]. Under ideal conditions, SEI formation gradually reaches a dynamic equilibrium within the ESW[57]. Its electronically insulating nature further suppresses continuous electrolyte reactions by preventing electron transport, whereas its ion-conductive nature maintains Li^+ ion transport across the interphase, enabling stable electrode reactions[58,59]. The chemical stability and mechanical properties of SEI directly affect active-material utilization and interfacial resistance

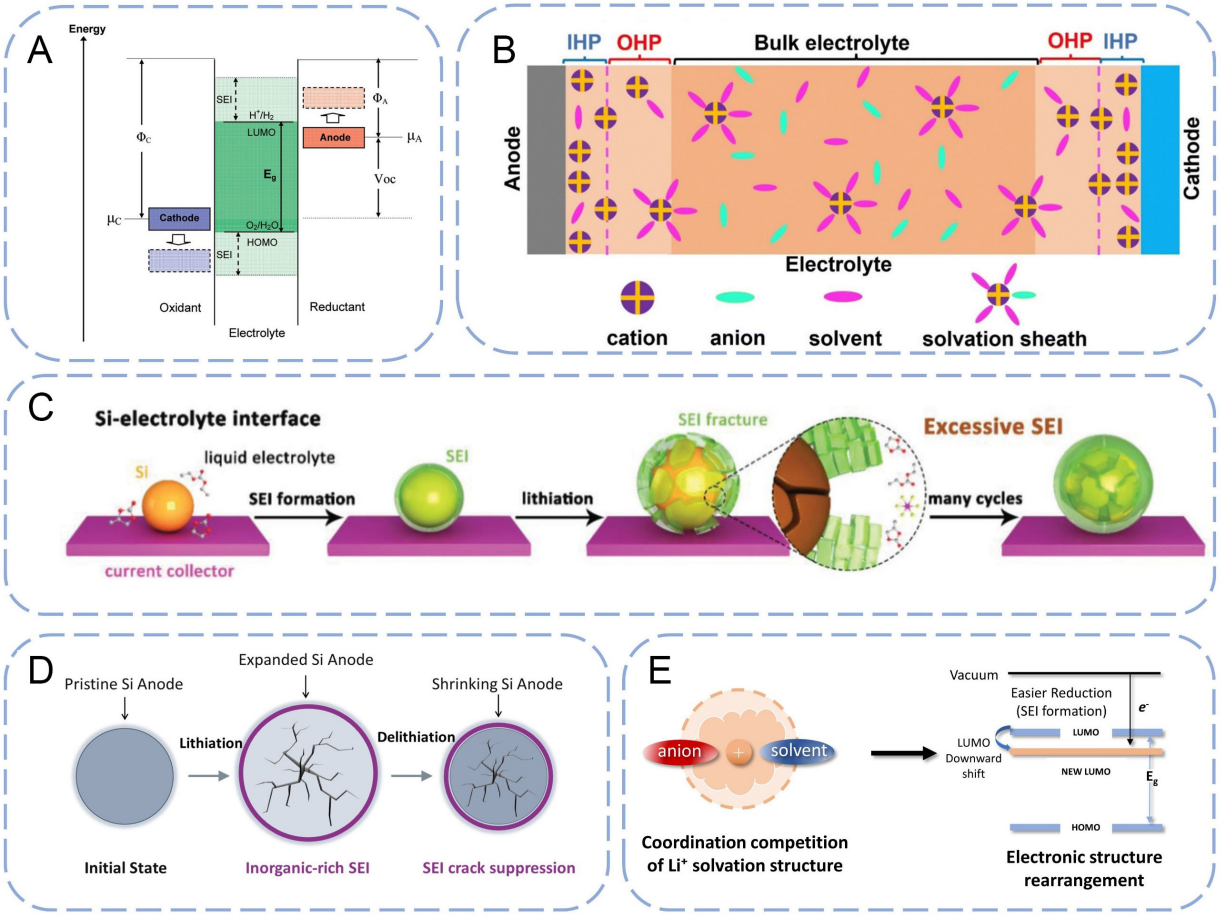

Figure 1. (A) The electrolyte open-circuit energy diagram. ΦA and ΦC represent the work functions of the anode and cathode; Eg indicates the thermodynamic stability window of the electrolyte; μA and μC denote the redox potentials of the anode and cathode; Figure 1A is reprinted with permission from Ref.[52]. Copyright © 2019 American Chemical Society; (B) Schematic showing the spatial redistribution of ions and solvent molecules during cycling; Figure 1B is reprinted with permission from Ref.[56]. Copyright © 2019 Copyright 2023 Royal Society of Chemistry; (C) Cycling failure due to SEI fracture, repeated growth, and electrolyte depletion at the Si-electrolyte interphase; Figure 1C is reprinted with permission from Ref.[61]. Copyright © 2022 Wiley; (D) Schematic diagram of the volume expansion of a rigid inorganic SEI film during lithiation/delithiation of the Si anode; (E) Influence of solvation-structure design on reduction potential. SEI: Solid electrolyte interphase; LUMO: lowest unoccupied molecular orbital; IHP: inner Helmholtz plane; OHP: outer Helmholtz plane.

during cycling, thereby underpinning the long-term stability of LIBs.

Requirements for SEI on Si anodes

During practical charge/discharge cycling, an unstable SEI cannot withstand the drastic volume expansion of the Si anode associated with Li-Si alloying, thus leading to rapid capacity fading [Figure 1C]. In detail, the initially formed unstable SEI undergoes continuous thickening, leading to active lithium loss and increased resistance to Li^+ transport. Meanwhile, the mechanically fragile SEI repeatedly fractures because of the drastic volume changes associated with the Li-Si alloy reaction, exposing fresh Si surfaces to the electrolyte. This repeated exposure continuously consumes Li^+ and electrolyte, thereby driving a self-accelerating interfacial deterioration process[60-62]. Besides, surface hydroxyl groups (-OH) on the native oxide (e.g., SiO_2) layer can further complicate the chemical composition of the SEI on Si anodes[63,64]. Thus, unlike the relatively intact bilayer SEI structure formed on the graphite anodes, the SEI on Si anodes is generally thicker, more heterogeneous, and chemically more complex[65,66].

Early investigations by Choi *et al.* revealed that the SEI formed on Si comprises metastable linear alkyl carbonates [e.g., Si-O-$CH_2CH_2OCO_2Li$, Si-$CH_2CH_2OCO_2Li$, and $R(OCO_2Li)_2$] derived from EC decomposition[67]. Subsequently, Parimalam *et al.* demonstrated that the SEI on thin-film Si continuously evolves through the reductive decomposition of anions and organic solvents, producing primary components such as Li_2CO_3, lithium alkyl carbonates, LiF, and Li_xPF_y[68]. Conversely, Chan *et al.* proposed that SEI formation was voltage-dependent, and that its composition, dominated by Li_2CO_3 and LiF, becomes relatively stable after the initial cycle[69]. However, subsequent studies have shown that the SEI is a dynamic interphase that continuously evolves during cycling because of the repeated volume changes of Si[70-73]. Additionally, for carbon-coated Si, Yen *et al.* identified siloxanes rather than fluorides as the dominant interfacial species[74]. Fundamentally, although the SEI formed on pristine, oxidized, or carbon-coated Si exhibits similar morphological characteristics, its chemical composition varies considerably because of the distinct interfacial reactions between different surface chemistries and electrolyte components. Using depth-profiling analysis, Philippe *et al.* identified Li_2O and Li_4SiO_4 together with lithiated Li_xSi_y phase(s) and unreacted Si during the first cycle on SiO_2-coated Si/C electrodes[75]. Li_2O was found to increase progressively during lithiation, resulting in a mixed interfacial region composed of Li_2O, Li_xSiO_y, and SiO_2. Based on similar observations, Cao *et al.*[76,77] and Kumar *et al.*[78,79] further proposed a bilayer SEI model consisting of a porous, compliant organic outer layer, rich in alkyl carbonates, alkyl bicarbonates, and ROLi, and a mechanically robust inorganic inner layer, containing LiF, Li_2CO_3, Li_2O, Li_4SiO_4, and SiO_xF_y. Furthermore, the mechanical and electrochemical properties of this bilayer are thickness-dependent. The organic outer layer generally exhibits higher resistance, whereas the inorganic inner layer provides efficient Li^+ transport pathways while maintaining mechanical integrity.

Thus, constructing an SEI with high mechanical strength to withstand the drastic volume changes of Si while maintaining high Li^+ ionic conductivity is a primary challenge for Si anodes. Currently, inorganic components, such as LiF and Li_2O, have been demonstrated to effectively protect Si electrodes, with LiF exhibiting higher electronic resistivity than Li_2O[23,80]. These inorganic species exhibit low solubility in conventional electrolytes, enabling the formation of stable and mechanically robust interphases [Figure 1D]. Moreover, their high Young's modulus enables effective stress redistribution, thereby buffering the mechanical stress induced by Si volume changes and suppressing crack initiation and propagation[81,82]. Recently, Xu *et al.* employed a pulse electrochemical activation strategy to construct a multilayer fine-grained SEI containing uniformly distributed inorganic particles (e.g., LiF, Li_3N)[83]. The resulting SEI exhibited a high Young's modulus of 12.5 GPa, thereby effectively mitigating the volume expansion of Si anodes while maintaining fast ion transport kinetics[83]. In addition, theoretical calculations revealed that LiF and Li_2O exhibit high interfacial energies (E_{int}) with Si substrates, thus enabling these inorganic domains to accommodate the drastic volume changes in Si microparticles (SiMPs) with lower interfacial stress[84]. Importantly, the inorganic-rich layer functions as an electron-blocking barrier (electronic conductivity < 10^{-10} S m^{-1}), effectively suppressing continuous electrolyte reduction and minimizing parasitic reactions[85,86]. In a recent study, Zhang *et al.* employed potentiostatic aging tests to reveal that both calendar and cycle degradation are governed by the coupled effects of SEI cracking and dissolution, although their relative contributions differ[87]. When SEI dissolution is not the dominant degradation pathway, a positive correlation exists between the calendar and cycle life of Si anodes. LiF-rich SEIs, which effectively suppress SEI cracking and dissolution, are expected to simultaneously improve the cycling stability and calendar life of μ-Si anodes. This prediction was further validated by full-cell test results, which demonstrated that LiF-rich SEIs effectively suppress cracking and dissolution, thereby significantly extending the calendar life of μ-Si[88]. In contrast, nano-silicon is more susceptible to SEI dissolution due to its larger electrode-electrolyte interfacial area, thereby necessitating the effective suppression of interfacial side reactions to improve stability. Ultimately, these findings provide insights into the mechanisms of calendar aging and guide the design of robust electrolytes for durable Si anodes[87,89].

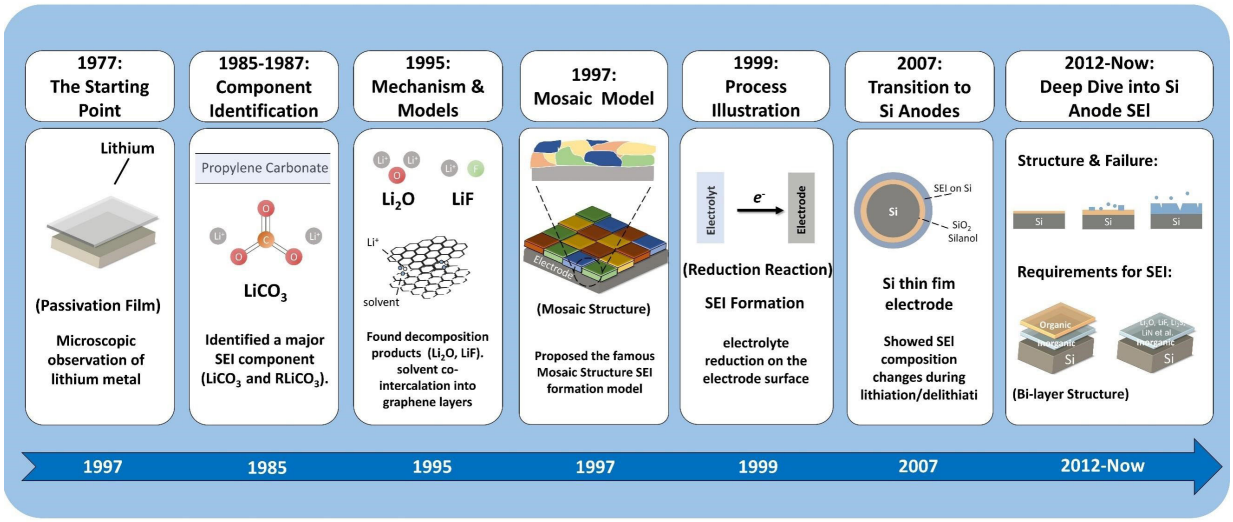

Figure 2. SEI formation on Si anode research historical chronicles (1977-Now). SEI: Solid electrolyte interphase.

Beyond electrolyte engineering, the chemical composition of the SEI is influenced by the morphology and composition of the Si surface. Unlike graphite, Si is inherently covered by a native oxide film (SiO_x) with oxygen-terminated dangling bonds, which alters the SEI formation pathway[28]. Numerous studies have shown that the nanometric SEI (1-100 nm) on Si, is a complex and heterogeneous interphase. The SEI generally consists of an outer organic layer with alkyl carbonates/ROLi and an inner inorganic layer dominated by Li_2O, Li_2CO_3, and LiF[90-92]. This bilayer SEI structure, featuring organic phases adjacent to the electrolyte and inorganic phases adjacent to the electrode, has been corroborated by diverse ex-situ techniques, including scanning force spectroscopy, atomic force microscopy, time-of-flight secondary ion mass spectrometry (TOF-SIMS), and X-ray photoelectron spectroscopy (XPS)[93].

Finally, Figure 2 shows the evolution of SEI research, from fundamental formation mechanisms to structural regulation on Si anodes. However, the composition and architecture of SEI are dynamic and strongly influenced by electrolyte solvents and salts[28]. Additionally, electrolyte additives and surface functionalization have both proven effective in enhancing the stability and electrochemical performance of Si anodes. SEI formation on Si anodes is governed by the synergistic effects of salts, solvents, additives, surface chemistry, and operating conditions. These factors determine the reduction pathways of electrolyte components and the stability of the resulting SEI layer [Figure 1E]. Building upon recent advances in electrolyte engineering for Si anodes, this review categorizes electrolyte components into supporting and sacrificial components and systematically discusses their mechanisms and design principles that govern SEI formation. Finally, advanced electrolyte engineering strategies developed for LMAs and Si/C composites are discussed to provide new insights into addressing the stability challenges of Si anodes.

SUPPORTING COMPONENTS

Supporting components are the bulk matrix of the electrolyte, of which the primary functions are to dissolve lithium salts and provide ion-transport pathways. Within the operating voltage window, supporting components should exhibit relatively high electrochemical stability, allowing them to serve as long-term carriers and frameworks for ion conduction[56,94]. Therefore, solvents are generally regarded as the supporting components.

Solvation ability and SEI formation

In electrolyte engineering for LIBs, the solvation chemistry of Li^+ ions is primarily governed by cation-solvent and cation-anion interactions, which can be classified as strong or weak solvation. In strong solvating electrolytes (SSEs), the cation-solvent interaction is significantly stronger than the cation-anion interaction[95]. Conversely, a weak solvating electrolyte (WSE) is characterized by relatively weak cation-solvent interactions that are comparable to, or weaker than, cation-anion interactions. While no strict criteria or absolute thresholds have been established to distinguish these categories, key parameters, such as the dielectric constant and donor/acceptor numbers, are widely used to evaluate the solvating capability of the solvents[56].

The dielectric constant (DC), defined as the ratio of the permittivity of a material to that of a vacuum, is a key descriptor of solvent polarity and its ability to promote lithium salt ionization and dissociation. Within a given electrolyte system, a higher solvent DC strengthens cation-solvent interactions, thereby promoting salt dissociation and increasing the concentration of mobile ions. Typically, cyclic carbonates exhibit significantly higher DCs than linear carbonates or ethers[96]. However, a high DC is often accompanied by high viscosity, which in turn impedes Li^+ transport. To balance these properties, electrolyte formulations usually employ a cosolvent strategy by combining high-DC solvents with low-viscosity diluents. In contrast, the Gutmann Donor Number (DN) quantifies the Lewis basicity of a solvent and is defined from the enthalpy of its reaction with antimonic(V) chloride in 1,2-dichloroethane. Salt dissociation is favored when the DN of the solvent exceeds that of the anion, owing to the stronger Lewis acid-base interaction between the cation and solvent. For instance, $LiNO_3$ is sparingly soluble in carbonates but dissolves readily in high-DN ethers[97]. Consequently, tailoring the DN represents an effective strategy for regulating solvation chemistry of electrolytes. It should be noted that neither DN nor DC accounts for steric hindrance or denticity and thus cannot fully describe the solvating ability. Thus, recent advances in theoretical calculations and characterization techniques have enabled a more comprehensive evaluation of solvating ability [Figure 3A-C][98,99], including descriptors such as the relative solvating power[100-102], surface electrostatic potential[103], binding energy between different components[103], positive maximum of the electrostatic potential energy[104], and the negative center of electrostatic potential[105].

The descriptors discussed above are widely used to evaluate the solvating ability of solvents and the strength of cation-solvent and cation-anion interactions. Due to its small ionic radius and strong Lewis acidity, Li^+ forms strong electrostatic interactions with simple anions in compounds such as LiF, Li_2O, and Li_2CO_3, resulting in poor solubility within organic media and precluding their use as electrolyte salts[94]. Consequently, only a limited number of lithium compounds can be used as lithium salts, including lithium hexafluorophosphate ($LiPF_6$), lithium tetrafluoroborate ($LiBF_4$), lithium bis(fluorosulfonyl)imide (LiFSI), lithium bis(trifluoromethylsulphonyl)imide (LiTFSI), lithium bis(oxalate) borate (LiBOB), lithium difluoro(oxalato)borate (LiDFOB), lithium difluorophosphate (LiDFP), lithium nitrate ($LiNO_3$), and related derivatives. Among these lithium salts, the binding energy between the cation and anion is non-uniform and depends on the specific chemical nature of the anion.

When anions (e.g., FSI^-, PF_6^-) enter the first solvation sheath of Li^+, they tend to undergo preferential reduction at the anode surface owing to their lower LUMO levels, ultimately forming inorganic SEI components (e.g., LiF, Li_2O)[106,107]. In contrast, solvent-dominated coordination (e.g., EC) promotes the formation of an organic-rich SEI, which provides greater flexibility but insufficient mechanical strength, often leading to crack propagation[108, 109]. Therefore, precisely designing electrolyte components with different solvating abilities to tailor the first solvation sheath of Li^+ ions is an effective way to regulate the chemical and physical properties of the SEI to accommodate the harsh operating conditions on Si anodes.

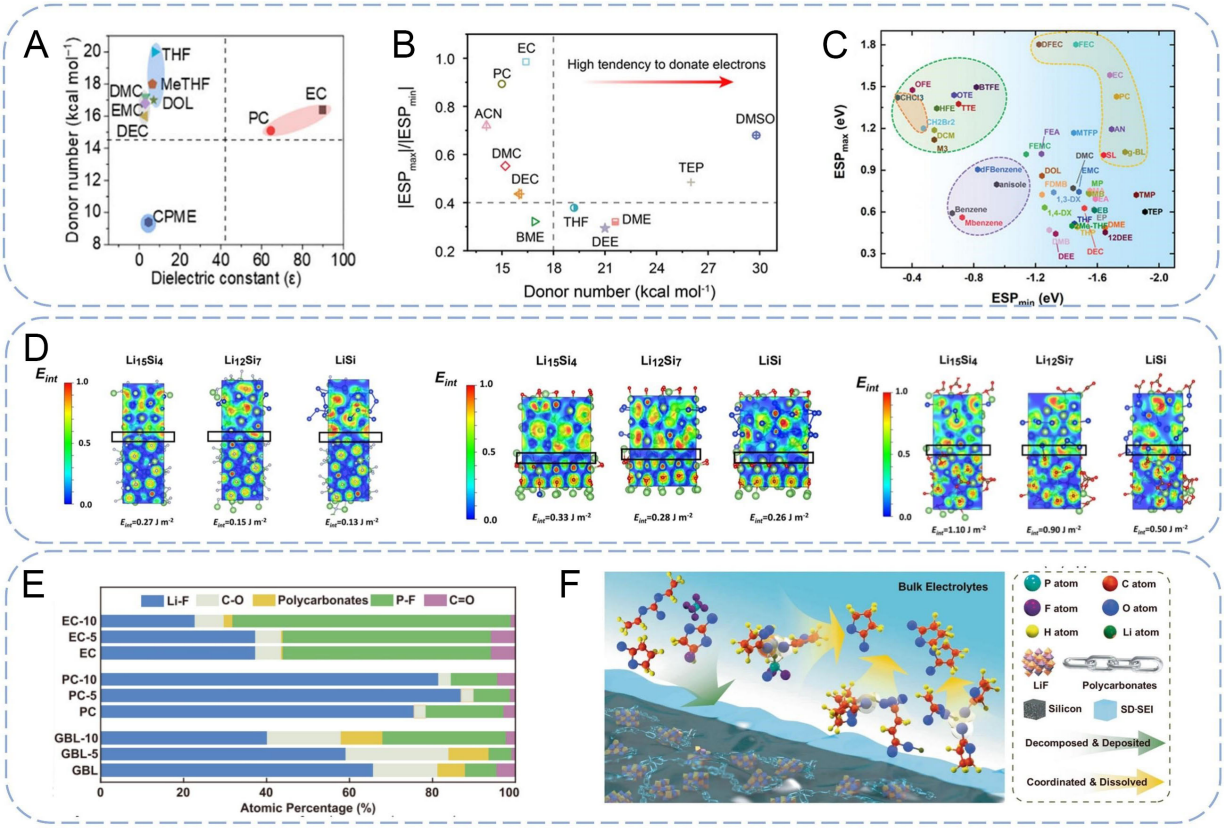

Figure 3. (A) Dielectric constant and donor number comparison of various solvents; Figure 3A is reprinted with permission from Ref.[98]. Copyright © 2026 Wiley, under CC BY 4.0 license; (B) Solvent criteria are based on donor number and the $|ESP_{max}|/|ESP_{min}|$ ratio; Figure 3B is reprinted with permission from Ref.[99]. Copyright © 2025 Wiley; (C) ESP of various solvents calculated via density functional theory under vacuum; Figure 3C is reprinted with permission from Ref.[103]. Copyright © 2023 Wiley; (D) Electron-localized function and E_{int} between Li_xSi ($Li_{15}Si_4$, $Li_{12}Si_7$, and LiSi) alloys and major SEI components (Left: LiF. Center: Li_2O. Right: Li_2CO_3); Figure 3D is reprinted with permission from Ref.[84]. Copyright © 2024 Springer Nature; (E) MALDI-TOF-MS profiling of SEI component distribution as a function of depth; (F) Schematic of the formation process of SD-SEI in the GBL-based electrolyte; Figure 3E and F are reprinted with permission from Ref.[112]. Copyright © 2023 Springer Nature. THF: Tetrahydrofuran; DMC: dimethyl carbonate; EMC: ethyl methyl carbonate; DEC: diethyl carbonate; DOL: 1,3-dioxolane; EC: ethylene carbonate; PC: propylene carbonate; CPME: cyclopentyl methyl ether; ACN: acetonitrile; BME: 1,2-dimethoxyethane; DEE: 1,2-diethoxyethane; DME: ethylene glycol dimethyl ether; TEP: triethyl phosphate; DMSO: dimethyl sulfoxide; OFE: 1,1,2,2-Tetrafluoroethyl ether; OTE: 1,1,2,2-Tetrafluoroethyl-2,2,2-trifluoroethyl ether; HFE: 2,2,3,3-tetrafluoropropyl ether; TTE: 1,1,2,2-tetrafluoroethyl-2,2,3,3-tetrafluoropropyl ether; DCM: dichloromethane; DFEC: difluoroethylene carbonat; DEC: diethyl carbonate; AN: acetonitrile; SL: sulfolane; g-BL: γ-butyrolactone; FEA: fluoroethyl acetate; FEMC: methyl 2,2,2-trifluoroethyl carbonate; MTFP: methyl trifluoropropyl ether; FDMB: fluoro-1,3-dimethoxybenzene; MP: methyl propionate; MB: methyl butyrate; MA: methyl acetate; TMP: trimethyl phosphate; DMB: dimethoxybutane; DX: 1,3-dioxane; SD-SEI: solvent-derived solid electrolyte interphase.

Strong solvating electrolytes

Strongly solvating solvents typically possess cyclic structures with high DC values, such as cyclic carbonates [e.g., EC, propylene carbonate (PC)], cyclic carboxylates [e.g., γ-butyrolactone (GBL)], and cyclic sulfonates [e.g., 1,3-propane sultone (PS), sulfolane (SL)][110-113]. The cyclic structures enable the dipole moments of the polar bonds to align synergistically, resulting in a markedly enhanced net molecular dipole and superior solvating ability[94]. These solvents possess delocalized intramolecular polarity and strongly coordinate with Li^+ via intense dipole-ion interactions, thereby effectively excluding anions from the first solvation sheath and limiting their contribution to interfacial reactions[114,115]. Strong solvating electrolyte formulations often achieve high ion-transport efficiency because of reduced Li^+ diffusion activation energy resulting from solvent-dominated solvation structures[116].

For instance, at the low potentials, the reduction of EC or PC predominantly proceeds via a one-electron pathway. In this process, the reduced solvent molecule reacts with another radical anion to form alkyl

carbonates [$ROCO_2Li$, $(CH_2OCO_2Li)_2$][58]. At higher potentials, the reduction mechanism shifts to a two-electron reduction process, in which the solvent molecule interacts either directly with a Li^+ to generate inorganic lithium carbonate or with a Li-coordinated solvent molecule to form alkyl carbonates[117,118]. Extensive research has been reported on the decomposition of EC on Si surfaces, with Shin *et al.* comprehensively summarizing the underlying elementary reaction steps in 2017[119]. The process is initiated by the ring-opening of EC, generating alkyl carbonate radical anions[120-122]. These anions subsequently dimerize to form lithium ethylene dicarbonate (LEDC) accompanied by the release of ethylene gas[123-125]. Fourier-transform infrared spectroscopy (FTIR), nuclear magnetic resonance spectroscopy (NMR), and XPS analyses consistently identified LEDC as a component of the outer layer of the SEI[126-128]. However, as LEDC migrates toward the reactive Si/silicide interface, it undergoes further electrochemical or chemical decomposition into inorganic compounds such as CO_2, Li-oxalate, Li_2CO_3, and Li-alkoxides[129-131]. Beyond the formation of LEDC, the alkyl carbonate radical anion can participate in nucleophilic attacks on unreacted EC molecules or decompose to release ethylene. The former pathway generates a radical-terminated linear carbonate ethylene oxide, which polymerizes into long-chain PEO-based polymers. The latter pathway produces ethylene oxide radicals, which trigger secondary nucleophilic attacks and subsequent polymerization[132]. Concurrently, during the formation of additional PEO-based polymers, CO_2 is reduced to $LiCO_2$ radicals, which abstract hydrogen to form lithium formate ($LiCO_2H$)[133,134]. In the presence of linear carbonates such as DMC, EC-derived radicals[135] or oligomers[136] can also nucleophilically attack DMC to form additional PEO-type polymers[121]. The relative proportions of oligomers and polymers depend on the polymerization rate. Crucially, a stable SEI requires a composition dominated by polymers rather than oligomers or other small molecules. Small molecules (oligomers) are highly soluble, thereby forming a thicker and less dense SEI that becomes more permeable to the electrolyte and promotes further electrolyte decomposition[119].

Li *et al.* demonstrated that SL molecules dominate the first solvation sheath of Li^+ in the fluoroethylene carbonate (FEC)/SL/1,1,2,2-tetrafluoroethyl-2,2,3,3-tetrafluoropropyl ether (TTE) electrolyte (FST), thereby promoting the formation of a Li_2O-rich SEI with fewer organic species[84]. SL is a highly polar aprotic solvent with a dielectric constant of 43.4 at 303.2 K. Density functional theory (DFT) calculations revealed that SL coordinated with two Li^+ ions is reduced at 1.3-2 V *vs.* Li/Li^+, forming Li_2O. This reduction potential overlaps with that for LiF formation via the reduction of FEC and TTE[84,137]. Combined with LiF derived from FEC reduction, the LiF/Li_2O-rich SEI exhibited pronounced Si-phobic characteristics [Figure 3D], where the high interfacial energy and weak adhesion toward Li_xSi alloys enabled SiMPs to expand and contract within the SEI layer, thereby significantly extending cycling life. Notably, pouch cells employing the FST electrolyte retained a capacity of 172 mAh g^{-1} after 120 cycles at 0.2 C. As oligomeric, low-modulus SEI components generally provide limited mechanical durability for Si anodes[138,139]. Tian *et al.* introduced a selective dissolution strategy using the high-DN solvent GBL to remove mechanically weak SEI species such as lithium ethylene dicarbonate, lithium fluorophosphates, and various oligomers, while retaining LiF and elastic polycarbonates[112]. Compared with the fragile SEI typically formed in EC- or PC-based electrolytes, this strategy produced a robust inorganic-polymer hybrid SEI [Figure 3E] capable of accommodating the drastic volume changes of micron-sized Si anodes, thereby enhancing cycling performance [Figure 3F].

Although strongly solvating electrolytes are characterized by high ionic conductivity, SEI formation on Si anodes primarily relies on the reduction of coordinated solvent molecules, inevitably leading to an organic-rich SEI with a heterogeneous interfacial structure. The resulting SEI exhibits poor mechanical robustness, high internal resistance, and limited ability to suppress dendrite growth or accommodate drastic volume changes[140,141]. To overcome these limitations, sacrificial additives have been introduced to construct a more robust and compatible interphase. By synergistically optimizing the solvation sheath structure and the decomposition pathways of sacrificial additives, the kinetics of SEI formation can be precisely regulated

without compromising the intrinsically high ionic conductivity of the electrolyte. The mechanisms will be discussed in the **SACRIFICIAL COMPONENTS** section.

Weak solvating electrolytes

By modulating the competitive binding energetics between Li^+-solvent and Li^+-anion interactions, WSEs exhibit distinct desolvation behaviors and unique solvation motifs, such as contact ion pairs (CIPs) and aggregates (AGGs). This unique solvation chemistry endows WSEs with superior compatibility, enhanced oxidation stability, and excellent adaptability to extreme temperature conditions. To regulate relative binding energy, three primary strategies are generally employed: increasing salt concentration, utilizing solvents with lower Li^+ affinity, and selecting anions with stronger binding capability. In WSE systems, anions displace solvent molecules from the first solvation sheath, thereby promoting the formation of CIPs and AGGs. Because the components within the first solvation sheath dictate the interfacial reaction pathways, their preferential decomposition leads to anion-derived, inorganic-rich SEI and CEI layers. These inorganic-rich electrode-electrolyte interphases exhibit high mechanical robustness, favorable interfacial stability, and improved ionic conductivity at high cut-off voltages[142]. A representative example is LiF, which, owing to its wide bandgap (8.9 eV), high shear modulus (48.6 GPa), and excellent anodic stability (> 6.5 V *vs.* Li^+), significantly enhances compatibility with both Li metal and high-voltage cathodes. Furthermore, when paired with low-viscosity solvents possessing wide liquid-temperature ranges, WSEs ensure reliable electrochemical performance over a broad temperature spectrum[143,144].

Reducing the polarity of solvents is an effective strategy for constructing weakly solvating electrolytes[145]. This can be achieved by selecting low-polarity solvents or attenuating polarity via molecular engineering, both of which weaken the Li^+-solvent interaction. As the coordination strength of Li^+ with solvent molecules decreases, the interaction between Li^+ and anions correspondingly strengthens. Consequently, more anions enter the first solvation sheath, giving rise to solvation structures dominated by CIPs and AGGs, thereby promoting the formation of an anion-derived SEI. Weakly coordinating solvents, such as ethers [e.g., 1,2-diethoxyethane (DEE), THF, DME] and linear esters (e.g., DMC, EMC), promote the formation of more CIPs and three-dimensional ionic AGGs through enhanced Coulombic interactions[146,147]. For example, Chen *et al.* formulated high-concentration electrolytes using weakly solvating cyclic ethers, including 2.0 M $LiPF_6$ in THF and 2-methyltetrahydrofuran (MTHF), which generated a robust SEI with low adhesion toward Li_xSi and sufficient elasticity to accommodate drastic volume changes[148]. Compared with conventional carbonate electrolytes (EC-DMC, 1:1), this electrolyte exhibited a significantly higher CIP fraction (87% *vs.* 38%), promoting AGG formation that further facilitated early LiF deposition and suppressed solvent decomposition, ultimately leading to a thinner LiF-organic bilayer SEI. When paired with SiMP anodes, this electrolyte delivered an initial capacity of 2,800 mAh g^{-1}, an initial Coulombic efficiency (ICE) > 90%, and a cycling CE > 99.9%.

Moreover, owing to the greater steric hindrance introduced by ethoxy groups relative to methoxy groups, DEE exhibits weaker solvation capacity than DME[149]. Liu *et al.* developed a dual-solvent electrolyte consisting of 3 M $LiPF_6$ in 1,3-dioxane (DX) and DEE, taking advantage of the ability of DX to dissolve $LiPF_6$ without self-polymerization[22]. This electrolyte constructed a mechanically durable SEI, in which the polymer-rich outer layer effectively encapsulated fractured Si particles, while the inorganic-rich inner layer promoted ionic transport and suppressed interfacial side reactions[22]. In addition, the higher CIP population arising from the combined effects of concentrated $LiPF_6$ and weakly solvating solvents enhanced oxidative stability [Figure 3G]. When paired with micrometer-sized Si anode material recovered from photovoltaic waste, the electrolyte retained 83.13% of its initial capacity after 200 cycles, together with an average CE of 99.94%. Similarly, a LiFSI/DEE electrolyte containing vinylene carbonate (VC) additive enabled the construction of a gradient SEI, in which inorganic species (e.g., LiF) gradually decreased while the polymeric

components [e.g., poly (VC)] progressively increased from the Si interface outward the electrolyte[150]. Specifically, due to the weak solvating ability of DEE molecules, an anion-rich first solvation sheath is formed when LiFSI is dissolved in DEE. The preferential reductive decomposition of FSI^- anions promotes the formation of a dense inorganic SEI layer. Meanwhile, the incorporation of the VC additive ensures its decomposition at an appropriate potential, forming a highly polymerized outer layer. The resulting gradient inorganic-polymer SEI not only enhances mechanical rigidity and flexibility but also establishes efficient Li^+ pathways, thereby mitigating the drastic volume expansion of Si particles, preserving the structural integrity of the electrode, and improving the electrode interfacial reaction kinetics.

Although HCEs can effectively maintain high CE and excellent cathode stability during Li^+ stripping/plating, their poor wettability, low ionic conductivity, and high cost hinder their practical application in next-generation rechargeable batteries. To address these limitations, inert solvents (diluents), with low viscosity and a wide liquid-phase temperature range, have been introduced. Owing to their low polarity, these diluents cannot dissolve lithium salts but exhibit excellent miscibility with HCE solvents, making them widely applicable[151,152]. In LHCEs, the non-solvating diluent resides outside the first Li^+-solvation sheath, thereby preserving the Li^+-anion-solvent clusters. The non-solvating diluent further strengthens both Li^+-solvent interactions and Li^+-anion interactions within the solvation structure by isolating the Li^+-anion-solvent clusters[151,153].

Yang *et al.* reported a glyme-based LHCE (GlyEIs), i.e., LiFSI-3DME-3TTE, which enabled the formation of a more robust SEI on Si anodes than the fluorine-rich bilayer SEI typically formed in carbonate electrolytes[154]. The outer GlyEI-SEI layer, enriched with elastic polyethers, accommodated the stress generated during repeated Li insertion/extraction, maintaining a conformal SEI on Si and mitigating fractures of amorphous Si (a-Si). Meanwhile, the inner GlyEI-SEI layer, composed of F- and S-rich inorganic species together with reduced carbonates and silicides, reduced interfacial resistance and polarization, enhancing cycling performance. Compared with the conventional FEC additive, the Si anode cycled in the GlyEI electrolyte exhibited a 62.5% reduction in early parasitic current and a 72.8% reduction in interfacial resistance, together with more than 7% improvement in capacity retention after 110 cycles[154].

To further construct a polymer-rich outer SEI layer while avoiding the formation of oligomers generated from DME decomposition, Yang *et al.* developed a THF-based LHCE by replacing DME with THF in the LiFSI/DME/TTE electrolyte[155]. THF forms a weakly solvating structure due to its limited coordination sites [Figure 4A and B], resulting in lower desolvation energy and promoting the formation of a thinner inorganic-rich inner SEI. Additionally, THF readily undergoes polymerization to form a highly elastic outer SEI layer, which mitigates stress-induced cracking while suppressing continuous side reactions and impedance growth. Pure Si anodes cycled in this THF-based LHCE exhibited excellent rate capability, outstanding long-term cycling stability, and high reversible capacity (1,995.7 mAh g^{-1} after 400 cycles at 1 A g^{-1} in a half-cell). When paired with the graphite anodes, the electrolyte delivered stable cycling performance in full cells. The electrolyte also exhibited excellent cycling performance in both Si||$LiFePO_4$ and Gr||$LiFePO_4$ full cells.

Furthermore, Guo *et al.* formulated a high-voltage LHCE by combining TTE and diethyl carbonate (DEC) with LiFSI for Si-anode LIBs[156]. The introduction of the diluent significantly increased the probability of anions entering the first Li^+ solvation sheath. TOF-SIMS 3D reconstruction revealed that the micron-sized Si anode formed a vertically aligned columnar SEI composed of LiF-sulfide composites. This steel-reinforced-concrete-like SEI enhanced interfacial mechanical stability, thereby enabling long-term cycling of Si anodes while maintaining excellent oxidative stability when paired with nickel-rich cathodes. Meanwhile, cycling tests revealed a uniform and thin CEI layer on the NCM cathode surface. Furthermore, Si||NCM full cells

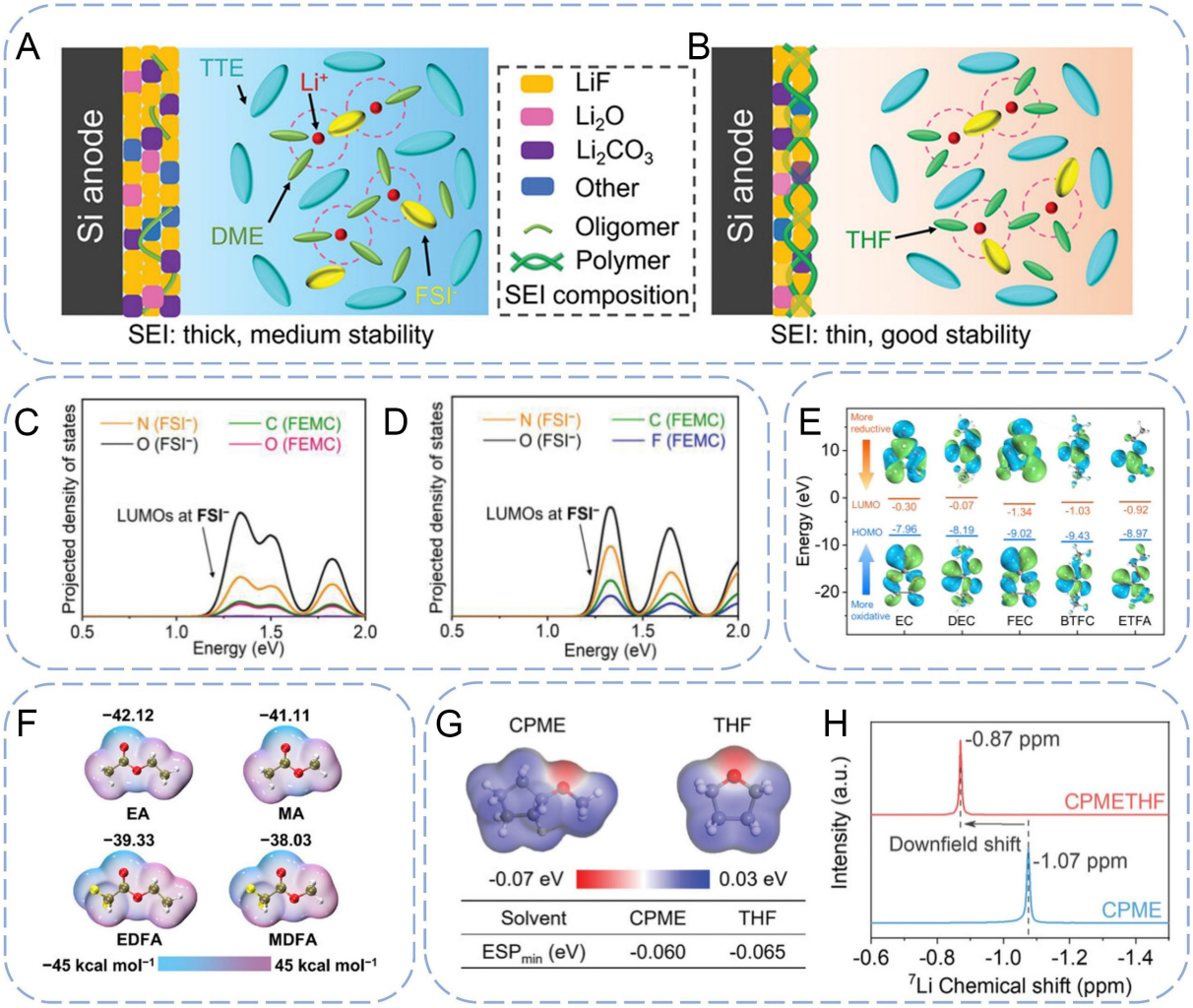

Figure 4. Schematic of SEI formation in (A) LHCE-DME-based electrolyte and (B) LHCE-THF-based electrolyte; Figure 4A and B is reprinted with permission from Ref.[155]. Copyright © 2023 Wiley; PDOS of (C) FEMC-HCE and (D) FEMC-LHCE from DFT-MD simulations; Figure 4C and D is reprinted with permission from Ref.[161]. Copyright © 2023 Wiley; (E) Frontier orbital energy levels of EC, DEC, FEC, BTFC, and ETFA solvents; Figure 4E is reprinted with permission from Ref.[164]. Copyright © 2022 American Chemical Society; (F) ESP maps of EA, MA, EDFA, and MDFA; Figure 4F is reprinted with permission from Ref.[165]. Copyright © 2025 Wiley; (G) Electrostatic potential mapping and (H) ^{7}Li NMR spectra of CPME and THF; Figure 4G and H is reprinted with permission from Ref.[24]. Copyright © 2025, Wiley. SEI: Solid electrolyte interphase; TTE: 1,1,2,2-tetrafluoroethyl-2,2,3,3-tetrafluoropropyl ether; DME: ethylene glycol dimethyl ether; FSI: fluorosulfonyl imide; THF: tetrahydrofuran; FEMC: methyl 2,2,2-trifluoroethyl carbonate; EA: ethyl acetate; MA: methyl acetate; EDFA: ethyl difluoroacetate; MDFA: methyl difluoroacetate; CPME: cyclopentyl methyl ether; ESP: electrostatic potential; LHCE: localized high-concentration electrolyte; PDOS: projected density of states; FEMC: methyl 2,2,2-trifluoroethyl carbonate; HCE: high-concentration electrolytes; DFT: density functional theory; MD: molecular dynamics; FEC: fluoroethylene carbonate; BTFC: bis(2,2,2-trifluoroethyl) carbonate; ETFA: ethyl trifluoroacetate; NMR: nuclear magnetic resonance spectroscopy.

employing the designed electrolyte delivered a high energy density (475 Wh kg^{-1}), together with excellent rate capability and stable high-voltage cycling performance.

The solvating ability of solvent molecules could also be regulated by tailoring their electronic and steric characteristics through the introduction of additional functional groups. For example, fluorine atoms, owing to their strong electron-withdrawing nature, substantially reduce the solvating ability of solvents while enhancing oxidative stability[157,158]. Kim *et al.* employed FEC to replace EC as a strategy to reduce the solvating ability of the electrolyte. Their study revealed that the lower DN and DC of FEC weakened Li^+-solvent interactions, thereby promoting the formation of a higher fraction of CIPs[159]. Furthermore, this

anion-participating solvation structure significantly improved desolvation kinetics, thereby enabling superior electrochemical performance even at high charging rates[159]. Beyond FEC, fluorination strategies based on ester solvents have also been widely explored to enhance the cycling stability of Si anodes. For example, Okada *et al.* employed highly fluorinated carbonates, i.e., methyl 2,2,2-trifluoroethyl carbonate (FEMC) as the solvent and bis(2,2,2-trifluoroethyl) carbonate (TFEC) as the diluent, to stabilize Si nanosheet anodes by forming ultrathin, compact, and LiF-rich SEI layers generated through the cooperative reduction of FSI^- anions and FEMC molecules within the first Li^+ solvation sheath[160]. Similarly, Fan *et al.* employed FEMC with LiFSI to construct a mechanically robust F-rich inorganic-organic bilayer SEI on SiMP anodes[161]. DFT-MD simulations revealed that FSI^- anions dominated the LUMO region of the conduction band, enabling their preferential reduction over FEMC to form a high-modulus inorganic SEI [Figure 4C and D]. The enhanced oxidative stability of the fluorinated solvents also enabled stable operation of 1.0 Ah-level SiMP||NMC811 pouch cells for over 200 cycles.

Fluorinated solvents with low LUMO energy levels undergo preferential reduction at the Si anode interface, thereby directing SEI formation through reductive decomposition pathways[162,163]. Cao *et al.* developed a fully fluorinated weakly solvating electrolyte consisting of 1.0 M LiFSI in a ternary mixture of FEC, bis(2,2,2-trifluoroethyl) carbonate (BTFC), and ethyl trifluoroacetate (ETFA)[164]. Computational analysis [Figure 4E] showed that FEC possesses the lowest LUMO energy (-1.34 eV), causing it to decompose first during the initial lithiation process, followed sequentially by BTFC (-1.03 eV) and ETFA (-0.92 eV). The resulting SEI, composed primarily of LiF and inorganic species, effectively suppresses continuous electrolyte decomposition.

The introduction of fluorine atoms not only reduces the solvating ability but also effectively improves low-temperature performance. For example, Gao *et al.* selected the fluorinated carboxylate ester methyl difluoroacetate (MDFA) as the solvent[165]. The electron density around the carbonyl oxygen in MDFA is significantly reduced by the combined effects of the weak electron-donating methyl groups and the strongly electron-withdrawing fluorine atoms. MDFA also exhibits a lower minimum electrostatic potential (ESP_{min}) [Figure 4F]. Consequently, the weak Li^+ affinity of MDFA results in a high proportion of CIPs and AGGs in the electrolyte. At low temperatures, the weakened Li^+-solvent interaction further strengthens the interaction between Li^+ and FSI^-. Consequently, the LiFSI/MDFA/FEC electrolyte enabled μSi||$Li_3V_2(PO_4)_3$ full cells to deliver excellent charge-discharge performance at low temperature.

Beyond fluorination, increasing steric hindrance through methyl substitution represents another effective strategy for tailoring the solvation structure. Peng *et al.* employed the ether-based solvent, ethylene glycol diethyl ether (EGDE), which exhibits strong compatibility with $LiPF_6$ and substantial steric hindrance[166]. XPS analysis of cycled Si electrodes demonstrated that the EGDE-derived electrolyte (D3) facilitated the formation of a thin, LiF-rich, and densely packed SEI, which effectively passivated the surface of Si, thereby reducing crack propagation and particle pulverization[167]. Kim *et al.* found that EGDE exhibited weaker Li^+-solvent interactions, faster charge-transfer kinetics, and lower desolvation barriers than DME and DGDE, enhancing interfacial Li^+ transport while suppressing side reactions[168]. Accordingly, they combined EGDE with LiFSI to formulate an electrolyte that increases anion accessibility by tailoring Li^+ coordination, thereby enhancing the stability of micrometer-sized Si. Operando Raman spectroscopy and MD simulations identified an anion-dominated solvation structure (78.7% as CIPs + AGGs). This unique solvation configuration attenuated the Li^+-solvent binding free energy, thereby promoting the formation of a LiF-rich inorganic SEI with improved chemo-mechanical integrity.

Similarly, Yang *et al.* developed a moderately solvated electrolyte (DPMPE/F/B) consisting of dipropylene glycol methyl propyl ether (DPMPE), 1.9 M LiFSI (base salt), 5 wt% FEC, and 0.1 M LiBOB[169]. The terminal propyl and mid-chain methyl groups of DPMPE introduce substantial steric hindrance, thereby weakening

Li^+-solvent coordination and promoting the preferential reduction of FSI^- anions, leading to the formation of inorganic SEI species. At the anode reduction potential, DPMPE undergoes molecular chain cleavage, accompanied by radicals that are triggered, thereby promoting the *in situ* formation of a highly elastic polymer within the SEI. Additionally, the boron-based additive LiBOB forms boron-containing polymers that synergize with the polyether phase to construct a more durable bipolymeric SEI. The optimized electrolyte enabled an NCM811||μm-Si full cell to retain 80.9% of its capacity over 200 cycles. Notably, the methyl groups not only increase steric hindrance but also serve as electron-donating moieties, reducing solvent polarity and further weakening Li^+-solvent coordination. Inspired by this strategy, Yang *et al.* developed a low-temperature electrolyte consisting of cyclopentyl methyl ether (CPME) combined with THF and LiFSI salt[24]. Radial distribution function analysis indicated that pure CPME electrolytes exhibited a higher FSI^- coordination number (coordination number, CN = 1.08) than CPME/THF blends (CN = 0.99), consistent with the lower ESP_{min} and weaker Li^+ solvating ability of CPME relative to THF [Figure 4G]. Furthermore, the addition of THF caused a downfield shift in the ^7Li NMR spectrum [Figure 4H], further confirming the weaker solvating ability of CPME. The resulting polymer-inorganic SEI, governed by coordinated decomposition of FSI^- and THF, provided dual stabilization of the Si-electrolyte interphase.

The core strategy of weakly solvating electrolytes is to balance solvent and anions in the first Li^+ solvation sheath, thereby regulating the interfacial reaction pathways of anions. Notably, weak solvation intrinsically lowers the Li^+ desolvation energy barrier, thereby significantly accelerating interfacial charge-transfer kinetics[170,171]. However, weakly solvating electrolytes typically possess low DC, which inevitably weakens lithium salt dissociation and consequently reduces the overall ionic conductivity of the electrolyte[172-174].

Exploration of solvent design

Beyond the strategies discussed above, tailoring solvent molecular structures remains a central approach to advancing electrolyte design. The integration of computation-driven approaches, particularly DFT calculations, has enabled predictive screening and inverse design of solvent molecules, promoting the rational optimization of solvation structures and microenvironment components[175-177].

To suppress the formation of an organic-rich SEI while promoting LiF generation on Si anodes, Li *et al.* found that conventional ionic liquids (such as imidazolium and ammonium-based cations) undergo preferential reduction to form an organic SEI because of their relatively high reduction potential (> 0.7 V *vs.* Li/Li^+), which is unfavorable for LiF. In contrast, pyrrolidinium-based cations possess a lower reduction potential (-0.2 V *vs.* Li/Li^+), but exist as solids at room temperature when paired with PF_6^-. Thus, they designed and synthesized N-methyl-N-(2-methoxyethoxy) methylpyrrolidinium hexafluorophosphate (NMEP), an ionic liquid electrolyte comprising pyrrolidinium cations, PF_6^- anions, and oligomeric DME fragments[23]. This asymmetric electrolyte structure enhances $LiPF_6$ compatibility with low-potential ether solvents. The extremely low reduction potentials of the pyrrolidinium cation and ether fragments promoted the preferential PF_6^- reduction on alloy anodes, thereby generating a LiF-rich SEI. This strategy enabled 50 μm Si anodes to deliver capacities exceeding 2,900 mAh g^{-1}, cycling CE exceeding 99.9%, and cycling stability over 400 cycles. Under lean electrolyte conditions (3 g Ah^{-1}), the NMEP/$LiPF_6$ electrolyte further enabled 90 mAh μSi||NMC811 pouch cells to sustain > 200 cycles with > 72% capacity retention, while 70 mAh $Li_{3.75}Si$||SPAN cells maintained > 85% capacity after 400 cycles [Tables 1 and 2][178,179].

Moreover, to elucidate the relationship between reduction stability and solvent molecular descriptors, Sun *et al.* systematically established quantitative correlations between electrolyte reduction stability (RS) and molecular parameters, including electronegativity differences ($\Delta\chi$) and the combined influence of electrophilicity (EPT) and coordination ability (CDA), as shown in Figure 5A and B[180]. The study revealed that EPT and CDA regulate the activation energy barriers by influencing ground-state and transition-state

Table 1. Li||Si half-cell electrochemical performance of selected strategies for supporting-component design

Electrolytes	Current density	Capacity[mAhg^{-1}] Retention [%]	Cycle	Refs.
1.0M $LiPF_6$ in FEC/SL/TTE	0.25 C	2,175/ > 80%	250	[84]
1M $LiPF_6$ in GBL/DEC/FEC	0.2 C	87.5%	100	[99]
2.0 M $LiPF_6$ in THF/Me-THF	0.2 C	90%	400	[112]
3 M $LiPF_6$ in DX/DEE	0.3 C	83.13%	200	[22]
3 M LiFSi in DEE + VC	1 A g^{-1}	80.5%	300	[150]
LiFSI in DME/TTE	1 C	3,266/ > 80%	110	[154]
1 M LiFSI in THF/TTE	1 A g^{-1}	1,995.7/79%	400	[155]
LiFSI in DMC/HFE	1 A g^{-1}	1,667	200	[156]
4 M LiFSI in FEMC/OTE	0.2 C	62%	150	[161]
LiFSI in FEC/BTFC/ETFA	0.2 C	1,842.5/81.1%	200	[164]
1 M LiFSI in MDFA/FEC	2 A g^{-1}	84.5%	100	[165]
2M $LiPF_6$ in EGDE + FEC	0.5 A g^{-1}	2,414/85.82%	200	[166]
LiFSI/LiBOB in DPMPE + FEC	1 A g^{-1}	95.87%	300	[169]
1 M LiFSI CPME/THF/TTE	1 A g^{-1}	2,194.5/73.1%	200	[24]
$LiPF_6$ in NMEP	0.125C	2,537/87%	400	[23]
1 M LiFSI TFSPY	0.2C	81%	600	[180]

FEC: Fluoroethylene carbonate; SL: sulfolane; TTE: 1,1,2,2-tetrafluoroethyl-2,2,3,3-tetrafluoropropyl ether; GBL: γ-butyrolactone; DEC: diethyl carbonate; THF: tetrahydrofuran; DX: 1,3-dioxane; DEE: 1,2-diethoxyethane; VC: vinylene carbonate; DME: ethylene glycol dimethyl ether; DMC: dimethyl carbonate; HFE: 2,2,3,3-tetrafluoropropyl ether; FEMC: methyl 2,2,2-trifluoroethyl carbonate; OTE: 1,1,2,2-Tetrafluoroethyl-2,2,2-trifluoroethyl ether; BTFC: bis(2,2,2-trifluoroethyl) carbonate; ETFA: ethyl trifluoroacetate; MDFA: methyl difluoroacetate; EGDE: ethylene glycol diethyl ether; DPMPE: dipropylene glycol methyl propyl ether; CPME: cyclopentyl methyl ether; NMEP: N-methyl-N-(2-methoxyethoxy) methylpyrrolidinium hexafluorophosphate; TFSPY: N-Pyrrolidine-trifluoromethanesulfonamide; $LiPF_6$: lithium hexafluorophosphate; LiFSI: lithium bis(fluorosulfonyl)imide; LiBOB: lithium bis(oxalate) borate.

energies, respectively. Lower EPT and CDA values correlate with enhanced resistance to solvent reduction, thereby promoting the formation of more homogeneous SEI layers. Guided by these design principles, they synthesized three previously unreported solvents, N-Pyrrolidine-trifluoromethanesulfonamide (TFSPY), N-Piperidine-trifluoromethanesulfonamide (TFSPD), and N-Morpholine-trifluoromethanesulfonamide (TFSMP), for Li or Si anode electrolytes. Electrochemical evaluation identified the 1 M LiFSI-TFSPY electrolyte as the optimal formulation. Li||Si cells employing this electrolyte exhibited 81% capacity retention after 600 cycles. Furthermore, Xu *et al.* developed anionic(-structure)-like fluorosulfonamide-dimethylsulfamyl fluoride (DMSF) and N, N-dimethyltrifluoromethanesulfonamide (DM) (e.g., DMSF/DM) as co-solvents[181]. ^{19}F NMR [Figure 5C] revealed an apparent downfield shift of DMSF (0.66 ppm), indicating its higher polarity. Additionally, strong ^{1}H-^{19}F coupling signals between DM and DMSF were observed in Figure 5D. By employing the space-charge depletion region arising from the semiconducting nature of Si during the initial lithiation process, they established an interfacial potential barrier for electron transfer. Under this electron-limited regime, the anionic-like sulfonamide solvents (DMSF/DM) underwent preferential single-electron reduction, thereby generating a dense and electrically insulating inorganic layer (composed of LiF and Li_2S).

SACRIFICIAL COMPONENTS

Sacrificial components are specifically introduced to enhance interfacial stability. They can preferentially undergo irreversible electrochemical (or chemical) reactions at the electrode/electrolyte interphase prior to the supporting components, thereby being consumed to generate a stable SEI[182,183]. Sacrificial components typically include lithium salts and additives. In the following, we discuss electrolyte design strategies for Si anodes from the perspective of these sacrificial component categories.

Table 2. Si-based full-cell electrochemical performance of selected supporting component design strategies

Electrolytes	Full-Cell materials	Current density	Capacity[mAhg^{-1}] Retention [%]	Cycle	Refs.
1.0M $LiPF_6$ in FEC/SL/TTE	μSi||NCA	0.25 C	81%	200	[84]
1M $LiPF_6$ in GBL/DEC/FEC	μSi||NCM811	0.2 C	83.7%	150	[112]
2.0 M $LiPF_6$ in THF/Me-THF	μSi||NCA μSi||LFP	0.2 C	92% 80%	30 100	[148]
3 M $LiPF_6$ in DX/DEE	μSi||NCM811	0.3 C	88.42%	150	[22]
3 M LiFSi in DEE+VC	Si||LPO Si||NCM811	0.3 C	85.7% 173.1	200 110	[150]
1 M LiFSI in THF/TTE	nSi||LPO	0.5 C	83.6%	600	[155]
LiFSI in DMC/HFE	μSi/NMC811	0.1 C	65%	200	[156]
$LiPF_6$ in EC/EMC/FEC	μSi||NCM811	3 C	76.6%	100	[159]
4 M LiFSI in FEMC/OTE	μSi||NCM811	0.2 C	70%	200	[161]
LiFSI in FEC/BTFC/ETFA	nSi||NMC532	0.2 C	153.8%	100	[164]
2M $LiPF_6$ in EGDE+FEC	μSi||LPO	0.2 C	77.6%	80	[166]
LiFSI/LiBOB in DPMPE+FEC	μSi||NCM811	0.25 C	85.4%	200	[169]
1 M LiFSI CPME/THF/TTE	nSi||LPO nSi||NCM811	0.2 C	97.2% 82.8%	100 160	[24]
$LiPF_6$ in NMEP	μSi||NMC811	0.125C	72%	200	[23]

$LiPF_6$: Lithium hexafluorophosphate; FEC: fluoroethylene carbonate; SL: sulfolane; TTE: 1,1,2,2-tetrafluoroethyl-2,2,3,3-tetrafluoropropyl ether; GBL: γ-butyrolactone; DEC: diethyl carbonate; THF: tetrahydrofuran; DX: 1,3-dioxane; DEE: 1,2-diethoxyethane; LiFSI: lithium bis(fluorosulfonyl)imide; VC: vinylene carbonate; DMC: dimethyl carbonate; HFE: 2,2,3,3-tetrafluoropropyl ether; EC: ethylene carbonate; EMC: ethyl methyl carbonate; FEMC: methyl 2,2,2-trifluoroethyl carbonate; OTE: 1,1,2,2-Tetrafluoroethyl-2,2,2-trifluoroethyl ether; BTFC: bis(2,2,2-trifluoroethyl) carbonate; ETFA: ethyl trifluoroacetate; EGDE: ethylene glycol diethyl ether; LiBOB: lithium bis(oxalate) borate; DPMPE: dipropylene glycol methyl propyl ether; CPME: cyclopentyl methyl ether; NMEP: N-methyl-N-(2-methoxyethoxy) methylpyrrolidinium hexafluorophosphate; NCA: lithium nickel cobalt aluminate oxide; NCM811: lithium nickel cobalt manganese oxide ($LiNi_{0.8}Co_{0.1}Mn_{0.1}O_2$); LFP: lithium iron phosphate ($LiFePO_4$); LPO: lithium phosphate (Li_3PO_4); NMC811: lithium nickel manganese cobalt oxide ($LiNi_{0.8}Mn_{0.1}Co_{0.1}O_2$); NMC532: lithium nickel manganese cobalt oxide ($LiNi_{0.5}Mn_{0.3}Co_{0.2}O_2$).

Lithium salt anions

The rational design of anion architectures exerts pronounced regulatory effects on both the formation mechanism and microstructural characteristics of the SEI at anode interfaces[184,185]. The chemical structure of anions (e.g., size, charge distribution, coordination ability, and LUMO/HOMO energy levels) determines their reactivity and decomposition pathways at electrode interfaces, thereby governing the composition and morphology of the resulting SEI[116,186]. Thus, lithium salts can modulate the solvation structure of electrolytes, thereby indirectly regulating the phase ratio and spatial distribution of organic and inorganic components within the SEI[187,188].

$LiPF_6$ is currently the most widely used lithium salt in commercial batteries, primarily owing to its strong solvation interactions with carbonate-based solvents (e.g., EC), which enable electrolytes with high ionic conductivity (> 10 mS cm^{-1}). The reduction products of PF_6^-, primarily high-modulus inorganic components such as LiF and $Li_xPO_yF_z$, contribute to the formation of a stable inorganic SEI [Figure 6A][23,189]. However, when paired with strongly solvating solvents such as EC, strong Li^+-EC coordination dominates the solvation sheath, forcing PF_6^- anions into the outer solvation layer. This spatial segregation significantly suppresses the reduction of PF_6^- at Si anode surfaces, resulting in an SEI with insufficient inorganic components and excessive organic constituents. The resulting mechanically weak, organic-dominated SEI accelerates capacity degradation[190,191]. Researchers have explored weakly solvating solvents to reduce Li^+-solvent coordination competition[148]. Nevertheless, the inherent high polarity of $LiPF_6$ limits its solubility in low-dielectric-constant weakly solvating solvents, leading to lower practical ionic conductivity compared with the

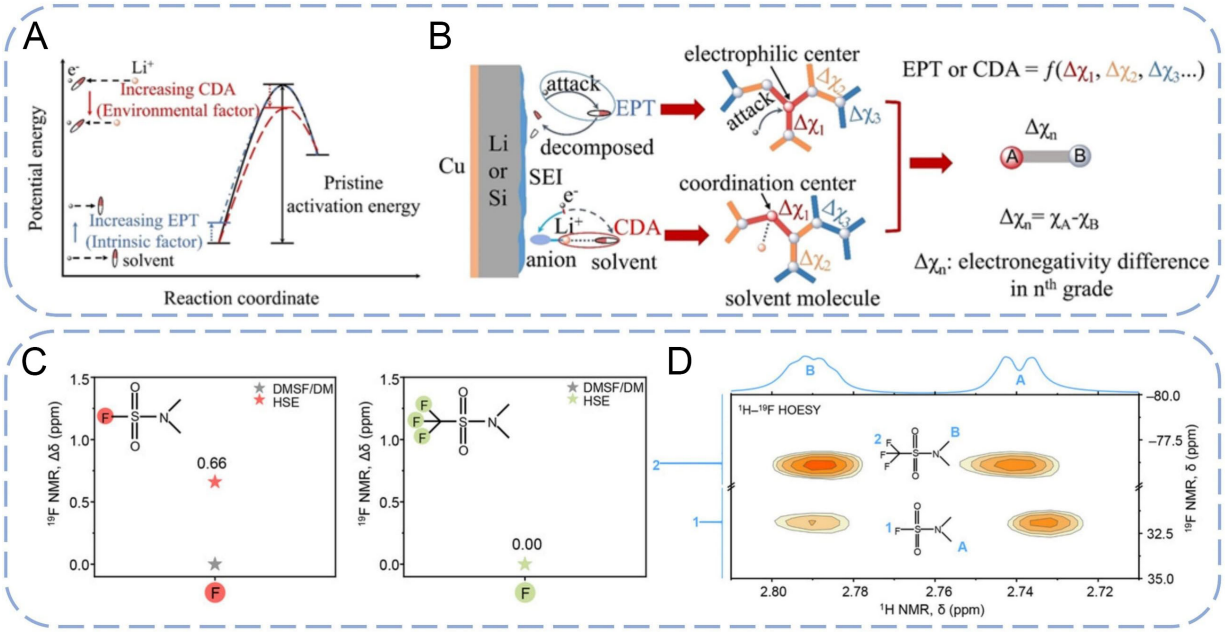

Figure 5. (A) EPT and CDA on solvent decomposition modeled as a reaction with activation energy; (B) Schematic of solvent decomposition processes at Li and Si anode interfaces; Figure 5A and B is reprinted with permission from Ref.[180]. Copyright © 2024 Wiley; (C) The ^{19}F NMR chemical shift differences between the DMSF/DM mixture (without 1 m LiFSI) and the HSE (with 1 m LiFSI) for the DMSF and the DM; (D) The ^{1}H-^{19}F heteronuclear Overhauser Effect Spectroscopy (HOESY) for the DMSF/DM mixture; Figure 5C and D is reprinted with permission from Ref.[181]. Copyright © 2025 Wiley. CDA: Coordination ability; EPT: effects of electrophilicity; Δχ: electronegativity differences; SEI: solid electrolyte interphase; NMR: nuclear magnetic resonance spectroscopy; DMSF: dimethylsulfamyl fluoride; DM: N, N-dimethyltrifluoromethanesulfonamide; HSE: hybrid sulfonamide electrolyte; LiFSI: lithium bis(fluorosulfonyl)imide.

conventional EC-based electrolyte[191,192]. Thus, the application of $LiPF_6$ in Si-based electrolytes is constrained by a dual challenge involving solvation structure and solubility, limiting its ability to optimize SEI architecture in such systems. To overcome these limitations and enhance lithium salt adaptability across diverse solvent environments, recent research efforts have focused on two main directions: developing alternative lithium salts and employing synergistic effects among composite lithium salts.

Novel lithium salt alternatives

Recent studies indicate that fluorine-containing lithium salts, such as LiFSI and LiDFOB, exhibit strong potential as alternatives to $LiPF_6$ in specific electrolyte systems[193-196]. Yu *et al.* employed electrochemical analysis and XPS to elucidate the formation mechanism of FSI-derived SEI and to identify electrolyte decomposition pathways in ether-based electrolytes[197,198]. As shown in Figure 6B, the reduction of FSI^- involves sequential S-F bond cleavage to form LiF and SO_x species; S=O bond cleavage to form Li_2S and Li_2O; stepwise N-S bond cleavage to form the N-SO_x intermediates and Li_3N. Meanwhile, interfacial dissolution between the SEI and the electrolyte also induces compositional evolution. Based on the relative abundance of individual components, the solubility trend follows the order: Li_3N/N-SO_x/-SO_2F > SO_x > Li_2S > LiF > Li_2O/LiOH. Similarly, Yang *et al.* employed LiFSI with VC as sacrificial components to form a stable SEI featuring an inorganic inner region and an organic outer region[150]. Furthermore, LiFSI exhibits a high dissociation constant, enabling the formation of higher-concentration electrolytes. Chang *et al.* formulated a highly concentrated electrolyte employing LiFSI and PC at a 1:2 molar ratio[199]. Owing to the increased concentration of CIPs and AGGs, the reduction of FSI^- anions is facilitated. Similarly, Jia *et al.* formulated an LHCE employing 1.8 M LiFSI in a carbonate solvent with a BTFE diluent[193]. As shown in Figure 6C, the high anion ratio enabled by the diluent leads to more FSI^- ions in the first solvation sheath, thereby promoting their preferential reaction to form the SEI. Compared with the SEI formed in a conventional 1.2

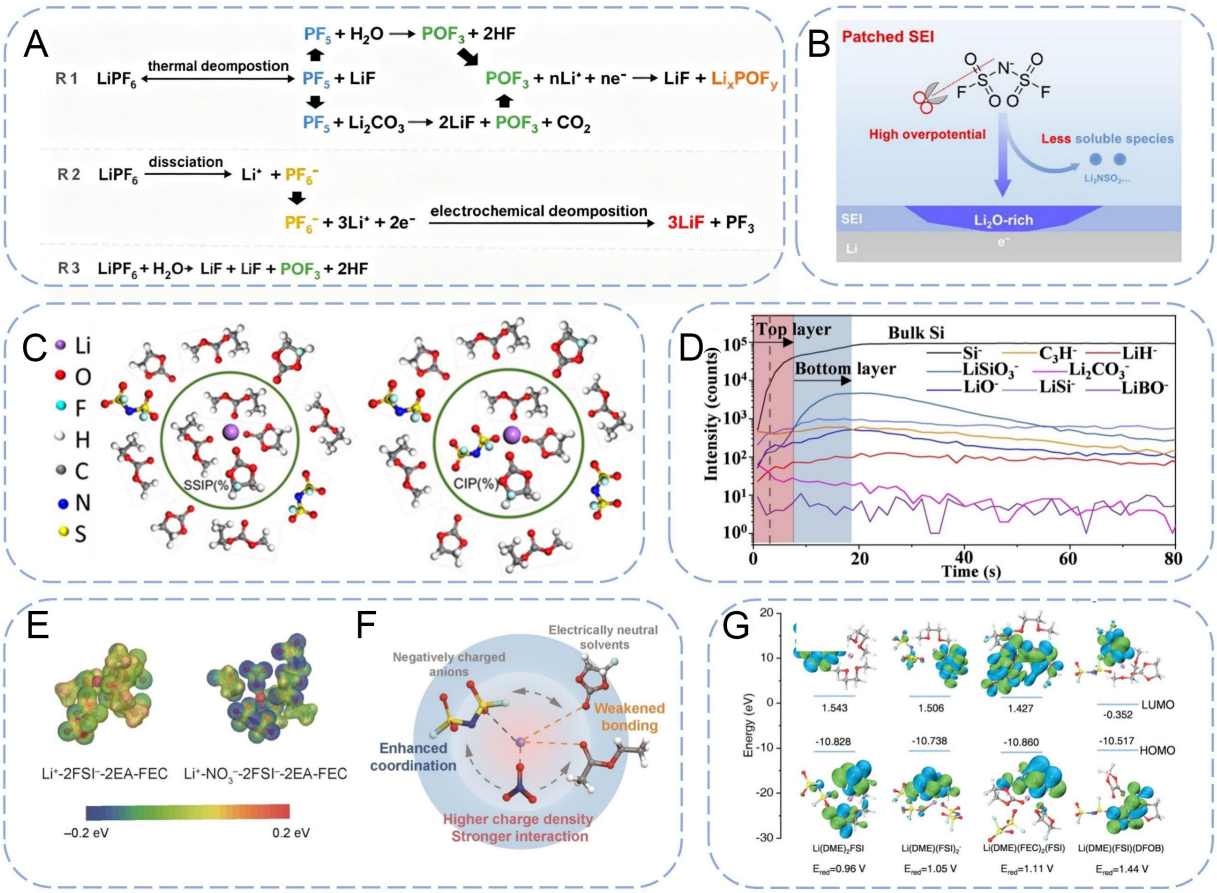

Figure 6. (A) Distinct reaction mechanisms of $LiPF_6$ in RCE systems; Figure 6A is reprinted with permission from Ref.[190]. Copyright © 2023 American Chemical Society; (B) Sequential SEI formation steps during FSI^- breakdown; Figure 6B is reprinted with permission from Ref.[198]. Copyright © 2025 Wiley; (C) Schematic of first-solvation-shell structures and CIP/SSIP ratios; Figure 6C is reprinted with permission from Ref.[193]. Copyright © 2020 American Chemical Society; (D) TOF-SIMS depth profiles of interphase species; Figure 6D is reprinted with permission from Ref.[33]. Copyright © 2023 Wiley; (E) Electrostatic potential evolution after $LiNO_3$ addition; (F) Schematic of NO_3^- regulating competitive coordination among Li^+, anions, and solvents in TIWSE; Figure 6E and F are reprinted with permission from Ref.[81]. Copyright © 2025 Wiley; (G) HOMO/LUMO levels and reduction potentials of four solvation structures in N-DHF electrolyte; Figure 6G is reprinted with permission from Ref.[213]. Copyright © 2021 Wiley. $LiPF_6$: Lithium hexafluorophosphate; SEI: solid electrolyte interphase; FSI: fluorosulfonyl imide; EA: ethyl acetate; FEC: fluoroethylene carbonate; LUMO: lowest unoccupied molecular orbital; HOMO: highest occupied molecular orbital; RCE: reference carbonate electrolyte; CIP: contact ion pair; SSIP: solvent-separated ion pair; TOF-SIMS: time-of-flight secondary ion mass spectrometry; TIWSE: temper-ature-inert weakly solvating electrolyte.

M $LiPF_6$ carbonate electrolyte, the SEI derived from this system contains a higher proportion of inorganic components. Furthermore, to investigate the decomposition pathways of FSI anions, Sankaran *et al.* employed imidazolium-based ILs with symmetric and asymmetric anions to study their impact on the SEI chemistry and morphology[200]. The study showed that electrolytes containing symmetric FSI^- {LiFSI-EMIFSI [1-ethyl-3-methylimidazolium bis(fluorosulfonyl)imide]} promote the formation of a more robust passivation layer. Moreover, this work elucidated the critical role of the decomposition product Li_2SO_4, revealing its significant contribution to enhancing the mechanical flexibility and ionic conductivity of the SEI[200].

LiDFOB possesses a lower LUMO energy level than $LiPF_6$, and its electronic structure enables preferential decomposition at a higher reduction potential of 2.8-3.0 V (*vs.* Li^+/Li), thereby forming a dense SEI film rich in LiF and borate species on the anode surface[201-203]. Zhang *et al.* developed a non-flammable lithium-ion electrolyte using LiDFOB as the salt in pure phosphate solvents[194]. The SEI formed from LiDFOB is thinner,

and the electrode maintains better structural integrity after cycling. Tests with micro-Si anodes indicated that this electrolyte significantly improved cycling performance by forming an SEI layer enriched with B and F containing species.

To address potential environmental concerns associated with fluorinated solvents, Li *et al.* developed a dual-functional fluorine-free electrolyte based on $LiBH_4$ (2 M $LiBH_4$ in THF/MeTHF)[33]. As revealed by TOF-SIMS [Figure 6D] and supported by COMSOL simulations, the BH_4^- anion enabled *in situ* chemical pre-lithiation of the native oxide layer on the Si surface, reconstructing the interfacial structure. The intrinsic stability of the $LiBH_4$-based electrolyte enables the formation of a denser, more inorganic interphase, which is beneficial for maintaining structural integrity during lithium alloying. Its superior mechanical strength suppresses Si particle pulverization and preserves particle integrity, enabling a high-capacity retention rate of 84.7% after 400 cycles at 0.2 C.

Beyond composite lithium-salt systems, multi-alkali metal molten salt electrolytes have emerged as a viable strategy for simultaneously enhancing interfacial stability and safety. Wang *et al.* reported a non-flammable molten-salt electrolyte consisting of lithium, potassium, and cesium bis(fluorosulfonyl)imide in a mole ratio of 0.3:0.35:0.35 (denoted as $Li_{0.3}K_{0.35}Cs_{0.35}FSA$)[204]. Both computational and experimental analyses revealed that FSA- anions facilitate the formation of an inorganic-rich SEI layer containing LiF, Li_3N, Li_2O, and Li_2S. This SEI exhibits excellent mechanical resilience and low interfacial resistance, thereby effectively accommodating the drastic volume changes of Si during repeated lithiation/delithiation cycles.

Synergistic effects of composite lithium salts

In lithium-ion batteries, single-component lithium salts are required to simultaneously fulfill the dual functions of ion transport and SEI formation. This dual functionality often induces Li^+ concentration gradients during cycling[205]. In contrast, composite multi-salt electrolytes leverage complementary charge distribution and coordination competition among different anions to regulate Li^+ concentration and promote the formation of a dense, inorganic-rich interphase[206,207]. Lv *et al.* developed a ternary $LiPF_6$-LiFSI-LiTFSI composite salt (molar ratio 7:1:2), which, compared with pure $LiPF_6$, generated a thinner SEI while suppressing $LiPF_6$ decomposition and HF formation through synergistic inter-anion effects[208].

Beyond conventional lithium salts, $LiNO_3$ and LiDFOB are also widely incorporated into composite electrolyte systems. Sang *et al.* developed a temperature-insensitive weakly solvating electrolyte composed of LiFSI and $LiNO_3$ in ethyl acetate (EA) and FEC for low-temperature μSi operation[81]. Incorporating high-DN NO_3^- into the first Li^+ solvation sheath decreased the electrostatic potential (ESP) around Li^+, generating a more negatively charged region that weakened dipole-dipole interactions between solvent molecules and Li^+ [Figure 6E]. Additionally, as illustrated in Figure 6F, the negatively charged region coordinated with more neighboring Li^+ ions, thereby stabilizing the anion-rich solvation structure. Full-cell μSi||NCM811 tests delivered capacity retention of 91.8% and 80.8% after 100 cycles at -20 °C and 30 °C, respectively.

Introducing $LiNO_3$ into the solvation sheath also enriches the SEI with N- and S-containing inorganic species (e.g., Li_3N, Li_2S), which exhibit high ionic conductivity and enhance Li^+ transport[209,210]. Moreover, owing to its high reduction potential (> 1.7 V *vs.* Li/Li^+), $LiNO_3$ effectively suppresses the LiFSI-triggered ring-opening polymerization of cyclic ethers (e.g., DOL), thereby preserving both the liquid-state nature and high ionic conductivity of the electrolyte[211]. Xu *et al.* co-incorporated $LiNO_3$ and FEC into a LiFSI-based LHCE[212]. Radial distribution function peaks at 1.6 Å and 2.0 Å, corresponding to Li-$O_{NO_3^-}$ and Li-O_{FEC} interactions, confirmed the incorporation of NO_3^- and FEC into the first solvation sheath, thereby altering overall LUMO-level distribution. Both FEC and $LiNO_3$ possess low LUMO energy levels, rendering them

thermodynamically susceptible to reduction[212]. The resulting organic-inorganic hybrid SEI exhibited excellent mechanical integrity and high-capacity retention on Si anodes[212].

The decomposition products of LiDFOB, including LiF and borate esters, also contribute to the formation of a uniform and dense SEI. Cao *et al.* incorporated FEC and LiDFOB into a LiFSI-based electrolyte to further improve SEI stability[213]. As shown in Figure 6G, the calculations of the LUMO and HOMO energy levels for different Li^+ solvation structures revealed that $DFOB^-$-containing clusters have the lowest LUMO energy level. Their preferential decomposition at the Si anode surface during lithiation promotes the early formation of LiF at relatively high potentials, thereby suppressing subsequent solvent reduction during SEI formation. The Si anode maintained a high discharge capacity after 200 cycles.

Electrolyte additive

The incorporation of film-forming additives into electrolytes is an effective strategy for addressing interfacial issues in Si anodes. Typically, an effective film-forming electrolyte additive should exhibit strong solvating ability and a low LUMO energy level, enabling preferential incorporation into the solvation sheath and prior reduction, thereby forming an effective passivation layer that suppresses continuous electrolyte decomposition[158,214]. With advanced characterization techniques elucidating SEI formation pathways, additive design has evolved from single-function passivation agents to multifunctional components with synergistic effects[215]. Here, additives are classified into conventional film-forming additives and emerging multifunctional additives to provide broader insights into future additive design.

Conventional film-forming additives

Unsaturated carbonate additives exhibit distinctive interfacial modulation behavior due to their unique molecular structures. Their C=C unsaturated bond lowers the LUMO energy, enabling preferential reduction at the anode surface compared with standard carbonate solvents. Vinylene carbonate (VC), one of the earliest film-forming additives, generates polycarbonate species that enhance SEI elasticity and partially mitigate volume expansion in Si and Si/C anodes[216-218]. After initial reduction, VC undergoes ring-opening to form a radical anion containing an unpaired electron, which can initiate radical polymerization at the C=C (homolytic cleavage) bond. The resulting polymer consists of repeating EC-derived units and is commonly referred to as poly(VC). Additionally, VC may also polymerize via its carbonate group, producing polycarbonate and/or polyethylene derivatives bearing-OCO_2Li groups. Poly(VC) can further undergo two-electron reduction to form Li_2CO_3 and polyacetylene. In addition, the ring-opened VC radical anion may undergo dimerization, generating dimers, such as lithium vinylene dicarbonate $(=CH\text{-}OCO_2Li)_2$, lithium divinylene dicarbonate $(=CH\text{-}CH\text{-}OCO_2Li)_2$, or lithium divinylene dioxide. These dimers may further aggregate via O-Li-O coordination into oligomer species consisting of three or more units. Furthermore, VC decomposition can generate inorganic species, such as lithium oxalate or Li_2CO_3[219]. However, subsequent studies have highlighted several limitations: the polycarbonate-rich SEI lacks sufficient mechanical robustness to withstand repeated Si volume changes, and the dense organic interphase impedes fast charging/discharging, leading to capacity fading [Figure 7A][220-222].

Fluorination significantly alters molecular electronic distribution through the strong electron-withdrawing inductive effect of C-F bonds[223]. Accordingly, FEC, the most widely used fluorinated additive, exhibits a higher reduction potential (approx. 1.2 V *vs.* Li^+/Li) than conventional EC (approx. 0.8 V). SEI layers formed in FEC-containing electrolytes exhibit stronger adhesion to the Si surface, enhancing the cycling stability and CE of Si-based anodes[214,224]. Upon accepting an electron at the negative electrode surface, FEC is converted into an unstable radical anion ($FEC^{\cdot -}$), a transient species that initiates the subsequent decomposition process[225]. Subsequently, $FEC^{\cdot -}$ undergoes ring-opening, accompanied by the simultaneous or stepwise elimination of a fluorine atom to generate VC, LiF, and CO_2[226]. This pathway directly links the

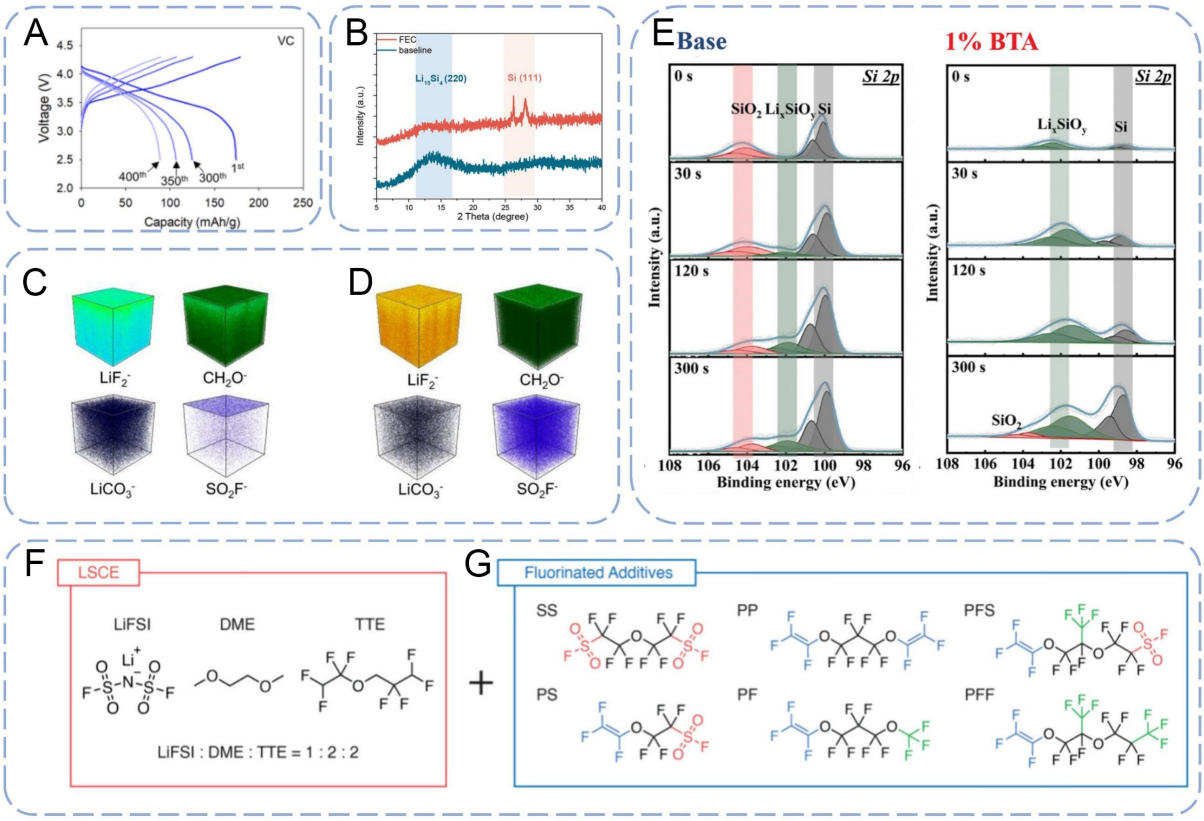

Figure 7. (A) Capacity-voltage profiles of NCM811/Si-C full cells with VC-containing electrolyte; Figure 7A is reprinted with permission from Ref.[222]. Copyright © 2021 Springer Nature, under CC BY 4.0 license; (B) XRD patterns of Si anodes after first delithiation; Figure 7B is reprinted with permission from Ref.[224]. Copyright © 2023 American Chemical Society; 3D TOF-SIMS sputtering images of typical secondary ion fragments under (C) 0.2 M-DTF and (D) 1 M-DTF; Figure 7C and D is reprinted with permission from Ref.[235]. Copyright © 2025 Wiley. (E) In-depth XPS etching of Si electrodes with Base and 1% BTA electrolytes (Si 2p); Figure 7E is reprinted with permission from Ref.[241]. Copyright © 2024 Wiley; (F) Chemical structures and molar ratios of LSCE; (G) Fluorinated additives containing fluoroalkyl sulfonyl fluoride or trifluorovinyl ether end-groups with a perfluoropolyether tether; Figure 7F and G is reprinted with permission from Ref.[34]. Copyright © 2021 American Chemical Society. VC: Vinylene carbonate; FEC: fluoroethylene carbonate; BTA: bis(trimethylsilyl)trifluoroacetamide; LSCE: localized super concentrated electrolytes; LiFSI: lithium bis(fluorosulfonyl)imide; DME: dimethyl ether; TTE: 1,1,2,2-tetrafluoroethyl-2,2,3,3-tetrafluoropropyl ether; SS: bis[2-(fluorosulfonyl)tetrafluoroethyl]ether; PS: 1,3-propane sultone; PP: hexafluoro-bis(trifluorovinyl)propane; PF: perfluoro-3,7-dioxaoct-1-ene; PFS: :perfluoro(4-methyl-3,6-dioxaoct-7-ene)-sulfonyl fluoride; PFP: perfluoro(5-methyl-3,6-dioxanon-1-ene); NCM811: lithium nickel cobalt manganese oxide ($LiNi_{0.8}Co_{0.1}Mn_{0.1}O_2$); XRD: X-ray diffraction; TOF-SIMS: time-of-flight secondary ion mass spectrometry; DTF: 2,2-difluoroethyl triflate; XPS: X-ray photoelectron spectroscopy.

decomposition of FEC and the formation of VC and LiF, two crucial components of the SEI. Additionally, $FEC^{\cdot-}$ may also undergo a more extensive decomposition pathway. This pathway involves the simultaneous cleavage of two C-O bonds, initiating a cascade of defluorination and decarboxylation reactions that ultimately generate the vinoxy radical ($\cdot CH_2CHO$), CO_2, and F^-[227]. A central issue regarding the decomposition mechanism of FEC concerns the origin of VC. Early studies proposed that FEC first converts to VC, which subsequently participates in SEI formation through its established decomposition mechanism[226]. However, subsequent studies employing radiochemistry and spectroscopic analysis suggest a more complex mechanism, in which direct FEC decomposition and indirect decomposition via VC likely occur simultaneously[225,228,229]. The final composition and structure of the SEI are governed by multiple factors, including the concentration of FEC, the nature of the negative electrode material (e.g., the distinct behaviors on Si versus graphite), and the specific electrochemical conditions. For instance, the film-forming mechanism of FEC at high-voltage conditions differs markedly from that at the negative electrode[230].

Jin *et al.* employed advanced dynamic nuclear polarization-enhanced solid-state NMR (DNP-NMR) spectroscopy to elucidate the differences in SEI compositions derived from FEC and VC[231]. They found that, despite their structural similarity, FEC undergoes a critical defluorination reaction during reduction, inducing the formation of a 3D cross-linked PEO-like polymer network with an inorganic LiF phase, whereas VC predominantly forms linear poly(vinylene carbonate). This FEC-derived inorganic nanocrystal/cross-linked polymer composite interphase exhibits superior mechanical rigidity and cohesive strength, thereby effectively preserving the structural integrity of Si particles during repeated volume expansion. The FEC-derived SEI primarily consists of Li_2CO_3, LiF, and polycarbonates, which contrasts significantly with the composition derived from conventional EC-based electrolytes[232,233]. Furthermore, Li *et al.* demonstrated that introducing FEC reduced the capacity loss associated with SEI growth by 52.9%, while decreasing the amount of dead lithium trapped within Si particles by 82.3%[234]. Post-cycling XRD analysis [Figure 7B] revealed that LiF incorporation into the Si phase effectively suppresses the formation of crystalline $Li_{15}Si_4$, thereby reducing lithium trapping during electrochemical cycling[234]. To promote the preferential participation of FEC in competitive interfacial reactions, Liu *et al.* developed a solvation engineering strategy to increase the coordination number of FEC molecules within the first Li^+ solvation sheath by minimizing anion participation[235]. Comparison of the TOF-SIMS depth profiles of the SEI under different lithium salt concentrations [Figure 7C and D] shows that, at low salt concentrations, FEC dominates the Li^+ solvation sheath, thereby promoting the formation of a uniform, LiF-rich SEI and enhancing the cycling stability. The Si anode exhibits a specific capacity of 2000 mAh g^{-1} over 200 cycles in a low-salt electrolyte consisting of 0.2 M LiFSI (or $LiPF_6$) in DMM (dimethoxymethane)/THF/FEC (4:3:3 by vol%). Despite its widespread application in Si anodes, FEC can induce detrimental effects on both the SEI film and the current collector-anode interface during cycling and calendar aging, highlighting the need for the continued development of new electrolyte additives to address these practical challenges[236,237].

Additionally, fluorinated derivatives, such as difluoroethylene carbonate (DFEC), have also been explored as film-forming additives, demonstrating considerable potential for interfacial regulation in Si-based anodes[238]. In a recent study, Ma *et al.* explored the interfacial behavior of trans-DFEC on Si anodes and highlighted the insufficient mechanical robustness of SEI layers derived from DFEC[239]. Typically, the decomposition of DFEC generates not only LiF but also substantial amounts of Li_2CO_3 and $ROCO_2Li$, which may compromise the stability of the SEI on Si electrodes. In contrast, incorporating LiDFOB promotes direct defluorination of DFEC during the initial decomposition step (i.e., cleavage of the C-F bond) rather than the conventional ring-opening reaction (i.e., cleavage of the C-O bond), thereby ensuring the exclusive formation of LiF instead of Li_2CO_3[240]. Consequently, LiDFOB was introduced as an initiator to regulate the defluorination-driven polymerization of DFEC. This strategy enabled the construction of a LiF-dominated hybrid interphase reinforced by a mechanically robust polymer network.

Multifunctional additives

Beyond film-forming functions, emerging electrolyte additives are designed to optimize the solvation structures and strengthen the cooperative interactions among electrolyte components. Deng *et al.* addressed ion-transport limitations arising from surface SiO_2 by introducing bis(trimethylsilyl)trifluoroacetamide (BTA) as a bifunctional additive[241]. Computational analysis revealed that BTA possesses a higher HOMO energy level and lower LUMO energy level. As shown in Figure 7E, BTA converts the inert SiO_2 layer into highly ion-conductive Li_xSiO_y by facilitating rapid electron transfer between Li^+ ions and Si-O bonds, enhancing the reactivity of SiO_2 toward lithiation. The resulting Li_xSiO_y layer becomes an integral part of the SEI, overcoming the kinetic limitations imposed by the native SiO_2 layer. Hou *et al.* further modulated the solvation structure through electrolyte additive engineering to regulate SEI formation. A weakly solvating electrolyte was formulated employing tris(hexafluoroisopropyl) borate (BTHE), 2,2,2-trifluoroethyl carbonate (FDEC), and FEC as solvents, with $LiPF_6$ as the lithium salt[242]. Depth-profile XPS analysis of

cycled Si anodes revealed that the electrolyte containing BTHE produced a robust and stable bilayer SEI. As an anion receptor, BTHE strengthens the Li^+-PF_6^- interaction, promoting the decomposition of PF_6^- and the formation of a high-purity LiF-rich inner SEI layer. Meanwhile, the -CF_3 groups in FDEC and FEC contribute to the formation of a fluorine-rich organic outer SEI layer upon reductive decomposition.

The functional groups of the electrolyte additives also play a critical role in SEI construction. Helms *et al.* employed molecular topology engineering to enhance the mechanical elasticity of the SEI[34]. They designed a series of reactive perfluoropolyether (PFPE) additives containing either an organosulfonyl fluoride or a trifluorovinyl ether functional group [Figure 7F and G][34]. These functional additives not only direct the *in-situ* formation of SEI components through their reactive moieties and molecular linkers, but also promote the oriented assembly of a hybrid inorganic-organic SEI via their unique topological anchoring structure. Experimental results demonstrated that difunctional additives (e.g., fluoroalkyl sulfonyl fluorides) simultaneously enriched both the LiF phase and the PFPE organic phase within the SEI, generating a hybrid interface reinforced by LiF-organic synergy[34,243]. This design significantly enhanced electrochemical performance, increasing the capacity retention of Si||LFP cells to 52% after 100 cycles at a C/3 rate, compared with only 36% for the control group, while markedly suppressing interface degradation.

Additionally, introducing catalytically active metal salts has emerged as another effective strategy for regulating interfacial reaction pathways. Li *et al.* demonstrated that incorporating an $Mg(TFSI)_2$ additive enables Mg^{2+} to synergistically participate in the lithiation process, fundamentally altering the conventional binary Li-Si alloying mechanism[244]. This process induces the *in-situ* formation of a thermodynamically stable ternary Li-Mg-Si Zintl phase, thereby modifying the phase transformation kinetics. Consequently, the altered reaction pathway results in higher CE and significantly improved capacity retention during long-term cycling. Similarly, Han *et al.* proposed a mixed salt electrolyte strategy. By introducing a small amount of multivalent metal salts [e.g., $Mg(TFSI)_2$ or $Zn(TFSI)_2$] into LiFSI-based electrolytes, they induced the *in-situ* formation of thermodynamically more stable ternary phases during lithiation[245]. The resulting mixed phase effectively suppressed the formation of the highly reactive crystalline $Li_{15}Si_4$ phase, thereby mitigating irreversible lithium consumption and particle pulverization by regulating bulk structure evolution, and thus significantly prolonging the cycle life of Si anodes. Moreover, the electrochemical performance of Si-based anodes in both half and full cells reported for representative sacrificial component strategies is summarized in Tables 3 and 4.

PROSPECTS FOR ELECTROLYTE DESIGN

Electrolyte innovation and refinement remain essential for improving SEI stability and extending the cycling durability of Si anodes. To identify new strategies for addressing these persistent challenges, this section draws inspiration from electrolyte strategies developed for other high-capacity anodes, including LMAs and Si/C composites. Because the alloying/dealloying potential of Si is slightly higher than that of lithium, some electrolyte components that have proven effective in Lithium metal batteries (LMBs) may also exhibit excellent performance in Si-based batteries[246,247]. Electrolyte design for LMBs has typically focused on regulating the solvation structures and constructing anion-derived inorganic SEIs, providing a systematic framework for the rational design of Si anode electrolytes. Such cross-system insights may facilitate the development of more effective electrolyte design principles for overcoming the limitations of Si anodes through the synergistic optimization of both sacrificial and supporting components.

Sacrificial component

Among the electrolyte components developed for LMAs, lithium difluorophosphate ($LiPO_2F_2$) has demonstrated remarkable advantages and considerable potential for addressing critical interfacial challenges[248]. Its ability to simultaneously construct robust SEI/CEI layers on both anode and cathode

Table 3. Li||Si half-cell electrochemical performance of the selection and design of sacrificial components

Electrolytes	Current density	Capacity[mAhg^{-1}] Retention [%]	Cycle	Refs.
LiFSI in PC	0.1C	1,997.9 /63.5%	100	[199]
0.2 M LiFSI in 0.8 M EMIFSI	0.5C	98%	100	[200]
1 M LiDFOB in TMP	0.2 A g^{-1}	950.27	100	[194]
2 M LiBH4 in THF/Me-THF	0.2 C	94.3%	100	[33]
$LiPF_6$: LiFSI: LiTFSI (7:1:2) in EC/DMC/DEC + VC/FEC	0.5 C	1,879.8	400	[208]
LiFSI/$LiNO_3$ in EA + FEC	0.5 C	76.1%	200	[81]
LiFSI/$LiNO_3$ in DME/TTE	1 A g^{-1}	96.1 %	100	[212]
LiFSI/ LiDFOB in DME/HFE + FEC	0.2 C	2,041.9	200	[213]
$Li_{0.3}K_{0.35}Cs_{0.35}FSA$	C/3	2,186.8/60.7%	100	[204]
0.2 M LiFSI ($LiPF_6$) in DMM/THF/FEC	0.2C	2000	200	[235]
1 M $LiPF_6$ in EC/DEC/DMC + LiDFOB + DFEC	2 A g^{-1}	1,487.3/67%	1,000	[240]
1 M $LiPF_6$ in EC/EMC+FEC/BTA	0.5 A g^{-1}	1,436.5	120	[241]
$LiPF_6$ in FEC/FDEC + BTHE	1 A g^{-1}	72.6%	300	[242]

LiFSI: Lithium bis(fluorosulfonyl)imide; PC: propylene carbonate; EMIFSI: 1-ethyl-3-methylimidazolium bis(fluorosulfonyl)imide; LiDFOB: lithium difluoro(oxalato)borate; TMP: trimethyl phosphate; THF: tetrahydrofuran; $LiPF_6$: lithium hexafluorophosphate; LiTFSI: lithium bis(trifluoromethylsulphonyl)imide; EC: ethylene carbonate; DMC: dimethyl carbonate; DEC: diethyl carbonate; VC: vinylene carbonate; FEC: fluoroethylene carbonate; $LiNO_3$: lithium nitrate; EA: ethyl acetate; DME: dimethyl ether; TTE: 1,1,2,2-tetrafluoroethyl-2,2,3,3-tetrafluoropropyl ether; HFE: 2,2,3,3-tetrafluoropropyl ether; FSA: bis(fluorosulfonyl)amide; DMM: dimethoxymethane; DFEC: difluoroethylene carbonate; EMC: ethyl methyl carbonate; BTA: bis(trimethylsilyl)trifluoroacetamide; FDEC: 2,2,2-trifluoroethyl carbonate; BTHE: tris(hexafluoroisopropyl) borate.

Table 4. Si-based full-cell electrochemical performance of the selection and design of sacrificial components

Electrolytes	Full-cell materials	Current density	Capacity[mAhg^{-1}] Retention [%]	Cycle	Refs.
LiFSI/$LiNO_3$ in EA + FEC	μSi||NCM811	0.5 C	80.8%	200	[81]
LiFSI/ LiDFOB in DME/HFE + FEC	nSi||NMC532	0.2 C	88.4%	60	[213]
1 M $LiPF_6$ in EC/DEC/DMC + LiDFOB + DFEC	nSi||NCM622	0.3 C	67%	100	[240]
$LiPF_6$ in FEC/FDEC + BTHE	nSi||NMC811	1 C	84.3%	1,000	[242]
LiFSI in DME/TTE + SS	nSi||LFP	C/20	52%	100	[34]

LiFSI: Lithium bis(fluorosulfonyl)imide; $LiNO_3$: lithium nitrate; EA: ethyl acetate; FEC: fluoroethylene carbonate; NCM811: lithium nickel cobalt manganese oxide ($LiNi_{0.8}Co_{0.1}Mn_{0.1}O_2$); LiDFOB: lithium difluoro(oxalato)borate; DME: dimethyl ether; HFE: 2,2,3,3-tetrafluoropropyl ether; NMC532: lithium nickel manganese cobalt oxide ($LiNi_{0.5}Mn_{0.3}Co_{0.2}O_2$); EC: ethylene carbonate; DEC: diethyl carbonate; DMC: dimethyl carbonate; DFEC: difluoroethylene carbonate; NMC622: lithium nickel manganese cobalt oxide ($LiNi_{0.6}Mn_{0.2}Co_{0.2}O_2$); FDEC: 2,2,2-trifluoroethyl carbonate; BTHE: tris(hexafluoroisopropyl) borate; NMC811: lithium nickel manganese cobalt oxide ($LiNi_{0.8}Mn_{0.1}Co_{0.1}O_2$); TTE: 1,1,2,2-tetrafluoroethyl-2,2,3,3-tetrafluoropropyl ether; SS: bis[2-(fluorosulfonyl)tetrafluoroethyl]ether; LFP: lithium iron phosphate ($LiFePO_4$).

surfaces has attracted increasing attention in recent studies[249,250]. As shown in Figure 8A, the $LiPO_2F_2$ anion exhibits a relatively low LUMO energy level and a high HOMO energy level, indicating strong electron affinity together with excellent oxidative stability[251]. For instance, Zheng *et al.* employed a dual-salt localized concentrated electrolyte (LCE) consisting of 0.1 M $LiPO_2F_2$ and 0.4 M LiBOB[252]. Figure 8B shows that the LMBs employing this dual-salt electrolyte achieved the highest capacity retention of 95.4% after 70 cycles at 1 C.

Although strongly coordinating anions (e.g., $DFOB^-$ and NO_3^-) are generally considered beneficial for SEI stabilization, weakly coordinating anions (e.g., AsF_6^- and PF_6^-) have been found to exhibit superior interfacial stability under fast charging conditions[253]. MD simulations revealed that these weakly coordinating anions

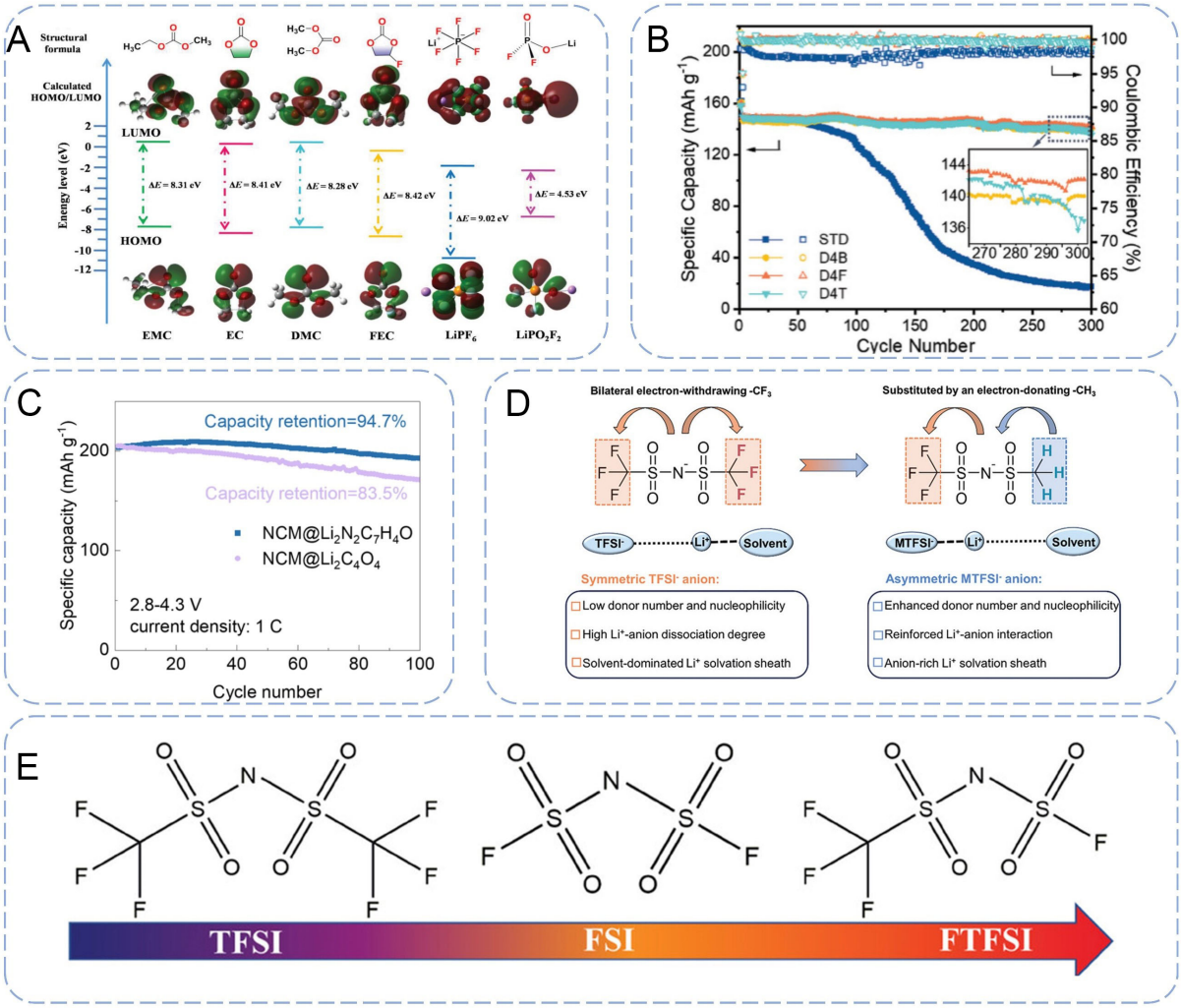

Figure 8. (A) HOMO and LUMO levels of EMC, EC, DMC, FEC, $LiPF_6$, and $LiPO_2F_2$; Figure 8A is reprinted with permission from Ref.[251]. Copyright © 2020 Wiley; (B) Cycling behavior of Li||Li symmetric cells at 0.5 mA cm^{-2}; Figure 8B is reprinted with permission from Ref.[252]. Copyright © 2020 Wiley; (C) Long-term cycling of NCM/$Li_2C_4O_4$ and NCM/$Li_2N_2C_7H_4O$ half-cells at 1 C; Figure 8C is reprinted with permission from Ref.[254]. Copyright © 2025, American Chemical Society; (D) Design principles of LiMTFSI based on LiTFSI; Figure 8D is reprinted with permission from Ref.[255]. Copyright © 2025 Wiley; (E) Chemical structures of the TFSI, FSI, and FTFSI anions.; Figure 8E is reprinted with permission from Ref.[257]. Copyright © 2025 Wiley. LUMO: Lowest unoccupied molecular orbital; HOMO: highest occupied molecular orbital; EMC: ethyl methyl carbonate; EC: ethylene carbonate; DMC: dimethyl carbonate; FEC: fluoroethylene carbonate; $LiPF_6$: lithium hexafluorophosphate; $LiPO_2F_2$: lithium difluorophosphate; STD: 0.1 M $LiPF_6$ electrolyte; NCM: nickel cobalt manganese oxide; TFSI: bis(trifluoromethylsulphonyl)imide; MTFSI: (methanesulfonyl)(trifluoromethanesulfonyl)imide; FSI: fluorosulfonyl imide; FTFSI: (fluorosulfonyl)(trifluoro-methanesulfonyl)imide.

exhibit minimal association with Li^+, generating excess positive charge on LiF cluster surfaces. The resulting electrostatic repulsion counteracts van der Waals attraction, stabilizing small LiF clusters and promoting the formation of thinner, more uniform SEI layers derived from AsF_6^-. To eliminate the toxicity associated with arsenic-containing anions, Kwon *et al.* employed theoretical calculations to identify tetraphenylborate (BPh_4^-) as a weakly coordinating anion based on its electrostatic potential minima and Li^+-binding energies[253].

Rational molecular design of anions has emerged as a major focus of recent research. Because anionic functional groups play a critical role in determining the reduction potential and coordination capability, Kang *et al.* employed a semi-supervised clustering approach to identify a nitrogen-centered organic lithium salt, Li-benzimidazol-2-one ($Li_2N_2C_7H_4O$), as an effective Li-ion compensation agent[254]. During the

compensation process, the anion generates benzimidazolone ($C_7H_4N_2O$) *in situ*, which subsequently functions as a sacrificial additive. Cycling tests showed that introducing the compensation lithium salt increased the capacity retention of full cells from 83.5% to 94.7% at 1 C [Figure 8C].

Furthermore, rational anion design can strengthen anion-cation interactions, thereby optimizing SEI chemistry. Zhou *et al.* designed an asymmetric lithium salt, lithium (methanesulfonyl)(trifluoromethanesulfonyl)imide (LiMTFSI), for LMBs[255]. Replacing the electron-withdrawing -CF_3 group in LiTFSI with an electron-donating -CH_3 group modulates anion nucleophilicity and strengthens Li^+-anion interactions [Figure 8D]. This modification increases anion participation within the first solvation sheath of Li^+, reducing solvent involvement and suppressing excessive solvent decomposition. Consequently, the resulting anion-rich solvation environment promotes the formation of an SEI enriched with Li_2S and Li_3N, whose high chemical stability and mechanical strength help lower the Li^+ diffusion barrier.

Asymmetric anion design can also modulate molecular polarity to fine-tune solvation structure. Liu *et al.* further developed lithium salts with improved oxidative stability, including lithium bis(sulfonyl)trifluoromethanesulfonyl imide (LiBSTFSI) and lithium sulfonyl(trifluoromethanesulfonyl)imide (LiSTFSI), which preserve SEI integrity while simultaneously enabling the formation of a mechanically robust CEI[256]. Tailored anion-solvent interactions can further suppress undesired solvent decomposition by regulating desolvation polarization, thereby promoting the formation of an inorganic-rich SEI. Xu *et al.* systematically investigated $TFSI^-$, FSI^-, and the asymmetric $FTFSI^-$ (fluorosulfonyl)(trifluoromethanesulfonyl)imide in bis(3-fluoropropyl) ether (BFPE) to develop a low-temperature electrolyte for LMBs [Figure 8E][257]. Assisted by H-F and H-O interactions between solvent molecules and anions, $FTFSI^-$ undergoes more rapid reductive decomposition while facilitating Li^+ desolvation. This anion promoted the formation of inorganic species such as Li_2O and LiF in the BFPE electrolyte. The 1.5 M LiFTFSI-BFPE electrolyte enables NMC811||Li full cells to cycle stably even at -40 °C, retaining more than 92% of the initial capacity (115 mAh g^{-1} after 100 cycles).

Recently, Park *et al.* introduced partially fluorinated -OCF_3 and -OTMS groups into the dimethyl vinylene carbonate (DMVC), synthesizing DMVC-OCF_3 and DMVC-OTMS as additives for Si/C anodes[222]. Computational analysis revealed that both additives possess low LUMO energy levels, ensuring their preferential reduction over other electrolyte components. Upon one-electron reduction, they generate DMVC-derived radicals together with OCF_3^- or $OTMS^-$ anions. As illustrated in Figure 9A, the -OCF_3-derived intermediates subsequently react with Li^+ to generate LiF, thereby reinforcing the mechanical robustness of the SEI. Meanwhile, DMVC-derived radicals attack the olefinic carbon of VC, initiating chain polymerization to form a LiF-rich cross-linked polymeric SEI. This elastic SEI more effectively accommodates volume changes of Si, thereby mitigating particle fracture and electrical isolation of Si.

Additionally, Wang *et al.* developed a dual-functional ester-based additive by combining 2,4,6,8-tetramethyl-2,4,6,8-tetravinylcyclotetrasiloxane (V4) with vinyltriethoxysilane (VTEO)[258]. As shown in Figure 9B, both VTEO and V4 exhibit nearly neutral electrostatic potential surfaces, promoting increased anion participation in the first Li^+ solvation sheath for priority reduction. Furthermore, VTEO functions as a molecular bridge, enabling addition polymerization of its vinyl group (-$CH=CH_2$) and the Si-based polymer framework generated from V4 decomposition. Meanwhile, the -OCH_2CH_3 groups in VTEO facilitate Li^+ transport and react with OH^- to form Si-O-Li linkages, thereby reinforcing interfacial stability.

Lan *et al.* identified N-tert-butyl-2-thiophenesulfonamide (NTSA) as a multifunctional electrolyte additive[259]. In the presence of NTSA and FEC, the resulting SEI was enriched with inorganic species, including LiF, Li_3N, and Li-S components. As shown in Figure 9C and D, comparison of radial distribution

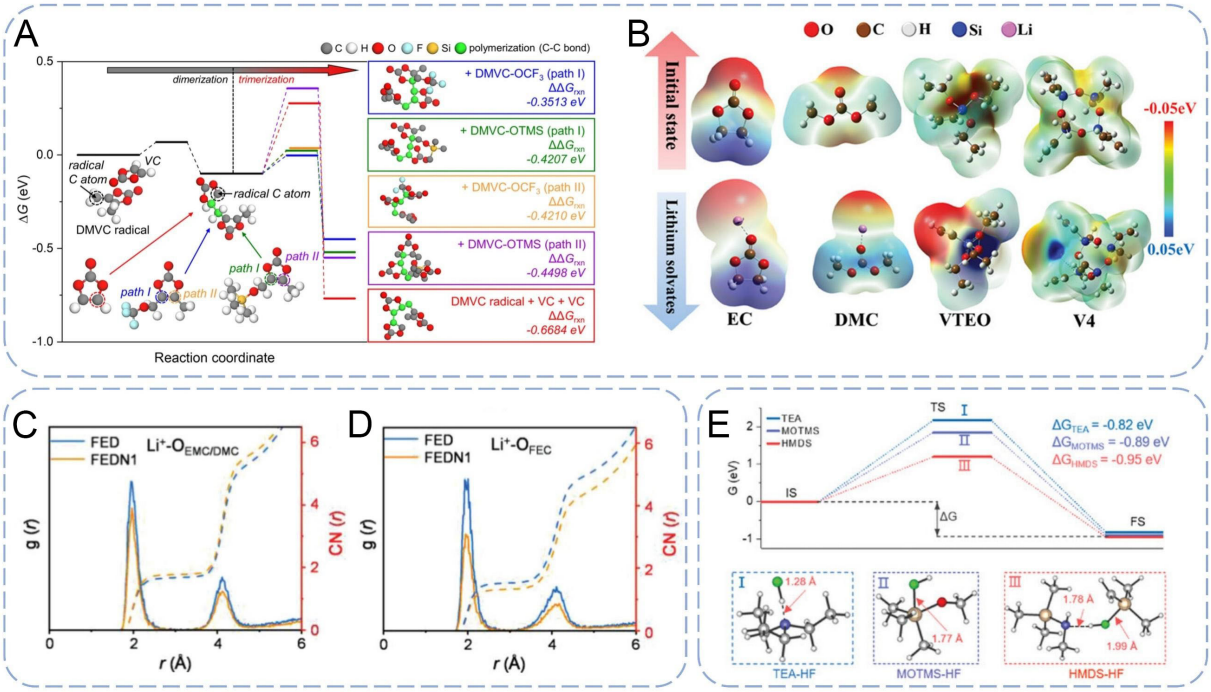

Figure 9. (A) Relative Gibbs free energy (ΔG) calculated at 1 atm and 298 K; Figure 9A is reprinted with permission from Ref.[222]. Copyright © 2021 Springer Nature, under CC BY 4.0 license; (B) Electrostatic potential diagrams of EC, DMC, VTEO, and V4 before and after Li^+ solvation; Figure 9B is reprinted with permission from Ref.[258]. Copyright © 2024 Wiley; (C) RDFs and CNs of Li^+-$O_{EMC/DMC}$, and (d) Li^+-O_{FEC}; Figure 9C and D is reprinted with permission from Ref.[259]. Copyright © 2023 Wiley; (E) Reaction pathways of selected additives with HF and transition-state complexes; Figure 9E is reprinted with permission from Ref.[263]. Copyright © 2025 Wiley. VC: Vinylene carbonate; DMVC: dimethyl vinylene carbonate; EC: ethylene carbonate; DMC: dimethyl carbonate; VTEO: vinyltriethoxysilane; V4: 2,4,6,8-tetramethyl-2,4,6,8-tetravinylcyclotetrasiloxane; FED: FEC : EMC : DMC (2 : 4 : 4 by volume); EMC ethyl methyl carbonate; FEC: fluoroethylene carbonate; MOTMS: methoxytrimethylsilane; TS: transition state; FS: final state; TEA: triethylamine; MOTMS-HF: reaction paths of MOTMS additives with HF molecules; HMDS: heptamethyldisilazane; HF: hydrogen fluoride; RDF: radial distribution function.

function (RDF) profiles reveals that Li^+-$O_{EMC/DMC}$ coordination remained essentially unchanged after the addition of NTSA additive. In contrast, Li^+-O_{FEC} at 2.0 Å decreased markedly, with the corresponding coordination number declining from 1.53 to 1.32, indicating a reduction in the population of FEC molecules within the first solvation sheath[259,260]. Moreover, the probability of NTSA participating directly in the first solvation sheath was extremely low and almost negligible, which demonstrates that NTSA reduces the number of solvent molecules coordinating with Li^+ without altering the fundamental solvation structure. The reduced coordination number of Li^+ facilitates desolvation, thereby accelerating interfacial charge-transfer kinetics and improving electrochemical performance.

In liquid electrolytes, $LiPF_6$ is highly susceptible to hydrolysis by trace amounts of water, generating HF that progressively attacks the originally compact and uniform SEI. This corrosion process transforms the dense interphase into a porous and mechanically fragile structure. Although the resulting LiF is chemically stable, its accumulation as nanoparticles produces a highly porous interfacial layer that is considerably less effective at passivating the anode surface than the original Li_2CO_3 layer[261,262]. Jiang *et al.* tackled SEI degradation induced by HF, a detrimental hydrolysis byproduct of $LiPF_6$[263]. They proposed an orbital contribution ratio (OCR)-based additive design strategy and identified heptamethyldisilazane (HMDS) as an effective HF-scavenging additive. As shown in Figure 9E, HMDS exhibits the lowest Gibbs free-energy change for reaction with HF, outperforming triethylamine (TEA) and methoxytrimethylsilane (MOTMS), thereby validating the

orbital-matching rule governing HF elimination. Cells employing HMDS retained 80% capacity after 2,528 cycles.

Supporting component

A critical strategy for enhancing the preferential reduction of anions is the rational regulation and molecular design of solvent solvating ability. Wang *et al.* exploited the conjugative interaction between the vacant 3d orbitals of Si and lone electron pairs on adjacent oxygen atoms to weaken Li^+-solvent interactions [Figure 10A][264]. ESP analysis of siloxanes revealed that increasing methoxy substitution delocalizes the negative charge distribution, which spatially redistributes Li^+ binding sites and further weakens Li^+-solvent coordination. When paired with LiFSI, TMOS (tetramethyl orthosilicate) promotes the formation of LiF and Si-O species in the SEI, reducing interfacial resistance and enabling rapid Li^+ conduction. Furthermore, Chen *et al.* demonstrated the weak-solvation characteristics of siloxane-based electrolytes[265]. The intrinsic electrochemical stability of the siloxane solvent was further validated by the frontier molecular orbital theory and bond energy decomposition analysis. AIMD simulations were performed to elucidate the decomposition mechanism of siloxane solvents on the Li surface [Figure 10B]. The designed solvent molecule, 2,2-dimethoxypropane (DDS), decomposes on the Li metal surface, generating species such as CH_3 and $SiO(CH_3)_2(OCH_3)$[249]. These decomposition products contain Si-O moieties, which contribute to the formation of a stable interfacial layer on the Li metal anode, thereby enhancing the stability of the electrode-electrolyte interphase. Similarly, Wang *et al.* designed a trimethylsilane (TMMS)-based solvent incorporating Si-O bonds and methyl groups, which exhibited excellent electrochemical performance [Figure 10C][266]. The weak solvating ability of TMMS facilitates the formation of an anion-rich solvation structure, thereby promoting the construction of inorganic-rich interphases on both the cathode and anode. Moreover, the TMMS-based electrolyte demonstrated excellent oxidation stability, enabling stable cycling in NCM811||Li full cells at a high voltage of 4.5 V. Notably, the cell maintained a high CE of 99.8% after 85 cycles. Beyond Si-O conjugation, hyperconjugation arising from interactions between σ-bonds (e.g., C-H, C-C) and adjacent π or vacant orbitals (e.g., p orbitals) also regulates the solvation structure through localized electron delocalization. Based on this concept, Zhu*et al.* proposed a fluorine-free cyclic ether solvent, 2-methoxy-1,3-dioxolane (MODOL), for LMAs[267]. As illustrated in Figure 10D, the non-bonding hybrid orbitals introduced by the methoxy oxygen partially overlap with those of the ring oxygen atoms, inducing hyperconjugation that delocalizes lone-pair electrons. This electronic modulation, together with the steric hindrance introduced by the methoxy substituent, limited Li^+ coordination numbers, endowing MODOL with weak solvating ability and excellent compatibility with Li metal. TOF-SIMS and XPS analyses confirmed that MODOL promotes an anion-dominated solvation structure, leading to the formation of a uniform, inorganic-rich SEI.

Beyond molecular structure engineering, regulating intermolecular interactions among solvents has emerged as another effective modification strategy for constructing robust SEI. Wang *et al.* demonstrated that solvent-solvent interactions can regulate orbital energy gaps, thereby enhancing the reduction stability of electrolytes[268]. This effect is particularly evident in long-chain multidentate ligands, using 1,1,1,3,3-pentafluorobutane (PFB) and TTE to anchor G2 molecules[269]. PFB anchors G2 through the interactions between $F^{\delta-}$ (PFB) and $H^{\delta+}$ (G2) [Figure 10E], which stretch the glyme chain and induce a conformational transition from D3 to D2, which enhances its coordination with anions and Li^+. The ^{17}O-NMR spectra [Figure 10F] showed a downfield shift in G2 oxygen signals, indicating reduced electron density. TTE further anchors exposed G2 oxygen sites through interactions between $O^{\delta-}$ in TTE and $H^{\delta+}$ in G2, thereby enhancing the oxidation stability of the glyme electrolyte. Consequently, full cells employing this electrolyte exhibited excellent cycling stability.

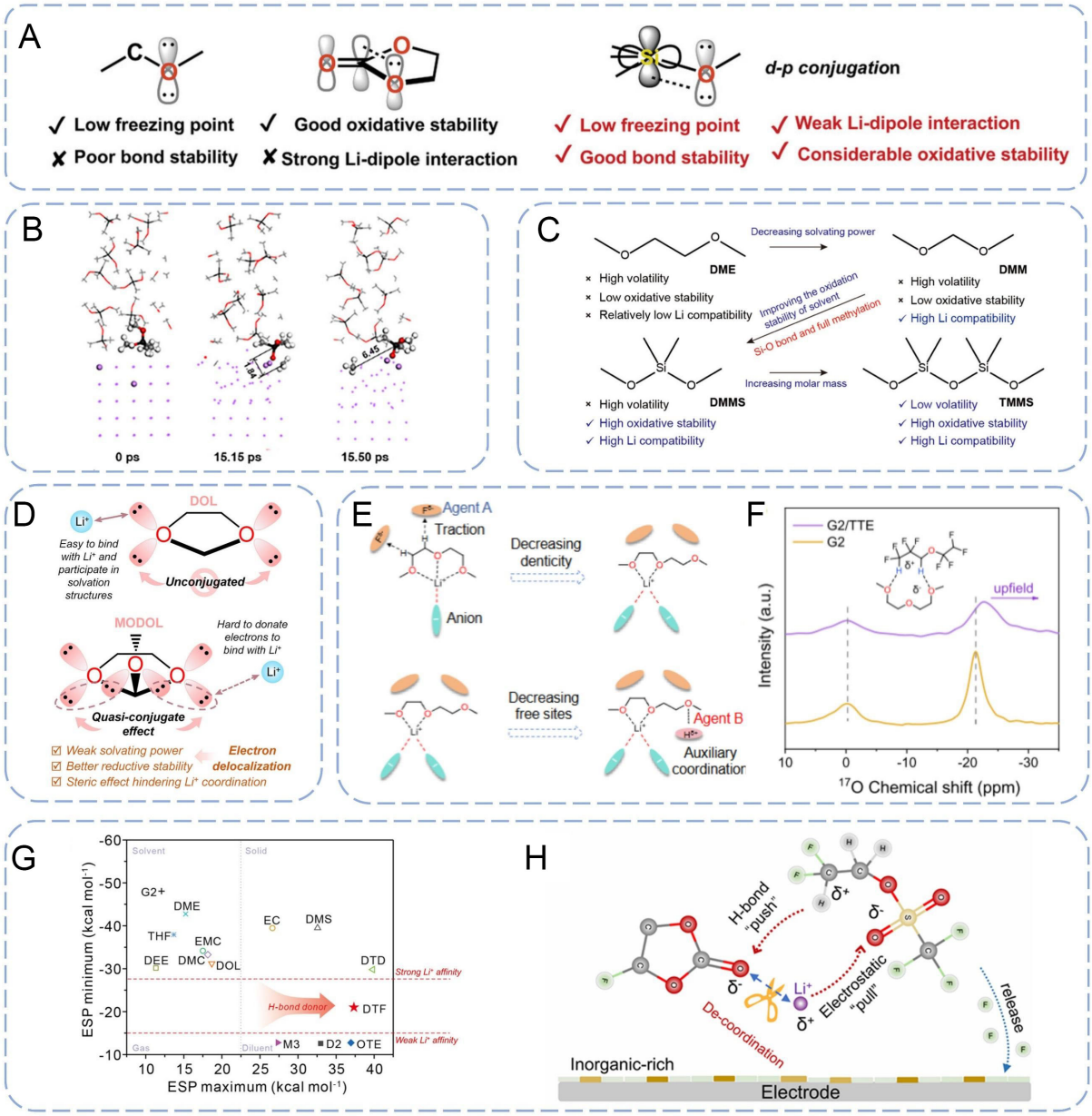

Figure 10. (A) Structures and properties of typical carbonate and ether solvents, along with the bonding structures and properties of siloxane solvents; Figure 10A is reprinted with permission from Ref.[264]. Copyright © 2025 Wiley; (B) AIMD simulation of the DDS decomposition process of siloxanes on the lithium (110) surface; Figure 10B is reprinted with permission from Ref.[265]. Copyright © 2025 Wiley; (C) Design strategy of a Si-containing solvent; Figure 10C is reprinted with permission from Ref.[266]. Copyright © 2025 American Chemical Society; (D) Schematic illustration of MODOL molecule design; Figure 10D is reprinted with permission from Ref.[267]. Copyright © 2025 Wiley; (E) Dual-anchoring design strategy for the synergistic effect of two anchoring agents; (F) Comparison of ^{17}O- NMR spectra between G2 and G2/TTE; Figure 10E and F is reprinted with permission from Ref.[269]. Copyright © 2025 Wiley; (G) Design strategy for electrolytes; (H) Schematic illustration of the "push-pull" mechanism; Figure 10G and H is reprinted with permission from Ref.[272]. Copyright © 2024 American Chemical Society. DME: Dimethyl ether; DMM: dimethoxymethane; DMMS: dimethyldimethoxysilane; TMMS: trimethylsilane; DOL: 1,3-dioxolane; MODOL: 2-methoxy-1,3-dioxolane; TTE: 1,1,2,2-tetrafluoroethyl-2,2,3,3-tetrafluoropropyl ether; THF: tetrahydrofuran; ESP: electrostatic potential; DEE: 1,2-diethoxyethane; DMC: dimethyl carbonate; EC: 1,2-diethoxyethane; DMS: dimethyl sulfite; DTD: 1,3,2-Dioxathiolane-2,2-dioxide; DTF: 2,2-difluoroethyl triflate; OTE: 1,1,2,2-Tetrafluoroethyl-2,2,2-trifluoroethyl ether; DDS: 2,2-dimethoxypropane; AIMD: Ab initio molecular dynamics; NMR: nuclear magnetic resonance spectroscopy.

Similarly, Li *et al.* regulated solvation by introducing hydrogen bonding interactions between DME and 2,2,2-trifluoroethyl trifluoromethanesulfonate (TFST)[270]. These intermolecular interactions weakened DME-Li^+ coordination, promoted anions participation in the first solvation sheath, and facilitated the formation of

AGG clusters, ultimately leading to the construction of inorganic-rich SEI/CEI. Depth-profiling analysis XPS revealed persistently high LiF content throughout the SEI formed from TFST/DME. Consequently, Li||NCM811 cells exhibited > 80% capacity retention and 99.8% average CE over 230 cycles. In another approach, a non-coordinating cyclic fluorinated ether diluent, 3,3,4,4-tetrafluorotetrahydrofuran (TFTHF), was introduced as a diluent into the DME[270]. Dipole-dipole interactions between C-F and H-C dipole weakened Li^+-DME coordination while strengthening Li^+-anion interactions. Consequently, the electrolyte exhibited an increased Li^+ transference number and facilitated the formation of an anion-derived SEI. XPS and cryo-TEM analyses further revealed that sequential reduction of $DFOB^-$ and BF_4^- produced a thin bilayer SEI, consistent with the difference in their reduction potentials. Li||NCM811 full cells employing TFTHF retained 80% capacity after 600 cycles, surpassing BTFE- and TTE-based electrolyte systems.

Beyond thermodynamic regulation of solvation structures, the kinetics of Li^+ desolvation plays a decisive role in governing interfacial reaction kinetics and activation barriers. To simultaneously accelerate interfacial kinetics and suppress solvent decomposition in LMAs, Ma *et al.* proposed a molecular-docking electrolyte (MDE) strategy based on intermolecular hydrogen-bond regulation[271]. Neither the latent solvents (e.g., BTP, BTE) nor inducers (e.g., fluorinated benzenes, halogenated alkanes) are individually capable of dissolving Li salts. However, hydrogen bonds interactions ($F^{\delta-}$-$H^{\delta+}$ or $H^{\delta+}$-$O^{\delta-}$) enable effective salt dissociation while providing low desolvation energies. The intermolecular interactions induce conformational rearrangement of the solvent molecules, enabling the latent solvents to effectively coordinate Li^+. Meanwhile, these interactions establish an energetically favorable solvation/desolvation process that significantly lowers the desolvation energy, a feature unattainable in conventional strongly solvating electrolytes. Furthermore, the dynamically regulated desolvation process facilitates Li^+-anion pairing, leading to the formation of an anion-derived SEI. The resulting SEI effectively suppresses continuous parasitic reactions of the MDE at the electrode interfaces.

Building upon desolvation-controlled kinetics, Cui *et al.* developed a "push-pull" electrolyte strategy to accelerate Li^+ desolvation[272]. Through molecular ESP screening, 2,2-difluoroethyl triflate (DTF) was identified as an optimal co-solvent for LiFSI-EMC/FEC. The moderate ESP_{min} of DTF attracts Li^+, whereas the difluoromethyl group, characterized by high ESP_{max}, competitively forms hydrogen bonds with coordinated solvent molecules [Figure 10G]. This complementary "push-pull" effect weakens Li^+-solvent coordination, reorganizes interfacial interactions, and substantially accelerates Li^+ desolvation [Figure 10H]. The accelerated desolvation kinetics effectively suppress unnecessary solvent decomposition at electrode surfaces, enabling high CE and long cycle life.

CONCLUSION

This review focuses on the regulation of the composition and structure of the SEI via rational electrolyte design. From a functional perspective, electrolyte components can be categorized into two types: sacrificial components (lithium salt anions and additives) and supporting components, namely solvents. These two categories do not function independently but operate in a highly coupled manner. The solvation structure established by the supporting components governs the coordination configuration of Li^+, thereby regulating the reduction priority and the interfacial reactivity of the sacrificial components. Representative strategies include introducing diluents to increase the proportion of anions in the first solvation sheath; enhancing anion reduction priority through fluorination to introduce electron-withdrawing effects or methylation to generate steric hindrance; developing multifunctional sacrificial components that simultaneously regulate solvation structure and promote robust SEI formation, thereby further improving the electrochemical stability of Si anodes.

The development of electrolytes for Si anodes should also draw extensively upon established design principles demonstrated in Si/C-based or Li metal-based battery systems. Research on supporting components should emphasize regulating the solvation structure to increase the proportion of effective sacrificial components. The solvation capability is governed by mechanisms ranging from intramolecular electronic regulation (e.g., conjugation-induced delocalization) to intermolecular engineering (e.g., topological design, molecular interactions, and desolvation kinetics). These strategies collectively weaken solvent coordination with Li^+, thereby suppressing excessive participation in interfacial reactions. The design of sacrificial components has evolved from a conventional focus on SEI formation mechanisms toward a deeper understanding of their behavior within the solvation sheath. This includes elucidating how intrinsic anion properties influence solvation capability and how anion-solvent interactions regulate the overall solvation structure. Meanwhile, the role of electrolyte additives has evolved from single-function SEI formation to multifunctional interfacial regulation.

CHALLENGE AND OUTLOOK

Currently, the design and development of electrolytes for Si anodes face the following scientific challenges and engineering bottlenecks:

(1) The trade-off between ionic conductivity and SEI stability. Owing to high mechanical modulus and excellent chemical stability, an inorganic-rich SEI provides effective interfacial passivation and mechanical protection for Si anodes. It can be constructed by tailoring the first solvation sheath of Li^+ ions through the use of weakly solvating solvents, (localized) high-concentration electrolytes, or sacrificial additives that undergo preferential reduction in the electrolyte. However, high salt concentrations and weakly solvating solvents inevitably increase electrolyte costs while suppressing lithium salt dissociation, thereby compromising ionic conductivity. Conversely, employing high DC solvents to promote salt dissociation, increases solvent molecule participation in the first solvation sheath of Li^+ and results in a solvent-derived organic-rich SEI. Although sacrificial additives preferentially decompose on Si anodes to construct inorganic-rich SEIs, their continuous consumption limits their ability to participate in the SEI regeneration. Therefore, achieving fast ionic transport while maintaining a continuously stable SEI remains a major challenge for future electrolyte design.

(2) Challenges in characterization techniques for the SEI on Si anodes. The drastic volume change exceeding 300% during repeated lithiation/delithiation continuously induces SEI fracture and regeneration. Conventional ex-situ characterization techniques (e.g., SEM, XPS, Cryo-TEM) provide only static snapshots outside electrochemical cycling and are highly susceptible to secondary reactions with trace air or moisture during sample transfer, making it difficult to accurately capture the dynamic evolution of the SEI. Moreover, the SEI on Si anodes is chemically complex and spatially heterogeneous, making it difficult for any single characterization technique to simultaneously resolve its chemical composition, multilayered structure, and spatial distribution. Although *in-situ* characterization techniques, such as *in-situ* TEM, *in-situ* Raman and *in-situ* IR, enable dynamic observations, they remain limited by specialized cell configurations, electron beam damage, and challenges in signal interpretation. Collectively, these limitations have hindered a comprehensive understanding of the SEI failure mechanisms on Si anodes, highlighting the urgent need for synergistic *in-situ* characterization strategies in the near future.

(3) Industrial cost dilemma. Currently, most high-performance electrolyte systems rely heavily on high-concentration lithium salts, fluorinated solvents, and fluorinated additives. However, supply-chain constraints associated with fluorinated fine chemicals, together with the high cost of concentrated lithium salts, may substantially compromise the economic viability of large-scale commercialization. More critically, electrolyte technologies remain highly diversified. From high-concentration to localized high-concentration

electrolytes, and from fluorinated carbonates to emerging weakly coordinating solvents, no consensus has yet been established regarding an industrially viable electrolyte platform. This technological fragmentation has significantly delayed the translation of laboratory advances into scalable manufacturing and product commercialization. Furthermore, substantial differences among various routes in viscosity, wettability, volatility, and processing characteristics require distinct manufacturing equipment and processing conditions. Consequently, the coexistence of multiple competing technological routes increases the uncertainty associated with equipment investments and manufacturing planning, thereby hindering industrial deployment.

Future electrolyte design for Si anodes is expected to integrate Artificial Intelligence (AI)-driven molecular engineering with macroscopic electrode structural optimization. With the improvement of computational capability, integrating computational modeling to accurately predict the influence of fluorination sites on orbital energy levels will become an important direction for balancing high-voltage stability with interfacial film-forming capability. Such a molecular-level digital design will gradually replace conventional trial-and-error methods, enabling the rapid identification of solvent and additive molecular structures. Moreover, solvent and additive molecular frameworks that simultaneously combine structural flexibility with intrinsically high DC are expected to simultaneously satisfy the requirement for moderate Li^+ coordination in weakly solvating electrolytes while maintaining a sufficiently polar environment for efficient lithium salt dissociation. Achieving this balance may provide a rational route to overcoming the intrinsic trade-off between ionic conductivity and the formation of a stable anion-derived SEI.

Electrolyte development should be coupled with the macroscopic structural engineering of Si anodes. Specifically, electrolyte design needs to be tailored for Si electrodes with different porosities, particle size distributions, and electrode thickness. Future electrolyte systems are expected to construct gradient interphase layers that evolve continuously from the bulk solution to the electrode surface through molecular design, thereby mitigating the interfacial stress generated by the drastic volume expansion of Si particles. Meanwhile, to address the low ICE of Si anodes, electrolytes should exhibit excellent wettability and low contact angles to penetrate the nanoscale gaps between Si particles. Controlled prelithiation strategies, including sacrificial or activatable Li sources that compensate for the irreversible active-Li loss, should also be further developed.

Furthermore, systematic investigations should be conducted to evaluate electrolyte adaptability under practical operating conditions, including wide-temperature-range charge/discharge performance, high-rate capability, and safety under extreme abuse conditions. Their practical feasibility should be validated in Ah-level cells or pouch-cell configurations to bridge the gap between laboratory studies and practical applications. Accordingly, electrolyte design should simultaneously ensure chemical and electrochemical compatibility with all key battery components, such as anodes, cathodes, separators, and current collectors. Only through such synergistic optimization and comprehensive system-level integration can a solid foundation be established for the long-term stable cycling and commercial viability of Si anodes, ultimately accelerating the transition of high-energy-density batteries from laboratory research to large-scale commercialization.

DECLARATIONS

Authors' contributions

Conceived the idea of this manuscript: Bayaguud, A.
Wrote the manuscript: Chen, Y.
Supervised and guided the academic expression of this work: Liu, H.; Bayaguud, A.; Wu, C.
Assisted in the collection of literature: Duan, A.
Further revised the logic, grammar, and professionalism of the manuscript: Liu, H.; Xu, Z.; Cao, J.; Wu, C.

Availability of data and materials

Not applicable.

AI and AI-assisted tools statement

Not applicable.

Financial support and sponsorship

This work was financially supported by the National Key R&D Program of China (2023YFB2405800), the Natural Science Foundation of Inner Mongolia Autonomous Region of China (2025MS02004), First-Class Discipline Scientific Research Special Project (YLXKZX-NGD-002), Science and Technology Planning Project of Hohhot (2023RC-LianHeTi-5), and Provincial-Level Scientific Research Support Project for Introduced Talents in Inner Mongolia (BJ2025003).

Conflicts of interest

All authors declared that there are no conflicts of interest.

Ethical approval and consent to participate

Not applicable.

Consent for publication

Not applicable.

REFERENCES

1. Mao, M.; Gong, L.; Wang, X.; et al. Electrolyte design combining fluoro- with cyano-substitution solvents for anode-free Li metal batteries. *Proc. Natl. Acad. Sci. U.S.A.* **2024**, *121*, e2316212121. DOI PubMed PMC
2. Du, H.; Wang, Y.; Kang, Y.; et al. Side reactions/changes in lithium-ion batteries: mechanisms and strategies for creating safer and better batteries. *Adv. Mater.* **2024**, *36*, 2401482. DOI
3. Cai, W.; Deng, Y.; Deng, Z.; et al. Quasi-localized high-concentration electrolytes for high-voltage lithium metal batteries. *Adv. Energy. Mater.* **2023**, *13*, 2301396. DOI
4. Chen, L.; Zhang, Q.; Song, C.; et al. A "flexible" solvent molecule enabling high-performance lithium metal batteries. *Angew. Chem. Int. Ed.* **2025**, *64*, e202422791. DOI
5. Fan, X.; Chen, L.; Borodin, O.; et al. Non-flammable electrolyte enables Li-metal batteries with aggressive cathode chemistries. *Nat. Nanotechnol.* **2018**, *13*, 715-22. DOI
6. Feng, K.; Li, M.; Liu, W.; et al. Silicon-based anodes for lithium-ion batteries: from fundamentals to practical applications. *Small* **2018**, *14*, 1702737. DOI
7. Mahajani, V.; Koratkar, N. Toward practical alloy anode based solid state batteries. *Small* **2023**, *21*, 2306388. DOI
8. Sun, L.; Liu, Y.; Shao, R.; Wu, J.; Jiang, R.; Jin, Z. Recent progress and future perspective on practical silicon anode-based lithium ion batteries. *Energy. Storage. Mater.* **2022**, *46*, 482-502. DOI
9. Chan, C. K.; Peng, H.; Liu, G.; et al. High-performance lithium battery anodes using silicon nanowires. *Nat. Nanotechnol.* **2007**, *3*, 31-5. DOI
10. Su, X.; Wu, Q.; Li, J.; et al. Silicon-based nanomaterials for lithium-ion batteries: a review. *Advanced. Energy. Mater.* **2013**, *4*, 1300882. DOI
11. Kim, N.; Kim, Y.; Sung, J.; Cho, J. Issues impeding the commercialization of laboratory innovations for energy-dense Si-containing lithium-ion batteries. *Nat. Energy.* **2023**, *8*, 921-33. DOI
12. Guo, J.; Dong, D.; Wang, J.; et al. Silicon-based lithium ion battery systems: stat-of-the-art from half and full cell viewpoint. *Adv. Funct. Mater.* **2021**, *31*, 2102546. DOI
13. Xiao, J.; Shi, F.; Glossmann, T.; Burnett, C.; Liu, Z. From laboratory innovations to materials manufacturing for lithium-based batteries. *Nat. Energy.* **2023**, *8*, 329-39. DOI
14. Sung, J.; Kim, N.; Ma, J.; et al. Subnano-sized silicon anode via crystal growth inhibition mechanism and its application in a prototype battery pack. *Nat. Energy.* **2021**, *6*, 1164-75. DOI
15. Han, X.; Gu, L.; Sun, Z.; et al. Manipulating charge-transfer kinetics and a flow-domain LiF-rich interphase to enable high-performance microsized silicon-silver-carbon composite anodes for solid-state batteries. *Energy. Environ. Sci.* **2023**, *16*, 5395-408. DOI

16. Zhang, Y.; Tang, W.; Gao, H.; et al. Monolithic layered silicon composed of a crystalline-amorphous network for sustainable lithium-ion battery anodes. *ACS. Nano.* **2024**, *18*, 15671-80. DOI
17. Wang, F.; Mao, J.; Zhao, Y. Crystal engineering of silica anode achieving intrinsic zero-strain. *Adv. Mater.* **2023**, *35*, 2307908. DOI
18. Liu, L.; Zhang, Y.; Xue, N.; et al. Mitigation of volumetric expansion in silicon anodes via engineered porosity: electrochemical performances and stress distribution implication. *Energy. Tech.* **2024**, *12*, 2400664. DOI
19. Zhang, Z.; Ma, X.; Li, Y.; et al. Highly ion-conductive Si Anode binder with optimized tensile strength and large deformation for lithium-ion batteries. *ACS. Appl. Mater. Interfaces.* **2025**, *17*, 43034-47. DOI
20. Ramdhiny, M. N.; Jeon, J. W. Design of multifunctional polymeric binders in silicon anodes for lithium-ion batteries. *Carbon. Energy.* **2023**, *6*, e356. DOI
21. Jang, W.; Kim, S.; Kang, Y.; Yim, T.; Kim, T. A high-performance self-healing polymer binder for Si anodes based on dynamic carbon radicals in cross-linked poly(acrylic acid). *Chem. Eng. J.* **2023**, *469*, 143949. DOI
22. Liu, T.; Dong, T.; Wang, M.; et al. Recycled micro-sized silicon anode for high-voltage lithium-ion batteries. *Nat. Sustain.* **2024**, *7*, 1057-66. DOI
23. Li, A.; Wang, Z.; Lee, T.; et al. Asymmetric electrolyte design for high-energy lithium-ion batteries with micro-sized alloying anodes. *Nat. Energy.* **2024**, *9*, 1551-60. DOI
24. Yang, Y.; Li, Z.; Zhang, M.; et al. Electrolyte chemistry modulation toward high-performance and ultralow-temperature silicon anode. *Adv. Mater.* **2025**, *37*, 2417981. DOI
25. Ko, M.; Chae, S.; Ma, J.; et al. Scalable synthesis of silicon-nanolayer-embedded graphite for high-energy lithium-ion batteries. *Nat. Energy.* **2016**, *1*, 16113. DOI
26. Quan, L.; Su, Q.; Lei, H.; et al. Integrated prelithiation and SEI engineering for high-performance silicon anodes in lithium-ion batteries. *Natl. Sci. Rev.* **2025**, *12*, nwaf084. DOI PubMed PMC
27. Huo, H.; Jiang, M.; Bai, Y.; et al. Chemo-mechanical failure mechanisms of the silicon anode in solid-state batteries. *Nat. Mater.* **2024**, *23*, 543-51. DOI PubMed PMC
28. Zhang, Y.; Du, N.; Yang, D. Designing superior solid electrolyte interfaces on silicon anodes for high-performance lithium-ion batteries. *Nanoscale* **2019**, *11*, 19086-104. DOI
29. Khan, M.; Yan, S.; Ali, M.; et al. Innovative solutions for high-performance silicon anodes in lithium-ion batteries: overcoming challenges and real-world applications. *Nano-Micro. Lett.* **2024**, *16*, 179. DOI PubMed PMC
30. Yang, G.; Browning, K.; Meyer, H. M.; et al. Mitigating calendar aging in Si-NMC batteries with advanced dual-salt Glyme electrolytes. *Chem. Mater.* **2024**, *36*, 10902-11. DOI
31. Wu, H.; Chan, G.; Choi, J. W.; et al. Stable cycling of double-walled silicon nanotube battery anodes through solid-electrolyte interphase control. *Nat. Nanotechnol.* **2012**, *7*, 310-5. DOI
32. *Silicon Anode Systems for Lithium-Ion Batteries*; Elsevier, 2022. DOI
33. Li, Q.; Ruan, J.; Weng, S.; et al. Interphasial pre-lithiation and reinforcement of micro-Si anode through fluorine-free electrolytes. *Angew. Chem. Int. Ed.* **2023**, *62*, e202310297. DOI
34. Ko, Y.; Bae, J.; Chen, G.; et al. Topological considerations in electrolyte additives for passivating silicon anodes with hybrid solid-electrolyte interphases. *ACS. Energy. Lett.* **2024**, *9*, 3448-55. DOI
35. Wu, Y.; Feng, X.; Yang, M.; et al. Thermal runaway of nonflammable localized high-concentration electrolytes for practical $LiNi_{0.8}Mn_{0.1}Co_{0.1}O_2$|graphite-SiO pouch cells. *Adv. Sci.* **2022**, *9*, 2204059. DOI
36. Zhang, F.; Wang, Z.; Wang, L.; et al. Constructing a universal artificial polymeric ionic liquid interfacial film for graphite anode and High-Voltage cathode. *Chem. Eng. J.* **2022**, *435*, 135101. DOI
37. Mu, T.; Sun, Y.; Wang, C.; et al. Long-life silicon anodes by conformal molecular-deposited polyurea interface for lithium ion batteries. *Nano. Energy.* **2022**, *103*, 107829. DOI
38. Dey, A. Lithium anode film and organic and inorganic electrolyte batteries. *Thin. Solid. Films.* **1977**, *43*, 131-71. DOI
39. Peled, E. The electrochemical behavior of alkali and alkaline earth metals in nonaqueous battery systems - the solid electrolyte interphase model. *J. Electrochem. Soc.* **2019**, *126*, 2047-51. DOI
40. Nazri, G.; Muller, R. H. Composition of surface layers on Li electrodes in PC, $LiClO_4$ of very low water content. *J. Electrochem. Soc.* **1985**, *132*, 2050-4. DOI
41. Aurbach, D.; Daroux, M. L.; Faguy, P. W.; Yeager, E. Identification of surface films formed on lithium in propylene carbonate solutions. *J. Electrochem. Soc.* **1987**, *134*, 1611-20. DOI
42. Kanamura, K.; Tamura, H.; Shiraishi, S.; Takehara, Z. I. XPS Analysis of lithium surfaces following immersion in various solvents containing $LiBF_4$. *J. Electrochem. Soc.* **1995**, *142*, 340-7. DOI

43. Edström, K.; Herstedt, M.; Abraham, D. P. A new look at the solid electrolyte interphase on graphite anodes in Li-ion batteries. *J. Power. Sources.* **2006**, *153*, 380-4. DOI
44. Guo, K.; Kumar, R.; Xiao, X.; Sheldon, B. W.; Gao, H. Failure progression in the solid electrolyte interphase (SEI) on silicon electrodes. *Nano. Energy.* **2020**, *68*, 104257. DOI
45. Lee, C. H.; Dura, J. A.; Lebar, A.; Decaluwe, S. C. Direct, *operando* observation of the bilayer solid electrolyte interphase structure: Electrolyte reduction on a non-intercalating electrode. *J. Power. Sources.* **2019**, *412*, 725-35. DOI
46. Liu, Y.; Guo, K.; Wang, C.; Gao, H. Wrinkling and ratcheting of a thin film on cyclically deforming plastic substrate: Mechanical instability of the solid-electrolyte interphase in Li-ion batteries. *J. Mech. Phys. Solids.* **2019**, *123*, 103-18. DOI
47. Besenhard, J.; Winter, M.; Yang, J.; Biberacher, W. Filming mechanism of lithium-carbon anodes in organic and inorganic electrolytes. *J. Power. Sources.* **1995**, *54*, 228-31. DOI
48. Peled, E.; Golodnitsky, D.; Ardel, G. Advanced model for solid electrolyte interphase electrodes in liquid and polymer electrolytes. *J. Electrochem. Soc.* **1997**, *144*, L208-10. DOI
49. Aurbach, D.; Weissman, I.; Zaban, A.; Chusid, O. Correlation between surface chemistry, morphology, cycling efficiency and interfacial properties of Li electrodes in solutions containing different Li salts. *Electrochim. Acta.* **1994**, *39*, 51-71. DOI
50. Aurbach, D.; Markovsky, B.; Shechter, A.; Ein-Eli, Y.; Cohen, H. A Comparative study of synthetic graphite and Li electrodes in electrolyte solutions based on ethylene carbonate-dimethyl carbonate mixtures. *J. Electrochem. Soc.* **1996**, *143*, 3809-20. DOI
51. Aurbach, D.; Gofer, Y.; Ben-Zion, M.; Aped, P. The behaviour of lithium electrodes in propylene and ethylene carbonate: Te major factors that influence Li cycling efficiency. *J. Electroanal. Chem.* **1992**, *339*, 451-71. DOI
52. Goodenough, J. B.; Kim, Y. Challenges for rechargeable Li batteries. *Chem. Mater.* **2010**, *22*, 587-603. DOI
53. Yan, C.; Li, H.; Chen, X.; et al. Regulating the inner Helmholtz plane for stable solid electrolyte interphase on lithium metal anodes. *J. Am. Chem. Soc.* **2019**, *141*, 9422-9. DOI
54. Wang, Z.; Sun, Z.; Li, J.; et al. Insights into the deposition chemistry of Li ions in nonaqueous electrolyte for stable Li anodes. *Chem. Soc. Rev.* **2021**, *50*, 3178-210. DOI
55. Chekushkin, P. M.; Merenkov, I. S.; Smirnov, V. S.; Kislenko, S. A.; Nikitina, V. A. The physical origin of the activation barrier in Li-ion intercalation processes: the overestimated role of desolvation. *Electrochim. Acta.* **2021**, *372*, 137843. DOI
56. Xiao, P.; Yun, X.; Chen, Y.; et al. Insights into the solvation chemistry in liquid electrolytes for lithium-based rechargeable batteries. *Chem. Soc. Rev.* **2023**, *52*, 5255-316. DOI
57. Goodenough, J. B.; Park, K. The Li-ion rechargeable battery: a perspective. *J. Am. Chem. Soc.* **2013**, *135*, 1167-76. DOI
58. Wang, A.; Kadam, S.; Li, H.; Shi, S.; Qi, Y. Review on modeling of the anode solid electrolyte interphase (SEI) for lithium-ion batteries. *npj. Comput. Mater.* **2018**, *4*, 15. DOI
59. Zhao, Q.; Stalin, S.; Archer, L. A. Stabilizing metal battery anodes through the design of solid electrolyte interphases. *Joule* **2021**, *5*, 1119-42. DOI
60. Hou, C.; Han, J.; Liu, P.; et al. *Operando* observations of SEI film evolution by mass-sensitive scanning transmission electron microscopy. *Adv. Energy. Mater.* **2019**, *9*, 1902675. DOI
61. Chen, Z.; Soltani, A.; Chen, Y.; et al. Emerging organic surface chemistry for Si anodes in lithium-ion batteries: advances, prospects, and beyond. *Adv. Energy. Mater.* **2022**, *12*, 2200924. DOI
62. He, Y.; Jiang, L.; Chen, T.; et al. Progressive growth of the solid-electrolyte interphase towards the Si anode interior causes capacity fading. *Nat. Nanotechnol.* **2021**, *16*, 1113-20. DOI
63. Tripathi, A. M.; Su, W.; Hwang, B. J. *In situ* analytical techniques for battery interface analysis. *Chem. Soc. Rev.* **2018**, *47*, 736-851. DOI
64. Moeremans, B.; Cheng, H. W.; Merola, C.; et al. *In situ* mechanical analysis of the nanoscopic solid electrolyte interphase on anodes of Li-ion batteries. *Adv. Sci.* **2019**, *6*, 1900190. DOI
65. Chon, M. J.; Sethuraman, V. A.; Mccormick, A.; Srinivasan, V.; Guduru, P. Real-time measurement of stress and damage evolution during initial lithiation of crystalline silicon. *Meet. Abstr.* **2011**, *MA2011-02*, 1336. DOI
66. Nie, M.; Abraham, D. P.; Chen, Y.; Bose, A.; Lucht, B. L. Silicon solid electrolyte interphase (SEI) of lithium ion battery characterized by microscopy and spectroscopy. *J. Phys. Chem. C.* **2013**, *117*, 13403-12. DOI
67. Choi, N.; Yew, K. H.; Lee, K. Y.; Sung, M.; Kim, H.; Kim, S. Effect of fluoroethylene carbonate additive on interfacial properties of silicon thin-film electrode. *J. Power. Sources.* **2006**, *161*, 1254-9. DOI
68. Parimalam, B. S.; Lucht, B. L. Reduction reactions of electrolyte salts for lithium ion batteries: $LiPF_6$, $LiBF_4$, LiDFOB, LiBOB, and LiTFSI. *J. Electrochem. Soc.* **2018**, *165*, A251-5. DOI
69. Chan, C. K.; Ruffo, R.; Hong, S. S.; Cui, Y. Surface chemistry and morphology of the solid electrolyte interphase on silicon nanowire lithium-ion battery anodes. *J. Power. Sources.* **2009**, *189*, 1132-40. DOI

70. Borodin, O.; Bedrov, D. Interfacial structure and dynamics of the lithium alkyl dicarbonate SEI components in contact with the lithium battery electrolyte. *J. Phys. Chem. C.* **2014**, *118*, 18362-71. DOI
71. Tasaki, K. Solvent decompositions and physical properties of decomposition compounds in Li-ion battery electrolytes studied by DFT calculations and molecular dynamics simulations. *J. Phys. Chem. B.* **2005**, *109*, 2920-33. DOI
72. Yang, Y.; Liu, X.; Dai, Z.; et al. *In situ* electrochemistry of rechargeable battery materials: status report and perspectives. *Adv. Mater.* **2017**, *29*, 1606922. DOI
73. Zheng, J.; Zheng, H.; Wang, R.; et al. 3D visualization of inhomogeneous multi-layered structure and Young's modulus of the solid electrolyte interphase (SEI) on silicon anodes for lithium ion batteries. *Phys. Chem. Chem. Phys.* **2014**, *16*, 13229-38. DOI
74. Yen, Y.; Chao, S.; Wu, H.; Wu, N. Study on solid-electrolyte-Interphase of Si and C-coated Si electrodes in lithium cells. *J. Electrochem. Soc.* **2009**, *156*, A95. DOI
75. Philippe, B.; Dedryvère, R.; Allouche, J.; et al. Nanosilicon electrodes for lithium-ion batteries: interfacial mechanisms studied by hard and soft X-ray photoelectron spectroscopy. *Chem. Mater.* **2012**, *24*, 1107-15. DOI
76. Cao, C.; Abate, I. I.; Sivonxay, E.; et al. Solid electrolyte interphase on native oxide-terminated silicon anodes for Li-ion batteries. *Joule* **2019**, *3*, 762-81. DOI
77. Cao, C.; Steinrück, H.; Shyam, B.; Stone, K. H.; Toney, M. F. *In situ* study of silicon electrode lithiation with X-ray reflectivity. *Nano. Lett.* **2016**, *16*, 7394-401. DOI
78. Kumar, R.; Lu, P.; Xiao, X.; Huang, Z.; Sheldon, B. W. Strain-induced lithium losses in the solid electrolyte interphase on silicon electrodes. *ACS. Appl. Mater. Interfaces.* **2017**, *9*, 28406-17. DOI
79. Kumar, R.; Tokranov, A.; Sheldon, B. W.; et al. *In situ* and operando investigations of failure mechanisms of the solid electrolyte interphase on silicon electrodes. *ACS. Energy. Lett.* **2016**, *1*, 689-97. DOI
80. Benitez, L.; Cristancho, D.; Seminario, J.; Martinez De La Hoz, J.; Balbuena, P. Electron transfer through solid-electrolyte-interphase layers formed on Si anodes of Li-ion batteries. *Electrochim. Acta.* **2014**, *140*, 250-7. DOI
81. Sang, X.; Hu, K.; Chen, J.; et al. Temperature-inert weakly solvating electrolytes for low-temperature lithium-ion batteries with micro-sized silicon anodes. *Angew. Chem. Int. Ed.* **2025**, *64*, e202500367. DOI
82. Cheng, K.; Tu, S.; Zhang, B.; et al. Material-electrolyte interfacial interaction enabling the formation of an inorganic-rich solid electrolyte interphase for fast-charging Si-based lithium-ion batteries. *Energy. Environ. Sci.* **2024**, *17*, 2631-41. DOI
83. Xu, C.; Jing, P.; Xia, P.; et al. Tailoring a multilayer fine-grained solid electrolyte interphase by pulse electrochemical activation maneuver for stable Si/C anodes. *Energy. Environ. Sci.* **2025**, *18*, 7060-70. DOI
84. Li, A.; Wang, Z.; Pollard, T. P.; et al. High voltage electrolytes for lithium-ion batteries with micro-sized silicon anodes. *Nat. Commun.* **2024**, *15*, 1206. DOI PubMed PMC
85. Mazur, P.; Markowski, L.; Grodzicki, M. Thermal stability of LiF thin films on 6H-SiC(0001) surface. *Vacuum* **2009**, *84*, 622-4. DOI
86. Bin Jassar, M.; Michel, C.; Abada, S.; et al. A Perspective on the molecular modeling of electrolyte decomposition reactions for solid electrolyte interphase growth in lithium-ion batteries. *Adv. Funct. Mater.* **2024**, *34*, 2313188. DOI
87. Zhang, W.; Zhang, N.; Wang, Z.; et al. Mechanistic understanding of interphase-driven ageing in silicon anodes. *Nat. Energy.* **2026**, *11*, 558-70. DOI
88. Wang, H.; Chew, H. B. Nanoscale mechanics of the solid electrolyte interphase on lithiated-silicon electrodes. *ACS. Appl. Mater. Interfaces.* **2017**, *9*, 25662-7. DOI
89. Mcbrayer, J. D.; Rodrigues, M. F.; Schulze, M. C.; et al. Calendar aging of silicon-containing batteries. *Nat. Energy.* **2021**, *6*, 866-72. DOI
90. Veith, G. M.; Doucet, M.; Sacci, R. L.; Vacaliuc, B.; Baldwin, J. K.; Browning, J. F. Determination of the Solid Electrolyte Interphase Structure Grown on a Silicon Electrode Using a Fluoroethylene Carbonate Additive. *Sci. Rep.* **2017**, *7*, 6326. DOI PubMed PMC
91. Key, B.; Bhattacharyya, R.; Morcrette, M.; Seznéc, V.; Tarascon, J.; Grey, C. P. Real-time NMR investigations of structural changes in silicon electrodes for lithium-ion batteries. *J. Am. Chem. Soc.* **2009**, *131*, 9239-49. DOI
92. Michan, A. L.; Leskes, M.; Grey, C. P. Voltage dependent solid electrolyte interphase formation in silicon electrodes: monitoring the formation of organic decomposition products. *Chem. Mater.* **2015**, *28*, 385-98. DOI
93. Liu, Z.; Lu, P.; Zhang, Q.; Xiao, X.; Qi, Y.; Chen, L. A bottom-up formation mechanism of solid electrolyte interphase revealed by isotope-assisted time-of-flight secondary ion mass spectrometry. *J. Phys. Chem. Lett.* **2018**, *9*, 5508-14. DOI
94. Xu, K. Nonaqueous liquid electrolytes for lithium-based rechargeable batteries. *Chem. Rev.* **2004**, *104*, 4303-418. DOI
95. Ren, K.; Li, Z.; Shen, X.; et al. Ion/dipole interactions in novel solvation structures for rechargeable batteries: a review. *Energy. Environ. Sci.* **2026**, *19*, 411-45. DOI
96. Seo, D. M.; Reininger, S.; Kutcher, M.; Redmond, K.; Euler, W. B.; Lucht, B. L. Role of mixed solvation and ion pairing in the solution structure of lithium ion battery electrolytes. *J. Phys. Chem. C.* **2015**, *119*, 14038-46. DOI

97. Chen, H.; Chen, K.; Luo, L.; et al. $LiNO_3$-based electrolytes via electron-donation modulation for sustainable nonaqueous lithium rechargeable batteries. *Angew. Chem. Int. Ed.* **2024**, *63*, e202316966. DOI
98. Luo, Z.; Hu, L.; Ye, Y.; et al. All-cyclic-solvent electrolyte design enables ultra-low-temperature and fast-charging sodium-ion batteries. *Angew. Chem. Int. Ed.* **2026**, *65*, e21433. DOI
99. Wu, S.; Liu, X.; Guo, M.; et al. Anion-induced bridged electrolyte design strategy mitigates capacity decay in lithium-sulfurized polyacrylonitrile batteries. *Angew. Chem. Int. Ed.* **2025**, *64*, e202517531. DOI
100. Su, C.; He, M.; Amine, R.; et al. Solvating power series of electrolyte solvents for lithium batteries. *Energy. Environ. Sci.* **2019**, *12*, 1249-54. DOI
101. Su, C. C.; He, M.; Amine, R.; Chen, Z.; Amine, K. The relationship between the relative solvating power of electrolytes and shuttling effect of lithium polysulfides in lithium-sulfur batteries. *Angew. Chem. Int. Ed.* **2018**, *57*, 12033-6. DOI
102. Su, C. C.; He, M.; Shi, J.; Amine, R.; Zhang, J.; Amine, K. Solvation rule for solid-electrolyte interphase enabler in lithium-metal batteries. *Angew. Chem. Int. Ed.* **2020**, *59*, 18229-33. DOI
103. Wu, Y.; Hu, Q.; Liang, H.; et al. Electrostatic potential as solvent descriptor to enable rational electrolyte design for lithium batteries. *Adv. Energy. Mater.* **2023**, *13*, 2300259. DOI
104. Wu, Z.; Li, R.; Zhang, S.; et al. Deciphering and modulating energetics of solvation structure enables aggressive high-voltage chemistry of Li metal batteries. *Chem* **2023**, *9*, 650-64. DOI
105. Zhang, H.; Li, R.; Chen, L.; et al. Simultaneous stabilization of lithium anode and cathode using hyperconjugative electrolytes for high-voltage lithium metal batteries. *Angew. Chem. Int. Ed.* **2023**, *62*, e202218970. DOI
106. Xu, Q.; Li, T.; Ju, Z.; et al. Li_2ZrF_6-based electrolytes for durable lithium metal batteries. *Nature* **2025**, *637*, 339-46. DOI
107. Tu, S.; Zhang, B.; Zhang, Y.; et al. Fast-charging capability of graphite-based lithium-ion batteries enabled by Li_3P-based crystalline solid-electrolyte interphase. *Nat. Energy.* **2023**, *8*, 1365-74. DOI
108. Liang, H.; Wang, L.; Song, Y.; et al. Manipulating ion transfer and interface stability by a bulk interphase framework for stable lithium metal batteries. *Adv. Funct. Mater.* **2023**, *33*, 2303077. DOI
109. Yoon, S. G.; Cavallaro, K. A.; Park, B. J.; Yook, H.; Han, J. W.; Mcdowell, M. T. Controlling solvation and solid-electrolyte interphase formation to enhance lithium interfacial kinetics at low temperatures. *Adv. Funct. Mater.* **2023**, *33*, 2302778. DOI
110. Qin, M.; Zeng, Z.; Wu, Q.; et al. Microsolvating competition in Li^+ solvation structure affording PC-based electrolyte with fast kinetics for lithium-ion batteries. *Adv. Funct. Mater.* **2024**, *34*, 2406357. DOI
111. Qin, M.; Liu, M.; Zeng, Z.; et al. Rejuvenating propylene carbonate-based electrolyte through nonsolvating interactions for wide-temperature Li-ions batteries. *Adv. Energy. Mater.* **2022**, *12*, 2201801. DOI
112. Tian, Y.; Tan, S.; Yang, C.; et al. Tailoring chemical composition of solid electrolyte interphase by selective dissolution for long-life micron-sized silicon anode. *Nat. Commun.* **2023**, *14*, 7247. DOI PubMed PMC
113. Tong, B.; Song, Z.; Wan, H.; et al. Sulfur-containing compounds as electrolyte additives for lithium-ion batteries. *InfoMat* **2021**, *3*, 1364-92. DOI
114. Chen, K.; Shen, X.; Luo, L.; et al. Correlating the solvating power of solvents with the strength of ion-dipole interaction in electrolytes of lithium-ion batteries. *Angew. Chem. Int. Ed.* **2023**, *62*, e202312373. DOI
115. Wang, J.; Luo, J.; Wu, H.; et al. Visualizing and regulating dynamic evolution of interfacial electrolyte configuration during de-solvation process on lithium-metal anode. *Angew. Chem. Int. Ed.* **2024**, *63*, e202400254. DOI
116. Lu, D.; Li, R.; Rahman, M. M.; et al. Ligand-channel-enabled ultrafast Li-ion conduction. *Nature* **2024**, *627*, 101-7. DOI
117. Gourdin, G.; Collins, J.; Zheng, D.; Foster, M.; Qu, D. Spectroscopic compositional analysis of electrolyte during initial SEI layer formation. *J. Phys. Chem. C.* **2014**, *118*, 17383-94. DOI
118. Schroder, K. W.; Dylla, A. G.; Harris, S. J.; Webb, L. J.; Stevenson, K. J. Role of surface oxides in the formation of solid-electrolyte interphases at silicon electrodes for lithium-ion batteries. *ACS. Appl. Mater. Interfaces.* **2014**, *6*, 21510-24. DOI
119. Shin, J.; Kim, T.; Lee, Y.; Cho, E. Key functional groups defining the formation of Si anode solid-electrolyte interphase towards high energy density Li-ion batteries. *Energy. Storage. Mater.* **2020**, *25*, 764-81. DOI
120. Soto, F.; Martinez De La Hoz, J.; Seminario, J.; Balbuena, P. Modeling solid-electrolyte interfacial phenomena in silicon anodes. *Curr. Opin. Chem. Eng.* **2016**, *13*, 179-85. DOI
121. Augustsson, A.; Herstedt, M.; Guo, J.; et al. Solid electrolyte interphase on graphite Li-ion battery anodes studied by soft X-ray spectroscopy. *Phys. Chem. Chem. Phys.* **2004**, *6*, 4185-9. DOI
122. Zhuang, G. V.; Xu, K.; Yang, H.; Jow, T. R.; Ross, P. N. Lithium ethylene dicarbonate identified as the primary product of chemical and electrochemical reduction of EC in 1.2 M $LiPF_6$/EC:EMC electrolyte. *J. Phys. Chem. B.* **2005**, *109*, 17567-73. DOI
123. Aurbach, D.; Levi, M. D.; Levi, E.; Schechter, A. Failure and stabilization mechanisms of graphite electrodes. *J. Phys. Chem. B.* **1997**, *101*, 2195-206. DOI

124. Yang, J.; Solomatin, N.; Kraytsberg, A.; Ein-Eli, Y. *In-situ* spectro-electrochemical insight revealing distinctive silicon anode solid electrolyte interphase formation in a lithium-ion battery. *ChemistrySelect* **2016**, *1*, 572-6. DOI
125. Andersson, A. M.; Edström, K. Chemical composition and morphology of the elevated temperature SEI on graphite. *J. Electrochem. Soc.* **2001**, *148*, A1100. DOI
126. Yamaguchi, K.; Domi, Y.; Usui, H.; Sakaguchi, H. Elucidation of the reaction behavior of silicon negative electrodes in a bis(fluorosulfonyl)amide-based ionic liquid electrolyte. *ChemElectroChem* **2017**, *4*, 3257-63. DOI
127. Shimizu, M.; Electrode Usui, H.; Suzumura, T.; Sakaguchi, H. Analysis of the deterioration mechanism of Si as a Li-ion battery anode using Raman microspectroscopy. *J. Phys. Chem. C.* **2015**, *119*, 2975-82. DOI
128. Dedryvère, R.; Martinez, H.; Leroy, S.; et al. Surface film formation on electrodes in a $LiCoO_2$/graphite cell: a step by step XPS study. *J. Power. Sources.* **2007**, *174*, 462-8. DOI
129. Zhang, Y.; Krishnamurthy, D.; Viswanathan, V. Engineering solid electrolyte interphase composition by assessing decomposition pathways of fluorinated organic solvents in lithium metal batteries. *J. Electrochem. Soc.* **2020**, *167*, 070554. DOI
130. Zafar Abbas Manj, R.; Zhang, F.; Ur Rehman, W.; Luo, W.; Yang, J. Toward understanding the interaction within silicon-based anodes for stable lithium storage. *Chem. Eng. J.* **2020**, *385*, 123821. DOI
131. Yoon, T.; Milien, M. S.; Parimalam, B. S.; Lucht, B. L. Thermal decomposition of the solid electrolyte interphase (SEI) on silicon electrodes for lithium ion batteries. *Chem. Mater.* **2017**, *29*, 3237-45. DOI
132. Ein-eli, Y.; Markovsky, B.; Aurbach, D.; Carmeli, Y.; Yamin, H.; Luski, S. The dependence of the performance of Li-C intercalation anodes for Li-ion secondary batteries on the electrolyte solution composition. *Electrochim. Acta.* **1994**, *39*, 2559-69. DOI
133. Koo, B.; Kim, H.; Cho, Y.; Lee, K. T.; Choi, N. S.; Cho, J. A highly cross-linked polymeric binder for high-performance silicon negative electrodes in lithium ion batteries. *Angew. Chem.* **2012**, *124*, 8892-7. DOI
134. Komaba, S.; Shimomura, K.; Yabuuchi, N.; Ozeki, T.; Yui, H.; Konno, K. Study on polymer binders for high-capacity SiO negative electrode of Li-ion batteries. *J. Phys. Chem. C.* **2011**, *115*, 13487-95. DOI
135. Tokranov, A.; Sheldon, B. W.; Li, C.; Minne, S.; Xiao, X. *In situ* atomic force microscopy study of initial solid electrolyte interphase formation on silicon electrodes for Li-ion batteries. *ACS. Appl. Mater. Interfaces.* **2014**, *6*, 6672-86. DOI
136. Leifer, N.; Smart, M. C.; Prakash, G. K. S.; et al. $_{13}$C solid state NMR suggests unusual breakdown products in sei formation on lithium ion electrodes. *J. Electrochem. Soc.* **2011**, *158*, A471-80. DOI
137. Gu, M.; Zhou, X.; Yang, Q.; et al. Anion-reinforced solvation structure enables stable operation of ether-based electrolyte in high-voltage potassium metal batteries. *Angew. Chem. Int. Ed.* **2024**, *63*, e202402946. DOI
138. Yin, Y.; Arca, E.; Wang, L.; et al. Nonpassivated silicon anode surface. *ACS. Appl. Mater. Interfaces.* **2020**, *12*, 26593-600. DOI
139. Yoon, I.; Larson, J. M.; Kostecki, R. The effect of the SEI layer mechanical deformation on the passivity of a Si anode in organic carbonate electrolytes. *ACS. Nano.* **2023**, *17*, 6943-54. DOI
140. Chen, Y.; Li, M.; Liu, Y.; et al. Origin of dendrite-free lithium deposition in concentrated electrolytes. *Nat. Commun.* **2023**, *14*, 2655. DOI PubMed PMC
141. Jiang, X.; Shi, X.; Yao, Y.; et al. Solid electrolyte interphase (SEI) for silicon anodes: from evolution to interface engineering and system-level optimization. *Energy. Storage. Mater.* **2026**, *88*, 105068. DOI
142. Tan, J.; Matz, J.; Dong, P.; Shen, J.; Ye, M. A growing appreciation for the role of LiF in the solid electrolyte interphase. *Adv. Energy. Mater.* **2021**, *11*, 2100046. DOI
143. Li, Y.; Qi, Y. Energy landscape of the charge transfer reaction at the complex Li/SEI/electrolyte interface. *Energy. Environ. Sci.* **2019**, *12*, 1286-95. DOI
144. Li, Z.; Chen, Y.; Yun, X.; Gao, P.; Zheng, C.; Xiao, P. Critical review of fluorinated electrolytes for high-performance lithium metal batteries. *Adv. Funct. Mater.* **2023**, *33*, 2300502. DOI
145. Jin, Y.; Le, P. M. L.; Gao, P.; et al. Low-solvation electrolytes for high-voltage sodium-ion batteries. *Nat. Energy.* **2022**, *7*, 718-25. DOI
146. Li, Z.; Liao, Y.; Ji, H.; et al. A tetrahydropyran-based weakly solvating electrolyte for low-temperature and high-voltage lithium metal batteries. *Adv. Energy. Mater.* **2024**, *15*, 2404120. DOI
147. Yang, Y.; Fang, Z.; Yin, Y.; et al. Synergy of weakly-solvated electrolyte and optimized interphase enables graphite anode charge at low temperature. *Angew. Chem. Int. Ed.* **2022**, *61*, e202208345. DOI
148. Chen, J.; Fan, X.; Li, Q.; et al. Electrolyte design for LiF-rich solid-electrolyte interfaces to enable high-performance microsized alloy anodes for batteries. *Nat. Energy.* **2020**, *5*, 386-97. DOI
149. Chen, Y.; Yu, Z.; Rudnicki, P.; et al. Steric effect tuned ion solvation enabling stable cycling of high-voltage lithium metal battery. *J. Am. Chem. Soc.* **2021**, *143*, 18703-13. DOI
150. Yang, Y.; Li, Z.; Wang, J.; Zhao, H. Inorganic-polymeric gradient interphase enabled by electrolyte chemistry modulation for highly stable silicon anode. *Chem. Eng. J.* **2025**, *517*, 164374. DOI

151. Cao, X.; Jia, H.; Xu, W.; Zhang, J. Review - localized high-concentration electrolytes for lithium batteries. *J. Electrochem. Soc.* **2021**, *168*, 010522. DOI
152. Dong, X.; Lin, Y.; Li, P.; et al. High-energy rechargeable metallic lithium battery at -70 °C enabled by a cosolvent electrolyte. *Angew. Chem. Int. Ed.* **2019**, *58*, 5623-7. DOI
153. Ren, X.; Gao, P.; Zou, L.; et al. Role of inner solvation sheath within salt-solvent complexes in tailoring electrode/electrolyte interphases for lithium metal batteries. *Proc. Natl. Acad. Sci. U.S.A.* **2020**, *117*, 28603-13. DOI
154. Yang, G.; Frisco, S.; Tao, R.; et al. Robust solid/electrolyte interphase (SEI) formation on Si anodes using Glyme-based electrolytes. *ACS. Energy. Lett.* **2021**, *6*, 1684-93. DOI
155. Yang, Y.; Yang, Z.; Li, Z.; Wang, J.; He, X.; Zhao, H. Rational electrolyte design for interfacial chemistry modulation to enable long-term cycling Si anode. *Adv. Energy. Mater.* **2023**, *13*, 2302068. DOI
156. Guo, Y.; Miao, M.; Wang, Y.; et al. A high-voltage and low-solvating electrolyte towards promising micro-Si/Ni-rich NMC full cells. *Energy. Storage. Mater.* **2024**, *67*, 103258. DOI
157. Mo, Y.; Liu, G.; Yin, Y.; et al. Fluorinated solvent molecule tuning enables fast-charging and low-temperature lithium-ion batteries. *Adv. Energy. Mater.* **2023**, *13*, 2301285. DOI
158. Chen, S.; Deng, Z.; Li, J.; et al. Tuning reaction kinetics of fluorinated molecules to construct robust solid electrolyte interphases on SiO_x anode. *Angew. Chem. Int. Ed.* **2025**, *64*, e202413927. DOI
159. Kim, M.; Moon, H.; Kim, S.; et al. Tunable solvation structures for fast charging of micron-Si anodes in energy-dense lithium-ion batteries. *Chem. Eng. J.* **2025**, *511*, 162079. DOI
160. Okada, R.; Aoki, Y.; Oda, M.; Nakazawa, M.; Inaba, M.; Doi, T. Effective formation of superior surface films on Si negative electrodes in a highly concentrated fluorinated carbonate ester solvent/diluent electrolyte solution system. *ACS. Appl. Energy. Mater.* **2022**, *6*, 546-53. DOI
161. Liu, Y.; Huang, Y.; Xu, X.; et al. Fluorinated solvent-coupled anion-derived interphase to stabilize silicon microparticle anodes for high-energy-density batteries. *Adv. Funct. Mater.* **2023**, *33*, 2303667. DOI
162. Peng, C.; Yang, X.; Tang, W.; et al. Fluorinated solvent coupled anions-derived hybrid interphase enabled highly reversible and cryogenic silicon anode. *J. Colloid. Interface. Sci.* **2025**, *699*, 138146. DOI
163. Zhang, W.; Zhang, S.; Fan, L.; et al. Tuning the LUMO energy of an organic interphase to stabilize lithium metal batteries. *ACS. Energy. Lett.* **2019**, *4*, 644-50. DOI
164. Cao, Z.; Zheng, X.; Zhou, M.; et al. Electrolyte solvation engineering toward high-rate and low-temperature silicon-based batteries. *ACS. Energy. Lett.* **2022**, *7*, 3581-92. DOI
165. Yang, J.; Wang, S.; Song, S.; et al. Cyclable micron-sized silicon-based lithium-ion batteries at -40 °C enabled by temperature-dependent solvation regulation. *Adv. Mater.* **2025**, *37*, 2501807. DOI
166. Peng, X.; Liu, B.; Chen, J.; Jian, Q.; Li, Y.; Zhao, T. A steric-hindrance-induced weakly solvating electrolyte boosting the cycling performance of a micrometer-sized silicon anode. *ACS. Energy. Lett.* **2023**, *8*, 3586-94. DOI
167. Geng, J.; Ni, Z.; Jiang, L.; et al. Engineering compact solvation structure of nonflammable electrolyte via an asymmetric fluorinated ether to enable stable high-voltage lithium-ion batteries with micron-sized silicon anodes. *Adv. Funct. Mater.* **2026**, *36*, e32086. DOI
168. Kim, D.; Han, J.; Park, S.; Kim, H.; Yoo, J. Anion-dominant coordinated weakly solvating ether electrolyte for silicon anodes. *J. Power. Sources.* **2026**, *668*, 239374. DOI
169. Liu, Q.; Sun, Y.; Li, M.; et al. Branched ether-driven electrolyte engineering for resilient inorganic-polymeric interface on micro-silicon anodes in high-energy Li-ion batteries. *Adv. Funct. Mater.* **2025**, *36*, e13046. DOI
170. Chen, Y.; Chen, X.; Yao, N.; et al. A molecular review on weakly solvating electrolytes for lithium batteries. *Materials. Today.* **2025**, *85*, 304-18. DOI
171. Zhang, J. H.; Zhang, Y.; Gu, Z. Y.; et al. Dampening lithium charge density by clustering solvents and anions to tame lithium de-coordination energy for low-temperature lithium-metal batteries. *Adv. Energy. Mater.* **2026**, *16*, e05551. DOI
172. Li, X.; Luo, F.; Zhou, N.; et al. Weakly solvating electrolytes for lithium and post-lithium rechargeable batteries: progress and outlook. *Adv. Energy. Mater.* **2025**, *15*, 2501272. DOI
173. Tiwari, R.; Kumar, D.; Verma, D. K.; et al. Fundamental chemical and physical properties of electrolytes in energy storage devices: a review. *J. Energy. Storage.* **2024**, *81*, 110361. DOI
174. Cui, Z.; Jia, Z.; Ruan, D.; et al. Molecular anchoring of free solvents for high-voltage and high-safety lithium metal batteries. *Nat. Commun.* **2024**, *15*, 2033. DOI PubMed PMC
175. You, Q.; Sun, Y.; Wang, F.; Cheng, J.; Tang, F. Decoding the competing effects of dynamic solvation structures on nuclear magnetic resonance chemical shifts of battery electrolytes via machine learning. *J. Am. Chem. Soc.* **2025**, *147*, 14667-76. DOI
176. Yao, N.; Chen, X.; Fu, Z.; Zhang, Q. Applying classical, *ab initio*, and machine-learning molecular dynamics simulations to the liquid electrolyte for rechargeable batteries. *Chem. Rev.* **2022**, *122*, 10970-1021. DOI

177. Yang, Y.; Yao, N.; Gao, Y. C.; et al. Data-knowledge-dual-driven electrolyte design for fast-charging lithium ion batteries. *Angew. Chem. Int. Ed.* **2025**, *64*, e202505212. DOI
178. Macfarlane, D. R.; Forsyth, M.; Howlett, P. C.; et al. Ionic liquids and their solid-state analogues as materials for energy generation and storage. *Nat. Rev. Mater.* **2016**, *1*, 15005. DOI
179. Huang, G.; Liao, Y.; Zhao, X.; et al. Tuning a solvation structure of lithium ions coordinated with nitrate anions through ionic liquid-based solvent for highly stable lithium metal batteries. *Adv. Funct. Mater.* **2022**, *33*, 2211364. DOI
180. Sun, C.; Li, R.; Weng, S.; et al. Reduction-tolerance electrolyte design for high-energy lithium batteries. *Angew. Chem. Int. Ed.* **2024**, *63*, e202400761. DOI
181. Xu, L.; Han, X.; Sung, J.; et al. 4.5-V-class safe lithium-ion batteries with silicon-majority-graphite anodes enabled by self-limiting interphase. *Adv. Mater.* **2025**, *38*, e15562. DOI
182. Haregewoin, A. M.; Wotango, A. S.; Hwang, B. Electrolyte additives for lithium ion battery electrodes: progress and perspectives. *Energy. Environ. Sci.* **2016**, *9*, 1955-88. DOI
183. Xiao, H.; Li, X.; Fu, Y. Advances in anion chemistry in the electrolyte design for better lithium batteries. *Nano-Micro. Lett.* **2025**, *17*, 149. DOI PubMed PMC
184. Hou, R.; Guo, S.; Zhou, H. Atomic insights into advances and issues in low-temperature electrolytes. *Adv. Energy. Mater.* **2023**, *13*, 2300053. DOI
185. Shen, S.; Chai, D.; Li, X.; Fu, Y. The synergistic effect of anion: design of stable ether electrolytes for li metal batteries beyond 4.6 V. *Adv. Funct. Mater.* **2025**, *35*, 2424072. DOI
186. Li, T.; Zhang, X. Q.; Yao, N.; et al. Stable anion-derived solid electrolyte interphase in lithium metal batteries. *Angew. Chem. Int. Ed.* **2021**, *60*, 22683-7. DOI
187. Liang, J. Y.; Zhang, Y.; Xin, S.; et al. Mitigating swelling of the solid electrolyte interphase using an inorganic anion switch for low-temperature lithium-ion batteries. *Angew. Chem. Int. Ed.* **2023**, *62*, e202300384. DOI
188. Kim, H.; Kim, T. H.; Kim, W.; Park, S. S.; Jeong, G. Interface engineering with nonsacrificial perfluorinated-anion additives for boosting the kinetics of lithium-ion batteries. *ACS. Appl. Mater. Interfaces.* **2023**, *15*, 9212-20. DOI
189. Philippe, B.; Dedryvère, R.; Gorgoi, M.; Rensmo, H.; Gonbeau, D.; Edström, K. Role of the $LiPF_6$ salt for the long-term stability of silicon electrodes in Li-ion batteries - a photoelectron spectroscopy study. *Chem. Mater.* **2013**, *25*, 394-404. DOI
190. Zhang, J.; Yue, X.; Wu, Z.; et al. A LiF-rich solid electrolyte interphase in a routine carbonate electrolyte by tuning the interfacial chemistry behavior of $LiPF_6$ for stable Li metal anodes. *Nano. Lett.* **2023**, *23*, 9609-17. DOI
191. Chen, Y.; Ma, Z.; Wang, Y.; et al. Trace ethylene carbonate-mediated low-concentration ether-based electrolytes for high-voltage lithium metal batteries. *Energy. Environ. Sci.* **2024**, *17*, 5613-26. DOI
192. Song, G.; Yi, Z.; Su, F.; et al. Boosting the low-temperature performance for Li-ion batteries in $LiPF_6$-based local high-concentration electrolyte. *ACS. Energy. Lett.* **2023**, *8*, 1336-43. DOI
193. Jia, H.; Gao, P.; Zou, L.; et al. Controlling ion coordination structure and diffusion kinetics for optimized electrode-electrolyte interphases and high-performance Si anodes. *Chem. Mater.* **2020**, *32*, 8956-64. DOI
194. Zhang, K.; Tian, Y.; Wei, C.; An, Y.; Feng, J. Building stable solid electrolyte interphases (SEI) for microsized silicon anode and 5V-class cathode with salt engineered nonflammable phosphate-based lithium-ion battery electrolyte. *Appl. Surf. Sci.* **2021**, *553*, 149566. DOI
195. Zhou, M.; Liu, W.; Su, Q.; et al. Ionic liquid additive mitigating lithium loss and aluminum corrosion for high-voltage anode-free lithium metal batteries. *ACS. Nano.* **2024**, *18*, 32959-72. DOI
196. Stehle, P.; Rutz, D.; Bazzoun, A. M.; Vrankovic, D.; Anjass, M. The optimal amount of lithium difluorophosphate as an additive for Si-dominant anodes in an application-oriented setup. *ChemSusChem* **2023**, *17*, e202301153. DOI
197. Yu, W.; Lin, K.; Boyle, D. T.; et al. Electrochemical formation of bis(fluorosulfonyl)imide-derived solid-electrolyte interphase at Li-metal potential. *Nature. Chem.* **2024**, *17*, 246-55. DOI
198. Li, J. L.; Zhang, X. Q.; Yu, P. P.; et al. Patching solid electrolyte interphase via modulating anion decomposition reactions for stable lithium metal batteries. *Angew. Chem. Int. Ed.* **2025**, *65*, e25130. DOI
199. Chang, Z. H.; Wang, J. T.; Wu, Z. H.; Gao, M.; Wu, S. J.; Lu, S. G. The electrochemical performance of silicon nanoparticles in concentrated electrolyte. *ChemSusChem* **2018**, *11*, 1787-96. DOI
200. Sankaran, A.; Laffir, F.; Maresca, G.; et al. Symmetric Vs asymmetric imide anion decomposition pathways and their influence on solid electrolyte interphase stability for Si anodes. *Angew. Chem. Int. Ed.* **2025**, *65*, e22709. DOI PubMed PMC
201. Jiang, Z.; Yang, T.; Li, C.; et al. Synergistic additives enabling stable cycling of ether electrolyte in 4.4 V Ni-rich/Li metal batteries. *Adv. Funct. Mater.* **2023**, *33*, 2306868. DOI

202. Lu, Z.; Liu, D.; Dai, K.; et al. Tailoring solvation chemistry in carbonate electrolytes for all-climate, high-voltage lithium-rich batteries. *Energy. Storage. Mater.* **2023**, *57*, 316-25. DOI
203. Xu, M.; Zhou, L.; Hao, L.; Xing, L.; Li, W.; Lucht, B. L. Investigation and application of lithium difluoro(oxalate)borate (LiDFOB) as additive to improve the thermal stability of electrolyte for lithium-ion batteries. *J. Power. Sources.* **2011**, *196*, 6794-801. DOI
204. Wang, W.; Zheng, C.; Zhang, S.; et al. Molten salt electrolyte enables micro-sized silicon anode in lithium-ion batteries. *Energy. Environ. Mater.* **2025**, *9*, e70111. DOI
205. Chen, S.; Wu, G.; Jiang, H.; et al. External Li supply reshapes Li deficiency and lifetime limit of batteries. *Nature* **2025**, *638*, 676-83. DOI
206. Zhang, A.; Yang, E.; Bi, Z.; et al. Unlocking 4.7 V $LiCoO_2$ with a counterintuitive low-concentration fluoroborate dual-salt electrolyte by anion-derived interfacial chemistry. *ACS. Energy. Lett.* **2025**, *10*, 1245-54. DOI
207. Kang, D. W.; Moon, J.; Choi, H.; Shin, H.; Kim, B. G. Stable cycling and uniform lithium deposition in anode-free lithium-metal batteries enabled by a high-concentration dual-salt electrolyte with high $LiNO_3$ content. *J. Power. Sources.* **2021**, *490*, 229504. DOI
208. Lv, L.; Wang, Y.; Huang, W.; Wang, Y.; Zhu, G.; Zheng, H. Effect of lithium salt type on silicon anode for lithium-ion batteries. *Electrochim. Acta.* **2022**, *413*, 140159. DOI
209. Cao, W.; Chen, W.; Lu, M.; et al. *In situ* generation of Li_3N concentration gradient in 3D carbon-based lithium anodes towards highly-stable lithium metal batteries. *J. Energy. Chem.* **2023**, *76*, 648-56. DOI
210. Ye, S.; Wang, L.; Liu, F.; et al. g-C_3N_4 derivative artificial organic/inorganic composite solid electrolyte interphase layer for stable lithium metal anode. *Adv. Energy. Mater.* **2020**, *10*, 2002647. DOI
211. Yang, W.; Li, S.; Liu, Y.; et al. Selective interfacial polymerization improves reversibility of Si anodes. *Chem. Eng. J.* **2025**, *514*, 163168. DOI
212. Xu, C.; Jing, P.; Deng, Z.; et al. Rectifying solid electrolyte interphase structure for stable multi-dimensional silicon anodes. *Energy. Storage. Mater.* **2025**, *74*, 103911. DOI
213. Cao, Z.; Zheng, X.; Qu, Q.; Huang, Y.; Zheng, H. Electrolyte design enabling a high-safety and high-performance Si anode with a tailored electrode-electrolyte interphase. *Adv. Mater.* **2021**, *33*, 2103178. DOI
214. Etacheri, V.; Haik, O.; Goffer, Y.; et al. Effect of fluoroethylene carbonate (FEC) on the performance and surface chemistry of Si-nanowire Li-ion battery anodes. *Langmuir* **2011**, *28*, 965-76. DOI
215. Liu, J.; Hao, W.; Fang, M.; et al. Screening of F-containing electrolyte additives and clarifying their decomposition routes for stable Li metal anodes. *Nat. Commun.* **2024**, *15*, 9356. DOI PubMed PMC
216. Martin, L.; Martinez, H.; Ulldemolins, M.; Pecquenard, B.; Le Cras, F. Evolution of the Si electrode/electrolyte interface in lithium batteries characterized by XPS and AFM techniques: the influence of vinylene carbonate additive. *Solid. State. Ionics.* **2012**, *215*, 36-44. DOI
217. Chen, L.; Wang, K.; Xie, X.; Xie, J. Effect of vinylene carbonate (VC) as electrolyte additive on electrochemical performance of Si film anode for lithium ion batteries. *J. Power. Sources.* **2007**, *174*, 538-43. DOI
218. Aurbach, D.; Gamolsky, K.; Markovsky, B.; Gofer, Y.; Schmidt, M.; Heider, U. On the use of vinylene carbonate (VC) as an additive to electrolyte solutions for Li-ion batteries. *Electrochim. Acta.* **2002**, *47*, 1423-39. DOI
219. Gogoi, N.; Lundström, R.; Hernández, G.; Berg, E. J. Base-driven ring-opening reactions of vinylene carbonate. *J. Electrochem. Soc.* **2024**, *171*, 050506. DOI
220. Wang, Y.; Nakamura, S.; Tasaki, K.; Balbuena, P. B. Theoretical studies to understand surface chemistry on carbon anodes for lithium-ion batteries: how does vinylene carbonate play its role as an electrolyte additive? *J. Am. Chem. Soc.* **2002**, *124*, 4408-21. DOI
221. Son, H. B.; Jeong, M.; Han, J.; et al. Effect of reductive cyclic carbonate additives and linear carbonate co-solvents on fast chargeability of $LiNi_{0.6}Co_{0.2}Mn_{0.2}O_2$/graphite cells. *J. Power. Sources.* **2018**, *400*, 147-56. DOI
222. Park, S.; Jeong, S. Y.; Lee, T. K.; et al. Replacing conventional battery electrolyte additives with dioxolone derivatives for high-energy-density lithium-ion batteries. *Nat. Commun.* **2021**, *12*, 838. DOI PubMed PMC
223. Li, Z.; Kong, L.; Peng, C.; Feng, W. Gas-phase fluorination of conjugated microporous polymer microspheres for effective interfacial stabilization in lithium metal anodes. *Carbon. Energy.* **2023**, *5*, e354. DOI
224. Tripathi, R.; Yesilbas, G.; Lamprecht, X.; et al. Understanding the electrolyte chemistry induced enhanced stability of Si anodes in Li-ion batteries based on Physico-chemical changes, impedance, and stress evolution during SEI formation. *J. Electrochem. Soc.* **2023**, *170*, 090544. DOI
225. Puget, M.; Shcherbakov, V.; Denisov, S.; et al. Reaction mechanisms of the degradation of fluoroethylene carbonate, an additive of lithium-ion batteries, unraveled by radiation chemistry. *Chem. Eur. J.* **2021**, *27*, 8185-94. DOI
226. Michan, A. L.; Parimalam, B. S.; Leskes, M.; et al. Fluoroethylene carbonate and vinylene carbonate reduction: understanding lithium-ion battery electrolyte additives and solid electrolyte interphase formation. *Chem. Mater.* **2016**, *28*, 8149-59. DOI

227. Sprowl, L. H.; Árnadóttir, L.; Chan, M. K. Y. Fluoroethylene carbonate breakdown mechanisms and energetics on two lithium silicide surfaces. *J. Phys. Chem. C.* **2019**, *123*, 26743-51. DOI
228. Shkrob, I. A.; Wishart, J. F.; Abraham, D. P. What makes fluoroethylene carbonate different? *J. Phys. Chem. C.* **2015**, *119*, 14954-64. DOI
229. Wang, Y.; Liu, Y.; Tu, Y.; Wang, Q. Reductive decomposition of solvents and additives toward solid-electrolyte interphase formation in lithium-ion battery. *J. Phys. Chem. C.* **2020**, *124*, 9099-108. DOI
230. Liu, D.; Qian, K.; He, Y.; et al. Positive film-forming effect of fluoroethylene carbonate (FEC) on high-voltage cycling with three-electrode $LiCoO_2$/Graphite pouch cell. *Electrochim. Acta.* **2018**, *269*, 378-87. DOI
231. Jin, Y.; Kneusels, N. H.; Marbella, L. E.; et al. Understanding fluoroethylene carbonate and vinylene carbonate based electrolytes for Si anodes in lithium ion batteries with NMR spectroscopy. *J. Am. Chem. Soc.* **2018**, *140*, 9854-67. DOI
232. Kim, J.; Chae, O. B.; Lucht, B. L. Perspective - structure and stability of the solid electrolyte interphase on silicon anodes of lithium-ion batteries. *J. Electrochem. Soc.* **2021**, *168*, 030521. DOI
233. Haridas, A. K.; Nguyen, Q. A.; Terlier, T.; Blaser, R.; Biswal, S. L. Investigating the compatibility of TTMSP and FEC electrolyte additives for $LiNi_{0.5}Mn_{0.3}Co_{0.2}O_2$ (NMC)-silicon lithium-ion batteries. *ACS. Appl. Mater. Interfaces.* **2021**, *13*, 2662-73. DOI
234. Li, Y.; Cao, Z.; Wang, Y.; et al. New Insight into the role of fluoro-ethylene carbonate in suppressing Li-trapping for Si anodes in lithium-ion batteries. *ACS. Energy. Lett.* **2023**, *8*, 4193-203. DOI
235. Liu, Z.; Zhang, Y.; Wang, S.; et al. Solvation-shell engineering enables additive-dominated coordination for stable silicon anodes under minimal salt conditions. *Angew. Chem. Int. Ed.* **2025**, *65*, e18092. DOI
236. Kim, J.; Yi, R.; Cao, X.; et al. Extending calendar life of Si-based lithium-ion batteries by a localized high concentration electrolyte. *ACS. Energy. Lett.* **2024**, *9*, 2318-25. DOI
237. Quinn, J.; Kim, J. M.; Yi, R.; Zhang, J. G.; Xiao, J.; Wang, C. Fluoro-ethylene-carbonate plays a double-edged role on the stability of Si anode-based rechargeable batteries during cycling and calendar aging. *Adv. Mater.* **2024**, *36*, 2402625. DOI
238. Shen, J.; Chen, H.; Yu, L.; Huang, D.; Luo, Z. 4, 5-difluoro-1, 3-dioxolan-2-one as an film forming additive on $LiNi_{0.8}Co_{0.15}Al_{0.05}O_2$/SiO@C full cells. *J. Electroanal. Chem.* **2019**, *834*, 1-7. DOI
239. Ma, Y.; Dai, Z.; Chang, Q.; et al. Freeze-resistant electrolyte with smart ion-pairing enables robust silicon anodes for high-energy lithium-ion batteries at low temperature. *Chem. Eng. J.* **2025**, *528*, 172063. DOI
240. Yang, Y.; Wang, J.; Li, Z.; Yang, Z.; Wang, B.; Zhao, H. Constructing LiF-dominated interphases with polymer interwoven outer layer enables long-term cycling of Si anodes. *ACS. Nano.* **2024**, *18*, 7666-76. DOI
241. Deng, Y.; Li, C.; Guo, R.; et al. Breaking kinetic barriers in silicon anodes via strategic electrolyte additive engineering. *Adv. Funct. Mater.* **2024**, *35*, 2415820. DOI
242. He, S.; Huang, S.; Liu, X.; et al. Electrolyte design for robust gradient solid-electrolyte interfaces to enable high-performance silicon anodes for pouch batteries. *Chem. Eng. J.* **2024**, *489*, 150620. DOI
243. Ou, Y.; Hou, W.; Zhu, D.; et al. Molecular design of electrolyte additives for high-voltage fast-charging lithium metal batteries. *Energy. Environ. Sci.* **2025**, *18*, 1464-76. DOI
244. Li, X.; Gilbert, J. A.; Trask, S. E.; et al. Investigating ternary Li-Mg-Si zintl phase formation and evolution for Si anodes in Li-ion batteries with $Mg(TFSI)_2$ electrolyte additive. *Chem. Mater.* **2021**, *33*, 4960-70. DOI
245. Han, B.; Liao, C.; Dogan, F.; et al. Using mixed salt electrolytes to stabilize silicon anodes for lithium-ion batteries via in situ formation of Li-M-Si Ternaries (M = Mg, Zn, Al, Ca). *ACS. Appl. Mater. Interfaces.* **2019**, *11*, 29780-90. DOI
246. Hüger, E.; Uxa, D.; Yang, F.; Schmidt, H. The lithiation onset of amorphous silicon thin-film electrodes. *Appl. Phys. Lett.* **2022**, *121*, 133901. DOI
247. Wu, Y.; Ge, G.; Wang, S.; Xiong, L.; He, Z. Formation mechanisms of solid electrolyte interphase and its influence on lithium battery performance. *Mater. Today. Energy.* **2025**, *54*, 102124. DOI
248. Wang, A.; Wang, L.; Liang, H.; et al. Lithium difluorophosphate as a widely applicable additive to boost lithium-ion batteries: a perspective. *Adv. Funct. Mater.* **2023**, *33*, 2211958. DOI
249. Kim, J. W.; Seong, M. J.; Park, D. W.; Jeong, G.; Yim, T. Anti-corrosive and surface-stabilizing functional electrolyte containing LiFSI and $LiPO_2F_2$ for SiO /NCM811-based batteries. *Corros. Sci.* **2022**, *198*, 110117. DOI
250. Lee, J. A.; Kim, S.; Cho, Y.; et al. Compositionally sequenced interfacial layers for high-energy Li-metal batteries. *Adv. Sci.* **2024**, *11*, 2310094. DOI
251. Chen, Y.; Zhao, W.; Zhang, Q.; et al. Armoring $LiNi_{1/3}Co_{1/3}Mn_{1/3}O_2$ cathode with reliable fluorinated organic-inorganic hybrid interphase layer toward durable high rate battery. *Adv. Funct. Mater.* **2020**, *30*, 2000396. DOI
252. Zhang, Y.; Lai, P.; Deng, X.; Zhang, P.; Zhao, J. Anion-oriented solvation regulation of a dual-salt electrolyte for lithium metal batteries. *Chem. Eng. J.* **2025**, *507*, 160482. DOI

253. Kwon, H.; Kim, S.; Hyun, J.; et al. Covariance of interphasic properties and fast chargeability of energy-dense lithium metal batteries. *Nat. Energy.* **2025**, *10*, 1132-45. DOI
254. Kang, Z.; Wang, S.; Wu, G.; et al. Nitrogen-centered organic salts enable stable lithium-ion supply for high-energy-density batteries. *J. Am. Chem. Soc.* **2025**, *147*, 30591-8. DOI
255. Zhou, P.; Ou, Y.; Feng, Q.; et al. Tuning the nucleophilicity of anion in lithium salt to enable an anion-rich solvation sheath for stable lithium metal batteries. *Adv. Funct. Mater.* **2024**, *35*, 2416800. DOI
256. Lu, Y.; Cao, Q.; Zhang, W.; et al. Breaking the molecular symmetricity of sulfonimide anions for high-performance lithium metal batteries under extreme cycling conditions. *Nat. Energy.* **2026**, 1679. DOI
257. Xu, J.; Koverga, V.; Phan, A.; et al. Revealing the anion-solvent interaction for ultralow temperature lithium metal batteries. *Adv. Mater.* **2023**, *36*, 2306462. DOI
258. Wang, S.; He, Y.; Zhang, G.; et al. Multifunctional silicon-based composite electrolyte additive enhances the stability of the lithium metal anode/electrolyte interface. *Adv. Energy. Mater.* **2024**, *14*, 2401384. DOI
259. Lan, X.; Yang, S.; Meng, T.; Zhang, C.; Hu, X. A multifunctional electrolyte additive with solvation structure regulation and electrode/electrolyte interface manipulation enabling high-performance Li-ion batteries in wide temperature range. *Adv. Energy. Mater.* **2023**, *13*, 2203449. DOI
260. Hou, T.; Yang, G.; Rajput, N. N.; et al. The influence of FEC on the solvation structure and reduction reaction of $LiPF_6$/EC electrolytes and its implication for solid electrolyte interphase formation. *Nano. Energy.* **2019**, *64*, 103881. DOI
261. Yang, B.; Hu, A.; Li, T.; et al. Eliminating water hazards and regulating electrode-electrolyte interfaces by multifunctional sacrificial electrolyte additives for long-life lithium metal batteries. *Energy. Storage. Mater.* **2024**, *70*, 103512. DOI
262. Ding, L.; Chen, Y.; Sheng, Y.; Yue, X.; Liang, Z. Eliminating hydrogen fluoride through piperidine-doped separators for stable Li metal batteries with nickel-rich cathodes. *Angew. Chem. Int. Ed.* **2024**, *63*, e202411933. DOI
263. Jiang, S.; Li, R.; Chen, L.; et al. Deciphering the purification additive chemistries for ultra-stable high-voltage lithium-ion batteries. *Adv. Mater.* **2025**, *37*, 2417285. DOI
264. Wang, Y.; Liu, J.; Ji, H.; et al. Optimizing Si-O conjugation to enhance interfacial kinetics for low-temperature rechargeable lithium-ion batteries. *Adv. Mater.* **2025**, *37*, 2412155. DOI
265. Chen, Y. P.; Niu, Y. L.; Zheng, Z.; et al. Origin of anion-rich solvation structures in siloxane electrolytes. *Angew. Chem. Int. Ed.* **2025**, *64*, e202508152. DOI
266. Wang, Y.; Ni, Y.; Xu, S.; et al. Fully methylated siloxane-based electrolyte for practical lithium metal batteries. *J. Am. Chem. Soc.* **2025**, *147*, 10772-83. DOI
267. Zhu, X.; Chen, J.; Liu, G.; et al. Non-fluorinated cyclic ether-based electrolyte with quasi-conjugate effect for high-performance lithium metal batteries. *Angew. Chem. Int. Ed.* **2024**, *64*, e202412859. DOI
268. Wang, Y.; Cao, Z.; Ma, Z.; et al. Weak solvent-solvent interaction enables high stability of battery electrolyte. *ACS. Energy. Lett.* **2023**, *8*, 1477-84. DOI
269. Liu, Z.; Zhang, S.; Zhang, H.; et al. Regulating solvating sites for stable high-voltage lithium metal batteries. *Angew. Chem. Int. Ed.* **2025**, *64*, e202506395. DOI
270. Li, G. X.; Lyu, X.; Nguyen, A.; et al. Fine-tuning Li-ion solvation structure by enhanced solvent-diluent interactions for long-cycling lithium metal batteries. *Adv. Energy. Mater.* **2025**, *15*, 2405680. DOI
271. Ma, B.; Zhang, H.; Li, R.; et al. Molecular-docking electrolytes enable high-voltage lithium battery chemistries. *Nature. Chem.* **2024**, *16*, 1427-35. DOI
272. Cui, Z.; Wang, D.; Guo, J.; et al. Push-pull electrolyte design strategy enables high-voltage low-temperature lithium metal batteries. *J. Am. Chem. Soc.* **2024**, *146*, 27644-54. DOI